Technische Universiteit Delft

Detection of Drought, Flood and Snow Anomalies with 37GHz Passive Microwave Space-borne Data

The SSM/I case study over Europe

By Eleni Ioannidou

TU Delft Delft University of Technology

Detection of Drought, Flood and Snow Anomalies with 37GHz Passive Microwave Space-borne Data

The SSM/I case study over Europe

by

Eleni Ioannidou

to obtain the degree of Master of Science
at the Delft University of Technology,
to be defended publicly on April 23, 2019.

Student number: 4520483

Thesis committee:

Prof.dr.ir. Nick van de Giesen,	TU Delft-Chairman
Prof.dr.ir. Susan Steele-Dunne,	TU Delft
Dr. Lorenzo Iannini,	TU Delft

TU Delft

Content

List of figures 7
List of tables 11
Acknowledgements 13
Abstract 15
Introduction 17
Research Objective 19
Thesis outline 19
Chapter 1. Remote Sensing Background 21
1.1 Categories of remote sensing 22
1.2 Satellite microwave sensing 23
1.3 SSM/I sensor 25
Chapter 2. Modelling approach 29
2.1 Study area and data 29
2.2 Brightness Temperature 31
2.3 Polarization Difference 33
2.4 Microwave Polarization Difference Index (MPDI) 36
Chapter 3. Methodology approach 39
3.1 Data Pre-Processing 39
3.2 Temporal Analysis 39
3.2.1 Histograms 39
3.2.2 Standard deviation and mean plots 42
3.3 Spatial Analysis 44
3.3.1 Brightness Temperature 45
3.3.2 Polarization Difference Brightness Temperature 47
3.3.3 Normalized Polarization Difference Brightness Temperature 48
Chapter 4. Results and discussion 51
4.1 Spain 52
4.2 South France 55
4.3 Bosnia and Herzegovina 58
4.4 Czech Republic 61
4.5 Poland 63

4.6 Ukraine 65
Chapter 5. Conclusions and Recommendations 69
Appendix A. Time series 73
A.1. Brightness Temperature time series 73
A.2. Polarization Difference Brightness Temperature time series 75
A.3. Microwave Polarization Difference Index time series 76
Appendix B. Polarization Difference Brightness Temperature statistics 79
B.1. Histogram plots 79
B.2. Standard deviation and mean plots 81
Appendix C. Methodology of creation of scatter plots 85
Bibliography 87

List of figures

Figure 1. Passive and Active remote sensors(Bakker et al. 2004) 23
Figure 2. Representation of the passes of the satellite (Kaya 2014) 25
Figure 3. Passing time of all the SSM/I instruments 26
Figure 4. Global image of Brightness Temperature 30
Figure 5. Investigated areas 30
Figure 6. Brightness Temperature time series for the Horizontal Polarization for Spain, event occurring in days 200-210 31
Figure 7. Brightness Temperature time series for the Vertical Polarization for Spain, event occurring in days 200-210 32
Figure 8. Brightness Temperature time series for the Horizontal Polarization for Bosnia and Herzegovina, event occurring in days 140-150 32
Figure 9. Brightness Temperature time series for the Vertical Polarization for Bosnia and Herzegovina, event occurring in days 140-150 32
Figure 10. Brightness Temperature time series for the Horizontal Polarization for Ukraine, event occurring in days 80-90 33
Figure 11. Brightness Temperature time series for the Vertical Polarization for Ukraine, event occurring in days 80-90 33
Figure 12. Polarization Difference Brightness Temperature time series for Spain, event occurring in days 200-210 34
Figure 13. Polarization Difference Brightness Temperature time series for Bosnia and Herzegovina, event occurring in days 140-150 35
Figure 14. Polarization Difference Brightness Temperature time series for Ukraine, event occurring in days 80-90 35
Figure 15. Microwave Polarization Difference Index time series for Spain, event occurring in days 200-210 36
Figure 16. Microwave Polarization Difference Index time series for Bosnia and Herzegovina, event occurring in days 140-150 37
Figure 17. Microwave Polarization Difference Index time series for Ukraine, event occurring in days 80-90 37
Figure 18. Histogram of the Polarization Difference Brightness Temperature for the ascending pass for days 200-210 for Spain 40
Figure 19. Histogram of the Polarization Difference Brightness Temperature for the descending pass for days 200-210 for Spain 40
Figure 20. Histogram of the Polarization Difference Brightness Temperature for the ascending pass for days 140-150 for Bosnia and Herzegovina 40
Figure 21. Histogram of the Polarization Difference Brightness Temperature for the descending pass for days 140-150 for Bosnia and Herzegovina 41
Figure 22. Histograms of the Polarization Difference Brightness Temperature for the ascending pass for days 80-90 for Ukraine 41
Figure 23. Histograms of the Polarization Difference Brightness Temperature for the descending pass for days 80-90 for Ukraine 41

Figure 24. Standard deviation and mean plots for the ascending pass for Spain 42
Figure 25.Standard deviation and mean plots for the descending pass for Spain..... 42
Figure 26. Standard deviation and mean plots for the ascending pass for Bosnia and Herzegovina..... 43
Figure 27. Standard deviation and mean plots for the descending pass for Bosnia and Herzegovina..... 43
Figure 28. Standard deviation and mean plots for the ascending pass for Ukraine 43
Figure 29. Standard deviation and mean plots for the descending pass for Ukraine 44
Figure 30. Average T_B for the Horizontal Polarization for the ascending pass for time interval of 10 days 45
Figure 31. Average T_B for the Horizontal Polarization for the descending pass for time interval of 10 days 45
Figure 32. Average T_B for the Vertical Polarization for the ascending pass for a time interval of 10 days 46
Figure 33. Average T_B for the Vertical Pass for the descending pass for a time interval of 10 days..... 46
Figure 34. Polarization Difference Brightness Temperature for the ascending pass for a time interval of 10 days 47
Figure 35. Polarization Difference Brightness Temperature for the descending pass for a time interval of 10 days 47
Figure 36. Normal distribution and z-score..... 48
Figure 37. Detected anomalies for 2014 for last days of May 49
Figure 38. Scatter plots for the ascending pass for the last 10 days of July for Spain 52
Figure 39. Scatter plots for the descending pass for the last 10 days of July for Spain 52
Figure 40. Detected anomalies for 2014 for the last days of July 52
Figure 41. Detected anomalies for 2017 for the last days of July. 53
Figure 42. Yearly soil moisture data for Spain..... 53
Figure 43.Hourly precipitation data for Spain for July 2014 54
Figure 44. Hourly precipitation data for Spain for July 2017 54
Figure 45. Scatter plots for the ascending pass for the first 10 days for South France 55
Figure 46. Scatter plots for the descending pass for the first 10 days for South France 55
Figure 47. Detected anomalies for 2014 for the first days of August. 56
Figure 48. Detected anomalies for 2003 for the first days of August 56
Figure 49. Yearly soil moisture data for South France 57
Figure 50. Hourly precipitation data for South France for August 2014..... 57
Figure 51. Hourly precipitation data for South France for August 2003..... 58
Figure 52. Scatter plots for the ascending pass for the last 10 days for Bosnia and Herzegovina..... 58
Figure 53. Scatter plots for the descending pass for the last 10 days for Bosnia and Herzegovina..... 59
Figure 54. Detected anomalies for 2014 for the last days of May 59
Figure 55. Detected anomalies for 1991 for the last days of May 60
Figure 56. Yearly soil moisture data for Bosnia and Herzegovina..... 60
Figure 57. Hourly precipitation data for Bosnia and Herzegovina for May 2014..... 61
Figure 58. Scatter plots for the ascending pass for the first 10 days for Czech Republic 61

Figure 59. Scatter plots for the descending pass for the first 10 days for Czech Republic 61
Figure 60. Detected anomalies for 2002 for the last days of August 62
Figure 61. Detected anomalies for 1996 for the last days of August 62
Figure 62. Hourly precipitation data for Czech Republic for August 2002 63
Figure 63. Scatter plots for the ascending pass for the first 10 days for Poland 63
Figure 64. Scatter plots for the descending pass for the first 10 days for Poland 63
Figure 65. Detected anomalies for 2009 for the first days of December 64
Figure 66. Detected anomalies for 2010 for the first days of December 64
Figure 67. Hourly precipitation data for Poland for December 2009 65
Figure 68. Hourly precipitation data for Poland for December 2010 65
Figure 69. Scatter plots for the ascending pass for Ukraine 65
Figure 70. Scatter plots for the descending pass for Ukraine 66
Figure 71. Detected anomalies for 2013 for the last days of March 66
Figure 72. Detected anomalies for 2006 for the last days of March 67
Figure 73. Yearly soil moisture data for Poland 67
Figure 74. Hourly precipitation data for Poland 68
Figure 75. Hourly precipitation data for Ukraine for March 2006 68
Figure 76. Brightness Temperature time series for the Horizontal Polarization for South France, event occurring in days 200-210 73
Figure 77. Brightness Temperature time series for the Vertical Polarization for South France, event occurring in days 200-210 73
Figure 78. Brightness Temperature time series for the Horizontal Polarization for Czech Republic, event occurring in days 220-230 74
Figure 79. Brightness Temperature time series for the Vertical Polarization for Czech Republic, event occurring in days 220-230 74
Figure 80. Brightness Temperature time series for the Horizontal Polarization for Poland, event is occurring in days 340-350 74
Figure 81. Brightness Temperature time series for the Vertical Polarization for Poland, event occurring in days 340-350 75
Figure 82. Polarization Difference Brightness Temperature time series for South France, event occurring in days 200-210 75
Figure 83.Polarization Difference Brightness Temperature time series for Czech Republic, event occurring in days 220-230 76
Figure 84. Polarization Difference Brightness Temperature time series for Poland, event occurring in days 340-350 76
Figure 85. Microwave Polarization Difference Index time series for South France, event occurring in days 200-210 76
Figure 86. Microwave Polarization Difference Index time series for Czech Republic, event occurring in days 220-230 77
Figure 87. Microwave Polarization Difference Index time series for Poland, event occurring in days 340-350 77
Figure 88. Histogram of the Polarization Difference Brightness Temperature for the ascending pass for days 200-210 for South France 79
Figure 89. Histogram of the Polarization Difference Brightness Temperature for the descending pass days 200-210 for South France 79

Figure 90. Histogram of the Polarization Difference Brightness Temperature for the ascending pass for days 220-230 for Czech Republic..... 80
Figure 91. Histogram of the Polarization Difference Brightness Temperature for the descending pass for days 220-230 for Czech Republic..... 80
Figure 92. Histogram of the Polarization Difference Brightness Temperature for the ascending pass for days 340-350 for Poland..... 80
Figure 93. Histogram of the Polarization Difference Brightness Temperature for the descending pass for days 340-350 for Poland..... 81
Figure 94. Standard deviation and mean plots for the ascending pass for South France..... 81
Figure 95. Standard deviation and mean plots for the descending pass for South France 81
Figure 96. Standard deviation and mean plots for the ascending pass for Czech Republic ... 82
Figure 97. Standard deviation and mean plots for the descending pass for Czech Republic . 82
Figure 98. Standard deviation and mean plots for the ascending pass for Poland..... 82
Figure 99. Standard deviation and mean plots for the descending pass for Poland 83

List of tables

Table 1. Six big floods in Europe (Kundzewicz et al. 2013) 18
Table 2. Drought events in Europe between 1985 and 2012 (Spinoni et al., 2016) 18
Table 3. Optical and thermal sensors used for water bodies identification (Shang 2017) 22
Table 4. Microwave sensors used for deriving soil moisture (Owe et al. 2008) 24
Table 5. Crossing Times as of 05-December-2018 26
Table 6. SSM/I instruments and their operating dates(Remote Sensing Systems n.d.) 27
Table 7.Type of event of the selected areas and their location 29

Acknowledgements

I would first like to thank my committee members for the support and information that they provided me with, pointing me towards the right direction. The door of Dr. Lorenzo Iannini was always open whenever I ran into troubles giving me guidance throughout this research.

I must express my gratitude to my parents and my sister for the continuous support and encouragement throughout all the years of my studies and for believing in me in my most difficult times. Without having them on my side, this accomplishment would not be possible.

Finally, I would like to thank my friends for bearing up with me all this time. Special thanks to my friends Iman and Lena who were always there for me and keeping me sane in this difficult journey.

Abstract

Europe is a continent with diverse climatic conditions. The dominant climates are the Oceanic, the Mediterranean and the Continental ones. The western part of Europe has an oceanic climate, southern Europe has a Mediterranean climate and eastern Europe has a continental climate. Because of such heterogeneities, a vast range of extreme climatic events might occur in different areas. We define extreme climatic events the droughts, floods and heavy snowfall. Those events will be generically referred to in this research as anomalies.

The purpose of this study is the identification of these extreme climatic events in the area of Europe, with the use of Special Sensor Microwave Imager (SSM/I) data at 37GHz frequency. The data that are used are Brightness Temperature (T_B) values. The detection of the events will be achieved with the Polarization Difference Brightness Temperature (PDBT). The PDBT values can be related to changes to surface wetness and the surface geometry. It could be used as an indicator of an anomaly, because the higher the values of PDBT the higher the surface wetness.

The methodological steps of the work consist in a statistical analysis of the SSM/I time-series, in the design of a detection algorithm of the anomalies under investigation and on the debate of its performance. The analysis of the temporally long SSM/I data will provide a first understanding of the data sensitivity to events under investigation and of their distribution for the statistical modelling of the Normalized Polarization Difference Brightness Temperature (NPDBT) indicator. The calculation of the NPDBT exploits the same principles as the well-known z-score index. The detection of the anomalies will be then achieved through thresholding the NPDBT index. Further information for the detection of anomalies is provided by the soil moisture time series from the Soil Moisture Active Passive (SMAP) sensor and the precipitation data from the Global Satellite Mapping of Precipitation (GSMAP). The soil moisture data appear to be more useful for the dry events, whereas the precipitation data for the flooding and the heavy snowfall events.

Introduction

Water is one of the most important parameters of human life. It is one of the main resources for surviving but at the same time it could be catastrophic. Natural disasters which are related to either the presence of water or not, such as floods and droughts not only affect the environment, but they have a huge impact in human life as well. Another event that is related to water and could be characterized as a natural disaster is heavy snowfall. Even though water does not have a liquid form, snow is water vapor in the form of crystals. These extreme climatic conditions could really affect not only the quality of human life and economy but its existence as well.

Snowfall events could sometimes be considered as helpful, whereas other times as lethal enemy. On one hand, snow cover can provide insulation on the Earth's surface and control its temperature and energy balance. Also, when it melts, it recharges the aquifers either by being absorbed by soil and recharging groundwater or ending up in a river, lake or sea through discharge (Snow and Climate | National Snow and Ice Data Center, n.d.). On the other hand, heavy snowfall could be fatal. When the melting of ice is followed by low temperatures, below zero, that leads to ice formation which could be very dangerous, especially for transportation. Also when heavy snowfall occurs in areas that this phenomenon is not so common, many casualties happen, mainly to vulnerable groups because of the low temperatures that could lead in hypothermia (Types of Disasters and Their Consequences, n.d.).

Drought is a climate related phenomenon that occurs due to the lack of precipitation in combination with high temperatures (Spinoni et al. 2015). Europe is a continent that suffers from droughts and not only in semi-arid areas such as the Mediterranean region, but also central Europe has suffered several droughts. One of the biggest was in 2003 and the latest one was recorded on July of 2018 with most of the countries of central and north Europe suffering from the heat wave. Indicatively, Sweden, France and Germany were some of the countries that were mostly affected by the high summer temperatures and the lack of rain. The main outcome, especially from the last drought was the severe impact in agriculture and dangerous fire events (Europe 2018).

Floods are hazardous natural events that can take human lives and destroy properties. The main natural cause of floods is extreme rainfall. One of the most important factors that cause heavy precipitation is mainly climate change. In central Europe in 1997 there was a severe flood causing the death of 114 people. The next big flood that followed was in 2002 and the most recent one was on July of 2018 (Kundzewicz et al. 2005, (Europe – FloodList)). Between the period 1950 and 2006, a big percentage of the deaths due to flood in Europe were caused due to flash floods. Flash floods appear to be an increasing event as a result of the growing agriculture cultivations and land use. It is expected that these events will happen more frequently as the years progress and this is due to climate change and the way that affects the hydrological cycle (Marchi et al. 2010). Flood risk is getting higher over the years due to urbanization, deforestation and the reduction of water storage in general (Kundzewicz et al. 2005).

In Table 1 are presented six of the biggest floods that occurred in Europe between 1985 and 2009.

Table 1. Six big floods in Europe (Kundzewicz et al. 2013)

Date of the flood	Country	Number of Deaths
01 August 2002	Germany, Czech Republic, Austria, Italy, Romania, Bulgaria, Slovakia, Ukraine, Hungary, Moldova	232
04 November 1994	Italy	64-83
04 November 1996	Italy	70-118
13 October 2000	Italy, France, Switzerland	13-38
25 August 1983	Spain	40-45
01 July 1997	Poland, Czech Republic, Germany	100-118

On the other hand, droughts are events that they do not happen very fast, they need time to progress and they usually affect bigger areas and they have an impact in economy as well. Long droughts can cause severe problems and destroy ecosystems. Between the years of 2006 and 2010, almost each year, 15% of the European area suffered extreme droughts, with the most affected regions to be the Mediterranean area. However, central and eastern Europe have become progressively to become areas of concern (Spinoni et al. 2016).

Drought is a complex phenomenon and it can undergo through several categories such as the agricultural, the socioeconomic, hydrological and groundwater droughts (Spinoni et al. 2016). This research is mainly focusing of the meteorological droughts, whose cause is the long-lasting lack of precipitation and the increase in temperature as well.

In Table 2are presented six of the most severe droughts that occurred in Europe between 1985-2012.

Table 2. Drought events in Europe between 1985 and 2012 (Spinoni et al., 2016)

Period of the drought	Area
1989-81	Southern Europe, Mediterranean
1999-2001	Southern/Eastern Europe
2003	European Heat Wave
2004-2005	Iberian Peninsula
2005-07	Baltic Republics
2007-08	Aegean Countries
2011	France, England, Central Europe

The identification of existence or not of water bodies was not an easy task in the past, but in the recent years it became a lot easier with the use of remote sensing technologies. Satellites orbit the Earth on a daily basis recording plenty of information of the global-scale, which in the past was very difficult to be collected, especially for remote areas where in situ measurements were inadequate (Ferraro et al. 1996). This gives the potential for bigger hydrological studies, studying bigger areas (Jackson 1997). With the use of remote sensing data, it is easy to monitor the current situation but also to predict extreme events. This could be achieved by analyzing the data and creating a pattern from their behavior. Also, with remote sensing techniques, qualitative and quantitative estimations about the damages that are caused by those extreme natural events are becoming more understandable and hence easier to use for co- and post-event

analysis and management, because there is an actual visualization. Constant monitoring could provide early warnings of the occurrence of the events. Those early warnings could be a useful tool in the prevention of catastrophic incidents that most of the times are irreversible (Csornai 2006).

Research Objective

As mentioned earlier, extreme climatic conditions could be catastrophic not only for human life but for ecosystems as well. Therefore, it is vital to develop a methodology that could detect these extremes and could be used in future research as a tool of prediction. Those extremes could be characterized as anomalies. The aim of this study is to develop a model with the use of space-borne data and connect the changes of surface wetness of an area with the detection of extreme phenomena, such as floods, droughts and heavy snowfall events in Europe.

This study will focus on the qualitative approach of the detection of the extremes and it will not be quantitative stating the level of the hazard. It will focus on confirming recorded events and recognize new ones that were not documented.

Thesis outline

In Chapter 1 information regarding some of the remote sensing techniques that exist and the one that is being used is described. In Chapter 2 there is a description of the modelling approach and information about the study area and the data that were used. This chapter describes in detail the selected areas and the investigated events. Chapter 3 describes the methodology approach and focuses more in the processing of the data. In Chapter 4 the results of the study are presented and discussed. This includes relevant observations on the detection of the anomalies and a brief validation of the analysis. Chapter 6 presents the conclusions and some of the limitations of the study, as well as recommendations for future research.

Chapter 1. Remote Sensing Background

Remote sensing is the science of monitoring and collecting data from the Earth's surface that are difficult to be obtained without making in situ contact with the object. The remote sensing data can be obtained by sensors mounted on different carriers, such as airplanes, satellites and drones, that can effortlessly cover large areas of the Earth surface. These images can be easily separated into smaller areas that are called pixels, containing digital values of the brightness of each area. The science of remote sensing is commonly used for mapping areas, in the field of meteorology, ecology, geomorphology, prediction of floods and so on, but they play a significant role in GIS. The list of applications of remote sensing is very big (Remote Sensing - Overview, Types and Applications; What is remote sensing and what is it used for?, n.d.). Another very important application of the remote sensing data seems to be the delineation of water bodies and the estimation of hydrological variables like soil moisture (Kumar and Tv 2013). Today, the detection and prediction of floods, droughts and heavy snowfall events are feasible with high resolution remote sensing data. Remote sensing uses electromagnetic radiation. Two of the most important features of the electromagnetic radiation are the wavelength and the frequency. As wavelength is characterized the distance between two identical high and low point of a wave and it is measured in meters (m). Frequency is called the number of iterations of an event in the unit of time and it is measured in Hz (Electromagnetic Radiation | Natural Resources Canada, n.d.).

The relationship between the frequency and the wavelength is described in the following equation.

$$c = \lambda \cdot f \tag{1}$$

Where,

c is the speed of light ($3 \cdot 10^8$ m/s)
λ is the wavelength (m)
f is the frequency (Hz)

When the value of the wavelength is high, the value of the frequency becomes small. This indicates that those two units are inversely proportional (Electromagnetic Radiation | Natural Resources Canada, n.d.).

One very important process that all the remote sensing data must undergo is calibration. Calibration is the procedure that insures that the data are consistent and accurate. There are two different calibration processes. The relative and the absolute calibration. In relative calibration it is ensured that any variation in data will be corrected by repeating the measurements over time. This gives the ability to the user to make comparisons between different images with confidence. However, if the user needs to establish physical relationships between the sensor measurements and the observed geophysical variables, then the absolute calibration must be

applied. Absolute calibration is more complicated than relative calibration. It requires detailed properties of the instrument page and the scattering properties of the black body (Natural Resources 2016).

1.1 Categories of remote sensing

The remote sensing data are subjected into two categories, the optical and the microwave. Their big difference is the wavelengths that they operate. Optical remote sensing is most commonly used when to inspect the data as the human eye sees it, whereas the microwave data provides a complementary and less intuitive set of features. A parameter that can really affect the quality of the optical data is the presence of clouds, whereas in the microwave spectrum, depending on the frequency, the impact of clouds is not always an issue. (Differences Between Optical & Radar Satellite Data | Pixalytics Ltd, n.d.).

The most commonly used sensors for the identification of water bodies are optical and thermal sensors (Shang 2017). The optical remote sensors produce images of the Earth's surface by operating at visible (0.4-0.7 μm) and infrared (0.7-1000 μm) wavelength. The way that they obtain their signal is by measuring the solar radiation re-irradiated from the objects on the ground. Each object reflects in a different way at specific wavelengths. So, each object can be categorized according to its reflectance and the number of bands that were used for the processing of the image (Principles of Remote Sensing - Centre for Remote Imaging, Sensing and Processing, CRISP, n.d.).

The thermal sensors detect thermal radiation, with the use of detectors that are sensitive to the photons. Those detectors are cooled down to such low temperature as -273.15 ^{o}C so that the signals that they receive will not be affected by their own emissions. Basically, thermal sensors measure the thermal properties of an object and its surface temperature. Thermal sensors operate in longer wavelengths than the visible, that there is not so much atmospheric scattering. On the other hand, because of the presence of atmospheric gases the physical phenomenon of absorption is quite evident. As the wavelength increases, the spatial resolution of the thermal sensors is becoming rough compared to the visible and infrared radiation (Thermal Imaging | Natural Resources Canada, n.d.).

As mentioned earlier, the identification of the existence or not of water bodies could be achieved with the use of optical and thermal sensors, because the reflectance of water is much lower that this of other objects. In Table 3, they are presented some of the optical and thermal sensors that are used for the identification of water bodies (Shang 2017).

Table 3. Optical and thermal sensors used for water bodies identification (Shang 2017)

Type of sensor	Instrument	Start date	Stop Date	Spatial resolution (m)	Revisiting time (days)
Optical and Thermal	Landsat	1972	Until now	15-30	16
	AVHRR	1978	Until now	1090	1
	SPOT	1986	Until now	105-20	4
	MODIS	2000	Until now	250-1000	≤ 1
	Sentinel 2	2015	Until now	≤ 20	5

However, those sensors are not able to penetrate dense vegetation and clouds in order to reach the water bodies underneath it, making their identification really difficult (Shang 2017). For

this reason, the use of microwave systems appears to be a better solution, because of their big wavelength (1cm to 1m) which gives them the ability to penetrate the beforementioned and, they are not so influenced by atmospheric scattering and absorption. This asset is extremely helpful because microwave energy can be detected under almost any environmental and weather conditions at any time (Microwave remote sensing | Natural Resources Canada, n.d.).

1.2 Satellite microwave sensing

The microwave systems fall under two categories. The active and the passive sensors. The active sensors emit energy to receive the backscattered radiation of an object. One of the advantages of the active sensors is that they can obtain measurements any time of the day (Passive vs. Active Sensing | Natural Resources Canada, n.d.).

On the other hand, the passive sensors receive radiation that is emitted from the surface itself, so the radiation that they receive is the reflected sunlight and the radiation that is emitted by the object itself. Passive remote sensors receive energy that is associated with the temperature and the moisture properties of the black body (Passive vs. Active Sensing | Natural Resources Canada, n.d.).

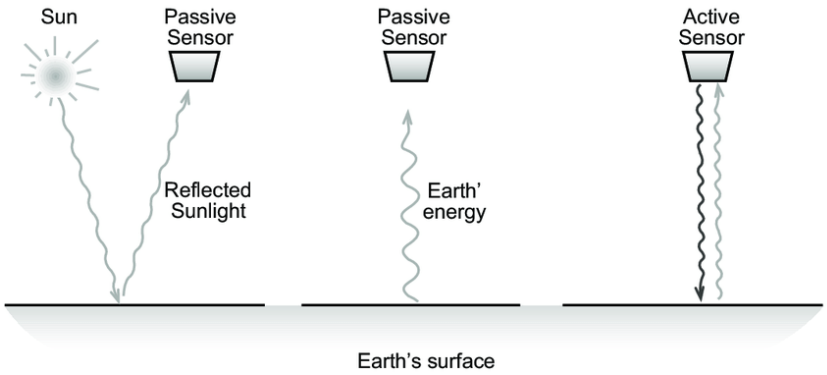

Figure 1. Passive and Active remote sensors(Bakker et al. 2004)

Active remote sensors can obtain data in any kind of weather conditions, however disturbances such as winds, turbulence, vegetation etc. could really affect the backscattering radiation that is received from the sensor, resulting in the identification of water bodies or surface wetness extremely difficult (Shang 2017).

On the other hand, the data obtained from passive sensors appear to be used for long term observations regardless the fact that the area might be covered with dense vegetation or even if there is a big variety of atmospheric conditions such as the presence of clouds (Fily et al. 2003, Shang 2017). Also, their revisiting time is fast and their spatial coverage is large enough for covering big areas, whereas their spatial resolution is low (Shang 2017). The main reason that the spatial resolution is low is because the energy of the passive microwave radiation is very low, leading to measuring larger areas to collect the radiation (Remote Sensing: Passive Microwave | National Snow and Ice Data Center n.d.).

The term revisiting time refers to the minimum amount of time that is needed for the same area to be sensed in two different images. Time is a vital factor in space-borne data because in one of the passes a phenomenon such as strong cloud absorption and scattering might appear whereas in the second pass not. (Kaya 2014).

The term spatial coverage corresponds to the area or a location were the data are collected and

could be described with latitude and longitude values (Spatial coverage, n.d.). On the other hand, the term spatial resolution refers to the ability of a sensor to provide a detailed image. Spatial resolution could be characterized as either high or low. When more pixels are included in the representation of one area, providing more details, then the spatial resolution is high, whereas when the number of pixels is limited, the spatial resolution is low (Spatial Resolution | fis.uni-bonn.de, n.d.).

Passive remote sensing is mostly used in meteorology, hydrology and oceanology. More specific, in meteorology the passive microwave data are used for the identification of water content in the atmosphere and for measuring atmospheric profiles. Hydrologists on the other hand use those data to detect soil moisture, because soil moisture considerably affects microwave emissivities. Also, oceanographers use passive remote sensing for mapping sea ice, surface winds and currents. Lastly, it is used it for detecting pollutants in the oceans (Passive vs. Active Sensing | Natural Resources Canada, n.d.).

The identification of the extremes could be achieved with the use of microwave emissivities. There are several sensors measuring surface's emissivity which is used for deriving surface moisture and surface wetness and are presented in Table 4.

Table 4. Microwave sensors used for deriving soil moisture (Owe et al. 2008)

Type of Sensor	Start date	Stop date	Frequency (GHz)
SSMR	Nov 1978	Aug 1987	6.6, 10.7, 18.3
SSM/I	Jul 1987	Until now	19.35, 37, 22.2, 85.5
TMI	Dev 1997	Until now	10.7, 19.4, 37
AMSR-E	May 2002	Until now	6.9, 10.7, 18.7, 36.5
SMAP	Jan 2015	Until now	1.26, 1.29
SMOS	Nov 2009	2017	1.4

The Soil Moisture Active Passive sensor (SMAP) is another sensor that directly measures the moisture in the top 5cm of the soil's surface. It operates in two different frequencies; 1.26GHz and 1.29GHz. It launched on January 31, 2015 and measures soil moisture every 2-3 days. It provides information about the water content of every surface that is not frozen or covered with water (Brown et al. 2013; Fournier et al. 2016; McColl et al. 2017).

Also, the Soil Moisture and Ocean Salinity (SMOS) is another satellite that measures directly soil moisture over land and salinity over oceans. The frequency that is operates is 1.4GHz. It launched on November 2, 2009 and operated until at least 2017, even though it was designed for only a five year mission (Baghdadi and Zribi 2016; Introducing SMOS / SMOS / Observing the Earth / Our Activities / ESA n.d.).

Both SMAP and SMOS operate in L-band which is very sensitive to soil moisture. However, these kinds of data are very sensitive to radio-frequency interference (RFI), which is the disturbance that is generated to the signal by an external source. This might cause to many errors in the data or even missing a lot of data (Baghdadi and Zribi 2016; What is RFI (EMI) / EMC? - FuseCo n.d.).

The Special Sensor Microwave Imager (SSM/I) appears to be a convenient choice because it is a sensitive and stable sensor whose measurements are continuous for the last three decades (Lakshmi et al. 1997). Even though it was not designed for directly detecting soil moisture and surface wetness, it could be used for this reason under some conditions (Jackson 1997). One of

the disadvantages of the SSM/I on land is that its high frequencies are significantly affected by the presence of vegetation. Also, the presence of clouds and rain could affect the quality of the data and some of the measurements might not be valid. This is addressed as noise most of the times and usually before using the data, a filtering process takes place (Prigent et al. 1997; Shang 2017). However, passive microwave data are capable of providing a lot of information related to inundated areas regardless of the presence of clouds (Sippel et al. 1994, Shang 2017).

1.3 SSM/I sensor

The Special Sensor Microwave Imager (SSM/I) started operating in July 1987 and continues operating until today, providing us with 31 years of data (Ferraro et al. 1996). The SSM/I is a passive remote sensing imager that retrieves numerous important hydrological and climate parameters such as the winds over oceans, precipitation, snow cover, atmospheric water vapor and cloud water (SSM/I | PO.DAAC, n.d.). The SSM/I is part of the Defense Meteorological Satellite Program (DMSP). It operates a conical scanning with an incidence angle of 53° (Jackson 1997). The SSM/I measures two polarizations, the horizontal and the vertical. The difference between those two is the direction of the electric field vector of the electro-magnetic (EM) wave to the Earth. In the case of the horizontal polarization the electro-magnetic wave is parallel to the Earth whereas in vertical polarization is perpendicular (Horizontal polarization vs Vertical polarization- Difference between Horizontal polarization and Vertical polarization n.d.). There are also two different passes of the SSM/I, the ascending and the descending. When the satellite travels towards the north side of the Earth the pass is called ascending, whereas when it travels towards the south side on the second half of its orbit, the pass is called descending (Horizontal polarization vs Vertical polarization- Difference between Horizontal polarization and Vertical polarization, n.d.).

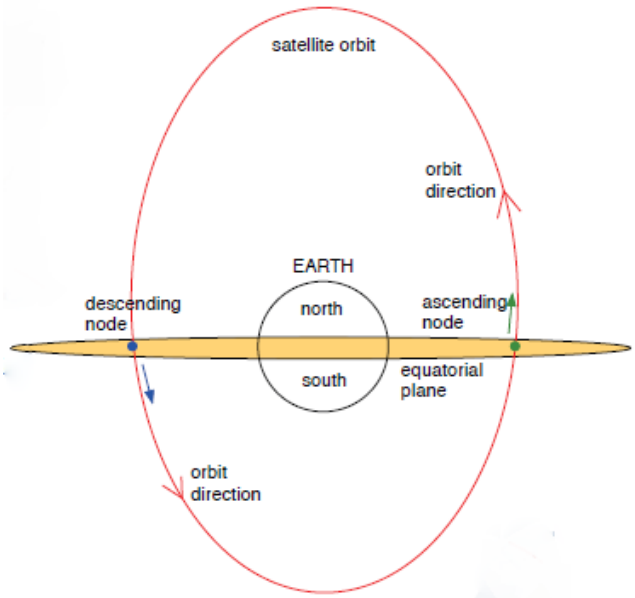

Figure 2. Representation of the passes of the satellite (Kaya 2014)

Both passes can happen in one day, depending on the geographic position of the under-investigation location. The elapsed time between the passes is approximately 12 hours (Jackson 1997). In the table below are presented the equatorial passing times according to the operating instruments that are used currently (Remote Sensing Systems n.d.).

Table 5. Crossing Times as of 05-December-2018

Platform	Instrument	Ascending pass	Descending pass
F15	SSM/I	14:59	02:59
F16	SSM/I	15:53	03:53
F17	SSM/I	18:36	06:36
F18	SSM/I	18:03	06:03

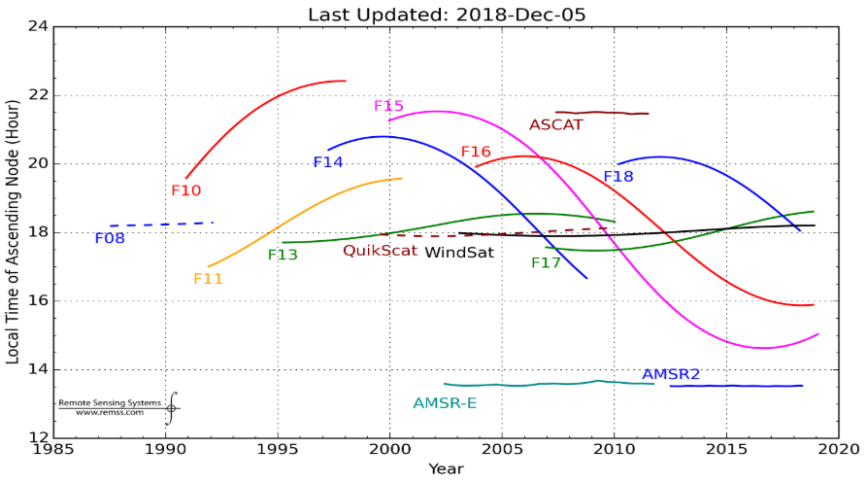

Figure 3. Passing time of all the SSM/I instruments

The SSM/I operates in four different frequency bands: 19.35GHz, 22.2GHz, 37GHz and 85.5GHz. In all of them, except for the 22.2 GHz, both polarizations are measured (Remote Sensing Systems, n.d.). According to the aim of each research, different frequencies are being used. For example, the measurements at the frequencies of 19.35 and 22.2 GHz provide more information regarding the variations in temperature and water vapor that usually happen at large scales. The 37 and 85.5 GHz frequencies respond to the previous mentioned variations, but they also respond to smaller-scale precipitation variations (because the scattering effects are more intense at high frequencies) (Grody 1991). The spatial resolution of SSM/I is 12.5 and 25km and its revisiting time is one day. However, between the orbits there are some missing data, just because the whole Earth cannot be covered in one day (Shang 2017).

The SSM/I measures radiation that is emitted from the Earth's surface called brightness temperature (Ferraro et al. 1996). The measurements are expressed in tenths of kelvins (Remote Sensing Systems, n.d.). The Brightness Temperature that is measured is affected by the air temperature and the atmospheric water vapor. Therefore, to minimize these effects and the variations that might result from them, the difference between the vertical and the horizontal polarization (Polarization Difference Brightness Temperature (PDBT)) is used (Sippel et al. 1994). It is known that the brightness temperature is sensitive to soil moisture, flooding and snow events when measured in relatively low frequencies (Paloscia et al. 2001; Prigent et al. 1997). However these events are usually associated with intense cloudiness that might affect the quality of the data (Prigent et al. 1997).

According to research that was done in the past, researches claimed that measurements at low frequencies, at 1.4 GHz (L-band) can provide vital information about soil moisture and moreover without any influence by the variation of vegetation (Paloscia et al. 2001; Velde et al. 2014). However, microwave sensors that operate at L-band and measuring soil moisture started operating relatively recently and as mentioned earlier they are very sensitive to RFI. The

instruments that are used for the measurements are presented in Table 6.

Table 6. SSM/I instruments and their operating dates(Remote Sensing Systems n.d.)

Instrument	Start Date	Stop Date
F08	July 1897	December 1991
F10	December 1990	November 1997
F11	December 1991	May 2000
F13	May 1995	May 2009
F14	May 1997	November 2009
F15	December 1999	August 2008
F16	October 2003	Until now
F17	December 2006	Until now
F18	October 2009	Until now
F19	April 2014	February 2016

The surface wetness can be estimated by the Polarization Difference Brightness Temperature (PDBT) at the frequency of 37GHz (Shang 2017; Sippel et al. 1994). The low values of PDBT indicate that the area is not flooded and that it is densely vegetated. In the current research the assumption that the low values of PDBT indicate that the area is dry is being made. On the other hand, the sparsely vegetated areas have high PDBT values. Variations in the PDBT throughout a year mirror the variation of seasons in areas that have high surface wetness rather than the water content of the canopy (Sippel et al. 1994).

In case of snow coverage there is a decline in polarization differences. This effect is more obvious in lower frequencies. However, there is a very important factor for this behavior, and it depends on the physical properties of the snow. For instance, if the snow is wet, the polarization differences become higher. The reason for that is because the scattering is becoming insignificant due to the big dielectric losses and the wet snow behaves and radiates like a black body. On the other hand, dry snow behaves in a completely different way. The scattering effect is much more obvious leading to lower emissivities (Prigent et al. 1997).

Chapter 2. Modelling approach

2.1 Study area and data

In this study, the SSM/I observations are examined for the area of Europe, for the years 1987-2017. However, Europe is a continent and an in-depth analysis would be too demanding in terms of time. For this reason, small- scale events analysis appears more efficient. Specific areas that belong in the continent and suffered extreme events in the last decade are being investigated. More specific, for the examination of the dry events, a selected location was close to Toledo, Spain. Another one was close to Toulouse, France. For the wet events, an area close to Kresevo, Bosnia and Herzegovina was selected as well as an area close to Prague, Czech Republic. Last, for the heavy snowfall events a location in the district of Lviv, Ukraine was selected and in Wroclaw, Poland. Those locations were not selected randomly, but they were selected according to recorded extreme events that occurred in specific date. For example, in Spain and South France there was a big drought event in late July and early August respectively in 2014. In Bosnia and Herzegovina there was a big flood in mid-May in 2014 and in Prague in mid-August of 2002. Last, there was a heavy snowfall in Ukraine in March of 2013 and in Poland in December of 2009. In the last event 62 people died due to extreme snowfall. In Table 7 are summarized the investigated area and their exact location is being presented.

Table 7.Type of event of the selected areas and their location

Country	Type of event	Latitude (degrees)	Longitude (degrees)
Spain	Drought	39.829139	-3.615099
South France	Drought	43.310225	1.486422
Bosnia and Herzegovina	Flood	43.872802	18.071143
Czech Republic	Flood	50.154559	14.456838
Ukraine	Heavy Snowfall	49.825940	23.478694
Poland	Heavy Snowfall	51.161902	16.975452

The SSM/I-SSMIS Pathfinder Daily EASE-Grid Brightness Temperatures were used at 37GHz frequency. Brightness Temperature (T_B) measures the upwelling microwave radiation from the surface of the Earth. The temporal coverage of the data is from the 9th July 1987 to the 5th July 2018 and are daily available since the revisiting time of the sensor is every day. The data have a binary format, meaning that the information is stored in the form of ones and zeros. The spatial resolution is 25×25km. The data of Brightness Temperature are provided in tenths of Kelvin. They have a global coverage based on Cylindrical, Equal area projection. (Armstrong Richard, Knowles Kenneth, Brodzik Mary, & Hardman Molly, 1994). The most common grid system that is used for this passive microwave data is the EASE-Grid (Shang 2017).

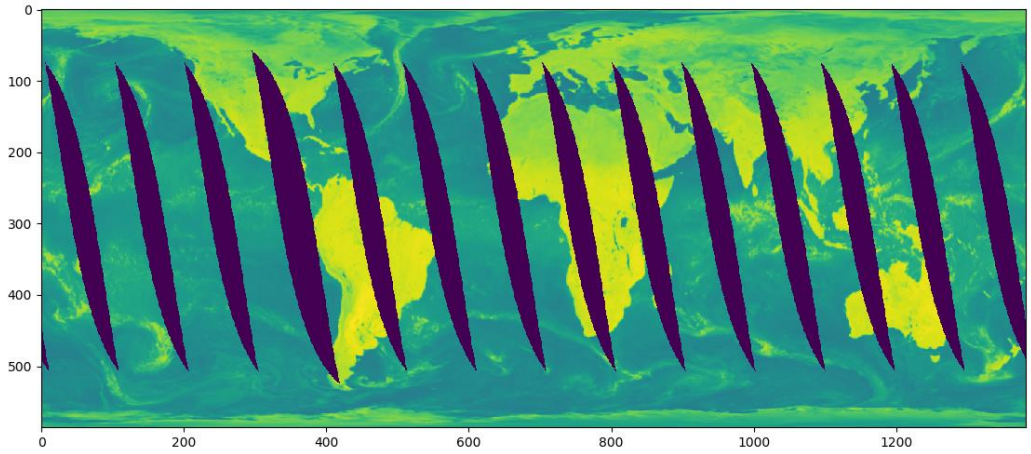

Figure 4. Global image of Brightness Temperature

The dark stripes that appear in Figure 4 are measurement gaps, meaning that there is no information on these areas.

In Figure 5 the under-investigation areas are presented, as described earlier and are depicted as black dots.

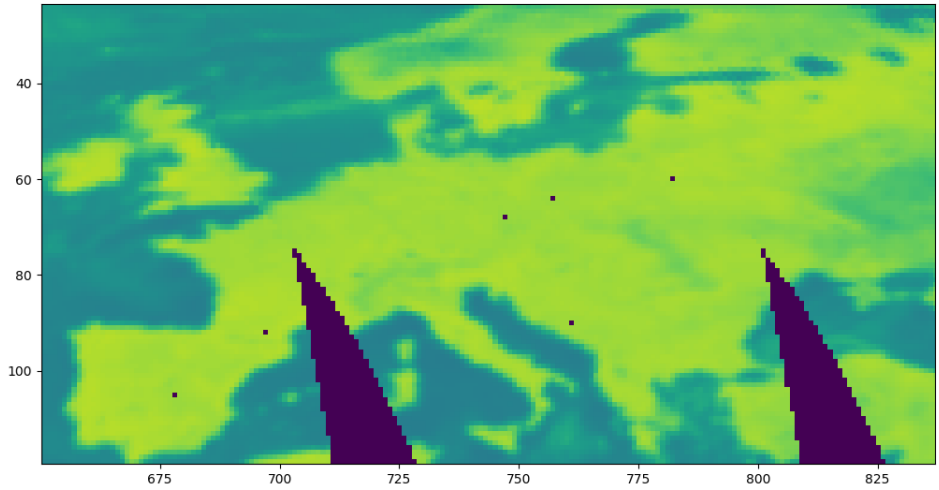

Figure 5. Investigated areas

The NASA-USDA Global soil moisture and the NASA-USDA SMAP Global moisture data were used and were obtained from Earth Engine Data Catalog. Their temporal coverage is from the 1st January of 2010 and they continue until now. Their spatial resolution is at 0.25°×0.25° and they are available every month. Those data could be expressed either in mm as soil moisture or in % as soil moisture profile (Bolten and Crow 2012; Bolten et al. 2010; Mladenova et al. 2017). The surface soil moisture can hold up to 25mm of water. In other words this is its full capacity (Surface Soil Moisture (WMO) n.d.). So, when we get an indication of 5mm of soil moisture, this means that is 5mm out of 25mm or $\frac{1}{5}$ which leads to 20% soil moisture profile.

The Global Satellite Mapping of Precipitation (GSMaP) data were used at a resolution of 0.1°×0.1° and were obtained from the Earth Engine Catalog. The obtained data were available at three-hour intervals and they are measured in mm. They are available since the 1st of March

of 2000 until the 12th of March of 2014 (Aonashi et al. 2009; Kubota et al. 2006; Kubota and Okamoto 2007).

2.2 Brightness Temperature

The radiative transfer equation can be expressed in terms of Brightness Temperature, neglecting the atmospheric radiation scattered by vegetation (Shang 2017, Prigent et al. 1997):

$$T_B(p,\theta) = \epsilon(p,\theta) \times t_v \times T_s + [1 + t_v \times \Gamma(p,\theta)] \times [1 - \omega_p] \times (1 - t_v) \times T_v + \Gamma(p,\theta) \times t_v^2 \times T_d \quad (2)$$

Where T_B is the satellite-measured brightness temperature at polarization p, referring to either vertical or horizontal; T_s is the soil temperature and T_v is the vegetation temperature; θ is the incidence angle; T_d is the down-welling brightness temperature of the atmosphere; $\epsilon(p,\theta)$ is the surface emissivity at polarization p and incidence angle θ; $\Gamma(p,\theta)$ is the surface reflectivity at polarization p; ω_p is the single scattering albedo at polarization p; t_v is the transmission function of the vegetation canopy.

The T_B is not the real surface temperature. In order to obtain the real surface temperature, the T_B has to be divided by the surface emissivity, which varies between 0 and 1(Rybicki and Lightman 1991).

In order to fully comprehend how the data behave, Brightness Temperature time series will be presented below. It should be mentioned that the data are averaged every 10 days. The plots that will be presented are for both polarizations and passes respectively, for a dry, a wet and a snow-covered area for the years that each event occurred, indicating a drought, a flood and a heavy snowfall event.

- *Dry event*

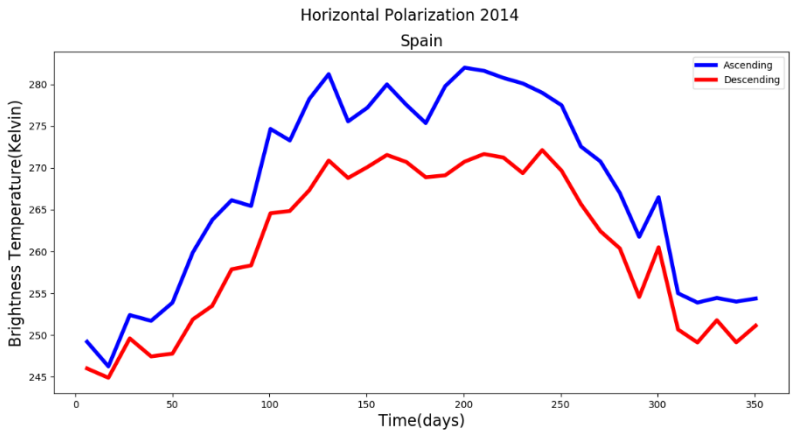

Figure 6. Brightness Temperature time series for the Horizontal Polarization for Spain, event occurring in days 200-210

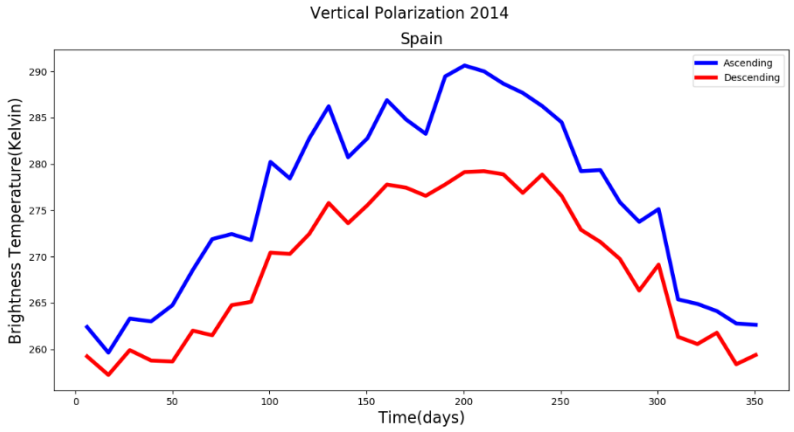

Figure 7. Brightness Temperature time series for the Vertical Polarization for Spain, event occurring in days 200-210

The drought in Spain occurred in late July of 2014. In Figure 6 and Figure 7 this period refers to days 200-210. It is obvious in both figures that for this time interval of 10 days the T_B values are very high compared to the rest of the year.

- *Wet event*

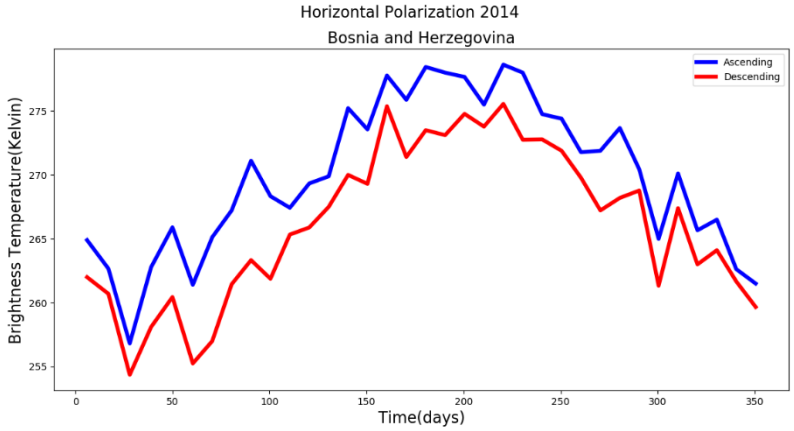

Figure 8. Brightness Temperature time series for the Horizontal Polarization for Bosnia and Herzegovina, event occurring in days 140-150

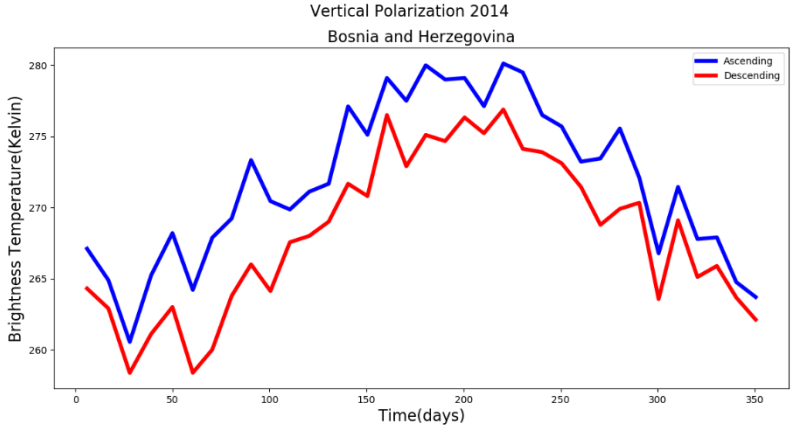

Figure 9. Brightness Temperature time series for the Vertical Polarization for Bosnia and Herzegovina, event occurring in days 140-150

The flood in Bosnia and Herzegovina happened in spring of 2014 and more specific between 14 and 19 May. This means that the days the event happened are 140-150. The values of the T_B are slowly increasing because is close to the end of spring season but compared to the previous case (drought event) the values of T_B are lower.

- *Snow event*

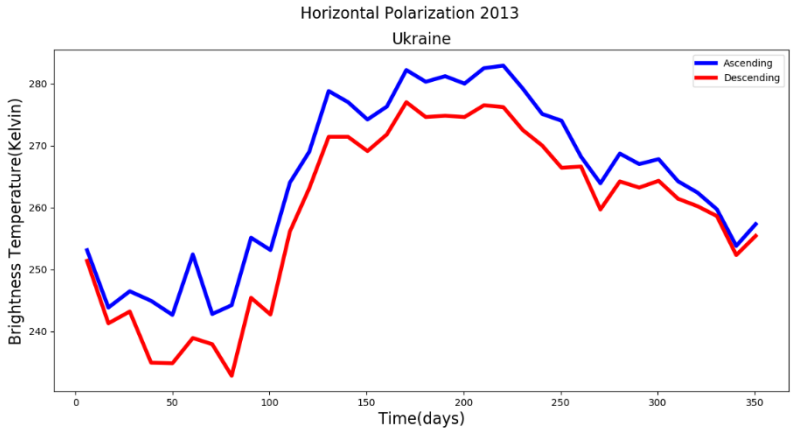

Figure 10. Brightness Temperature time series for the Horizontal Polarization for Ukraine, event occurring in days 80-90

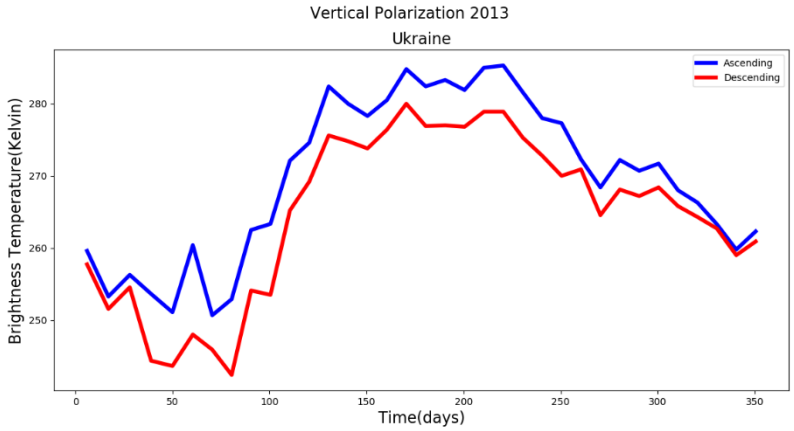

Figure 11. Brightness Temperature time series for the Vertical Polarization for Ukraine, event occurring in days 80-90

In Ukraine in 2013 a heavy snowfall occurred in March and more specific in days 80-90. This is obvious from Figure 10 and Figure 11 that the values of T_B are relatively low compared to the rest of the year, besides the beginning of the year.

From all the above figures, from all the cases, the more evident fact is that the T_B is higher during summer months and it makes sense because the real surface temperature is higher during this period. In all the cases the values are much lower in the beginning of the year and then slowly rising.

For the rest of the events, see Appendix A1.

2.3 Polarization Difference

For bare soil, as the incidence angle increases the values of brightness temperature at vertical polarization are higher than the ones at horizontal polarization. The polarization difference (PD) is a good indicator of soil moisture and more specifically it is supposed to increase for higher

values soil moisture, because of the differences in the dielectric properties of water and soil or vegetation. One of the benefits of using the PD values instead of the T_B is that the sensitivity due to temperature effects is significantly reduced. On the other hand, a disadvantage of using the PD is that a lot of atmospheric assumptions and assumptions about the vegetation have to be made, otherwise more complex modelling should take place removing the contributions of atmosphere, clouds and rain (Jackson 1997).

One assumption that is made is that in densely vegetated areas the estimation of inundated areas could be achieved with the calculation of PDBT at 37 GHz, because it could be assumed that the influence that the vegetation has on PDBT at 37 GHz is uniform (Shang 2017). Another assumption that is being made in this research is that the PDBT could also be used as an indicator for surface dryness. More specific, it is assumed that when the values of PDBT are low, then the area is characterized as dry.

The presence of vegetation can cause many problems in the prediction of extremes and the identification of flooded areas in many remote sensing techniques; however this is not the case in the passive microwave sensors with the use of Brightness Temperature Difference. Also, the effect that is caused by the atmospheric conditions could be mitigated by the calculation of the Brightness Temperature Difference (Shang 2017).

The up-welling atmospheric brightness temperature is filtered out by using the difference between the vertical and horizontal brightness temperature. The Polarization Difference Brightness Temperature (PDBT) for the case that the area is fully vegetated is presented below (Shang 2017):

$$\Delta T = T_B(V,\theta) - T_B(H,\theta) \tag{3}$$

The PDBT is an indicator of surface wetness. More specific, the brightness temperature difference increases with surface wetness and the moisture content of the soil (Shang 2017, Jackson 1997). Usually the PDBT has a positive value, meaning that the vertical polarization is higher than the horizontal one (Li et al. 2013).

In the figures below the Polarization Difference Brightness Temperature plots are presented. Once again, the data are averaged every 10 days. The figures refer to the three events that are being investigated; the dry, wet and snow ones.

- *Dry event*

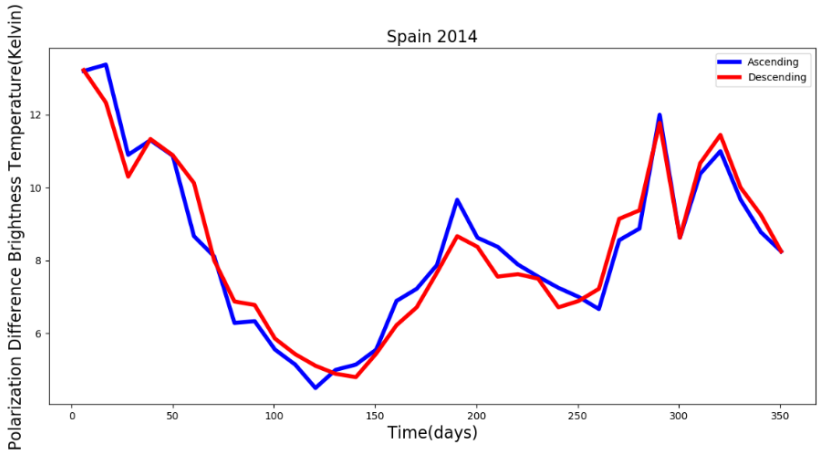

Figure 12. Polarization Difference Brightness Temperature time series for Spain, event occurring in days 200-210

As mentioned earlier the most critical period of the drought event that occurred in Spain was between days 200 and 210. With the assumption that was made earlier, that in case of a dry event the PDBT values would be low the results seem to agree.

- *Wet event*

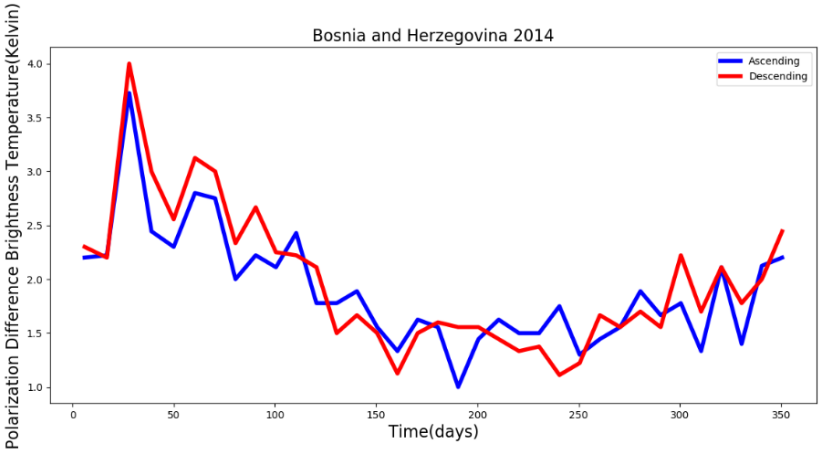

Figure 13. Polarization Difference Brightness Temperature time series for Bosnia and Herzegovina, event occurring in days 140-150

In case of Bosnia and Herzegovina, it was expected that the higher values would appear in days 140-150 because that was when the event happened, however the higher values appeared during January. Though, as it was mentioned earlier in the description of the study area, specific pixels were selected and not the whole area of Bosnia, meaning that it would be possible the pixel that was selected not to be so representative of the flood event.

- *Snow event*

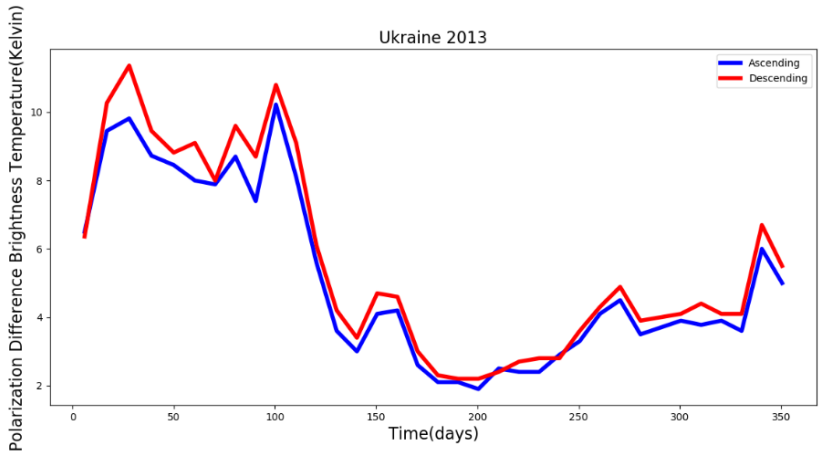

Figure 14. Polarization Difference Brightness Temperature time series for Ukraine, event occurring in days 80-90

The heavy snowfall event that Ukraine suffered from on March of 2013 is quite evident from Figure 14. The values of PDBT are relatively high compared to the ones after the event and until the end of the year. It is obvious that there was still wet snow, that is why the values of PDBT are high. If the snow was dry, then those values would be expected to be much lower.

The figures above give a better insight of how the PDBT data behave in each case. In general, at this stage it could be concluded that they can provide a handful amount of information and validation that the PDBT values are high when there is high soil moisture and high surface

wetness and low when there is not.

For the rest of the events, see Appendix A2.

2.4 Microwave Polarization Difference Index (MPDI)

Since brightness temperature contains information about the canopy and the soil surface an indicator that is sensitive to water content of plants is introduced and it is called Microwave Polarization Difference Index (MPDI) (Owe et al. 2011, Wen et al., 2005, Li et al. 2013, Becker and Choudhury 1988). The MPDI equation is based on the radiative transfer equation (Li et al. 2013):

$$MPDI = \frac{T_{BV} - T_{BH}}{T_{BV} + T_{BH}} \quad (4)$$

Where T_{BV} and T_{BH} are the brightness temperature in vertical and horizontal polarization respectively. MPDI is inversely proportional to frequency. More specific, the value of MPDI decreases as the frequency increases. The reasoning behind this statement is that as the frequency increases, the scattering increases as well, especially when there is dense vegetation. Also, MPDI values differ according to different vegetation types because they are related to vegetation density and the characteristics of the canopy (Li et al. 2013).

In areas and time periods that are covered by snow, the MPDI values are lower compared to the rest of year. This occurs, because the scattering increases and the contribution of the horizontal polarization is getting higher leading to the reduction of the MPDI. As the snow melts the MPDI values are getting higher (Li et al. 2013).

The differences in MPDI values are small during the summer and autumn, because that is the period when the vegetation starts to grow, and the depolarization effect takes place. The MPDI is closely related to soil moisture but also to the vegetation type that covers the investigated areas. It can be used for the description of parameters linked to vegetation, especially vegetation thickness (Li et al. 2013).

- *Dry event*

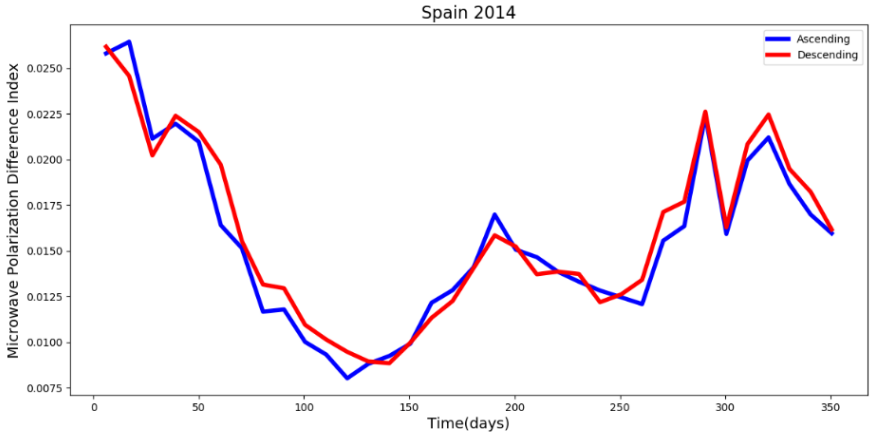

Figure 15. Microwave Polarization Difference Index time series for Spain, event occurring in days 200-210

- *Wet event*

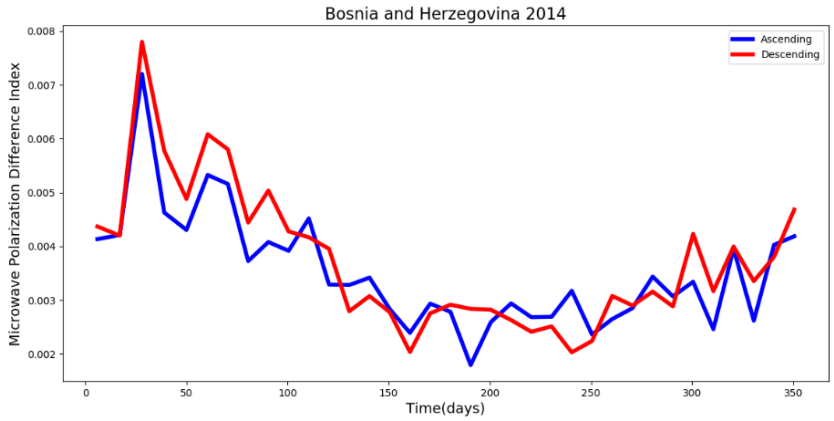

Figure 16. Microwave Polarization Difference Index time series for Bosnia and Herzegovina, event occurring in days 140-150

- *Snow event*

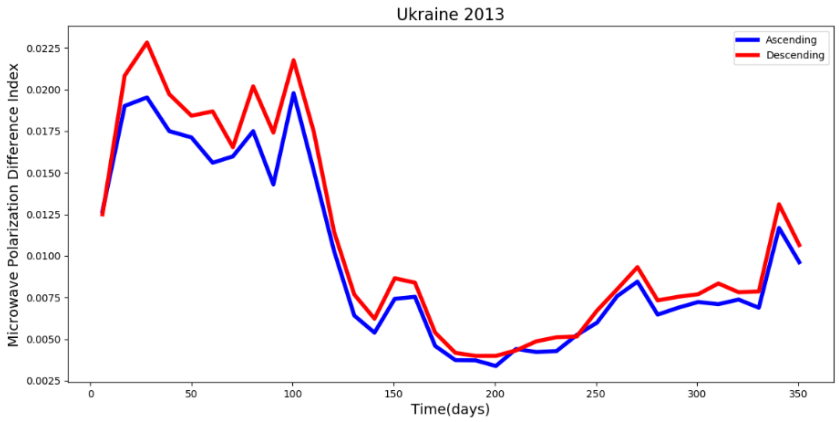

Figure 17. Microwave Polarization Difference Index time series for Ukraine, event occurring in days 80-90

As it can be seen in the above figures the calculation of the Microwave Polarization Difference Index (MPDI) time series did not provide us with significant information. It just provides the same information as the Polarization Difference Brightness Temperature (PDBT) but the values are significantly scaled down.

For the rest of the events, see Appendix A3.

Chapter 3. Methodology approach

3.1 Data Pre-Processing

In order to perform a statistical analysis on the SSM/I feature behavior the data were binned in groups of 10 days according to a fixed DoY index, and the cases of leap years they were binned in groups of 11 days, generating hence 36 groups for every year. The first bin collects for instance the acquisitions with $0 < DoY < 11$, the second $11 < DoY < 22$ and so on. This was done in order to perform averages that would allow to handle the issue gaps in swath coverage and to mitigate the effect of atmospheric perturbations. In practical terms, after averaging in each bin by the number of valid acquisitions, we hence attained a 2D array with shape (36,31) where 36 is the number of DoY bins and 31 is the number of years. This array contains the absolute values of Brightness Temperature for each selected location and it is created for both polarizations (vertical and horizontal) and for both passes (ascending and descending).

3.2 Temporal Analysis

3.2.1 Histograms

First the creation of histogram plots was conducted in order to provide us with a better insight of the distribution of the data and get a visual understanding on the sensitivity of the SSM/I to the extreme events under investigation. In those plots the best fitting gaussian distribution was plotted as well, in order to get a better estimation of how the data are distributed throughout the period that the extreme occurred.

A new 2D array was created obtaining the PDBT. This 2D array was averaged according to the month of interest (specified days), resulting in a 1D array containing the PDBT values of the selected period for the examined years.

The histograms were created for the PDBT for the selected pixel, for a specific month but only for 30 years and not 31, because the first year of the measurement that was 1987 had missing data since the SSM/I started operating on July of this year. Once again, the histograms that are presented in the next figures refer to the three different scenarios of events.

- *Dry event*

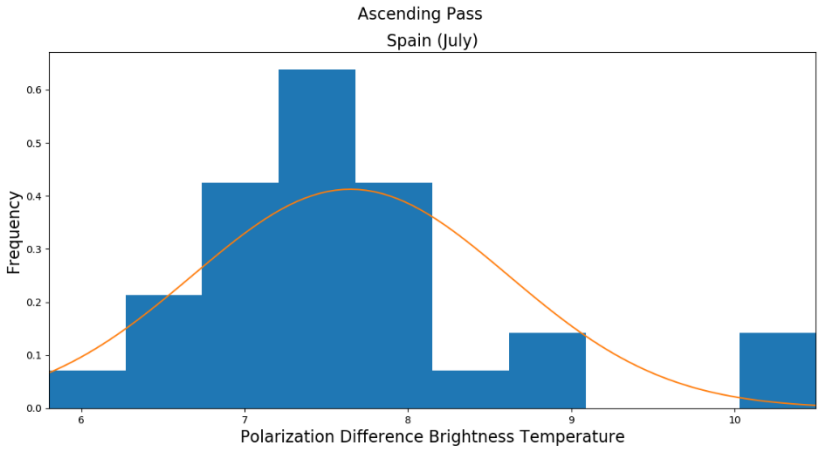

Figure 18. Histogram of the Polarization Difference Brightness Temperature for the ascending pass for days 200-210 for Spain

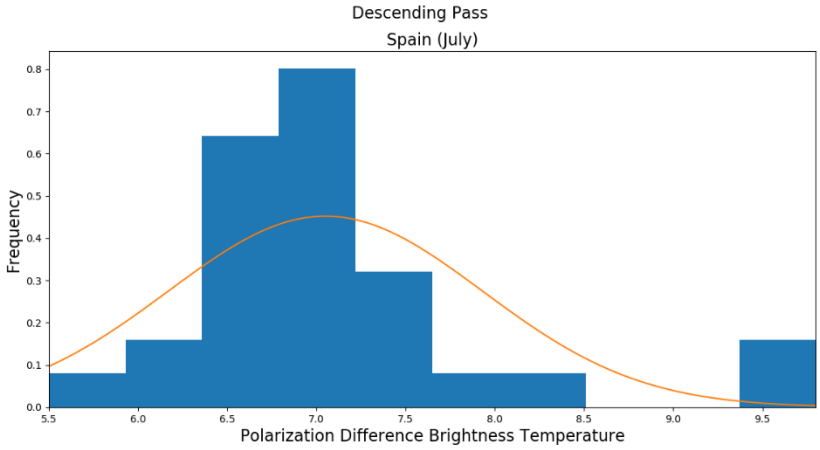

Figure 19. Histogram of the Polarization Difference Brightness Temperature for the descending pass for days 200-210 for Spain

For the dry event it is evident from Figure 18 and Figure 19 that mostly the values of PDBT vary between 6K and 9K. This is a variation of 3 units, showing a consistency in the behavior of the data for these kinds of events.

- *Wet event*

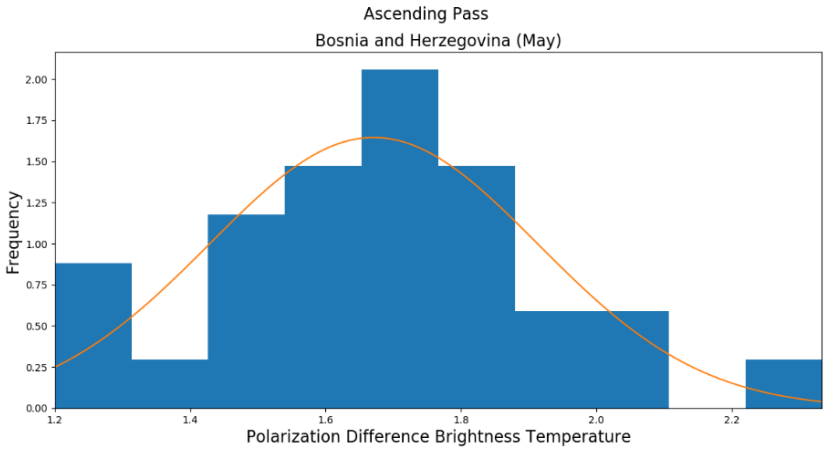

Figure 20. Histogram of the Polarization Difference Brightness Temperature for the ascending pass for days 140-150 for Bosnia and Herzegovina

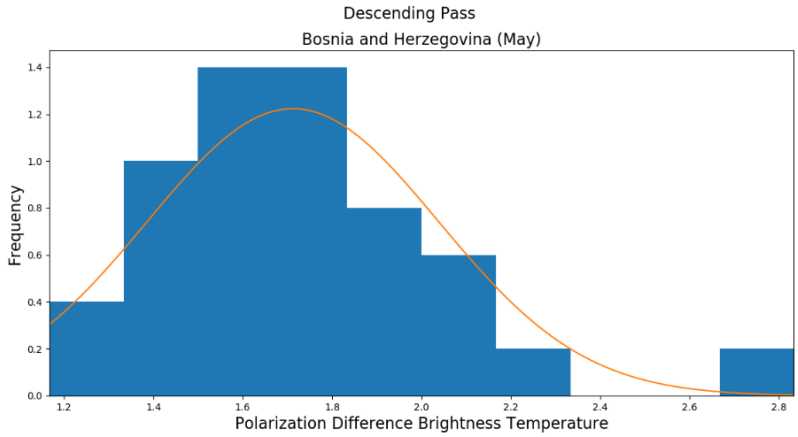

Figure 21. Histogram of the Polarization Difference Brightness Temperature for the descending pass for days 140-150 for Bosnia and Herzegovina

In the case of the wet events in Figure 20 which refers to the ascending pass most of the values are at around 15K, whereas in the descending pass they vary between 15 and 18K. It is evident that the PDBT values are higher in case of the wet event than the ones in the dry one. In the ascending pass the variance of the values is bigger than the one in the descending pass, meaning that they are more spread out than their average value.

- *Snow event*

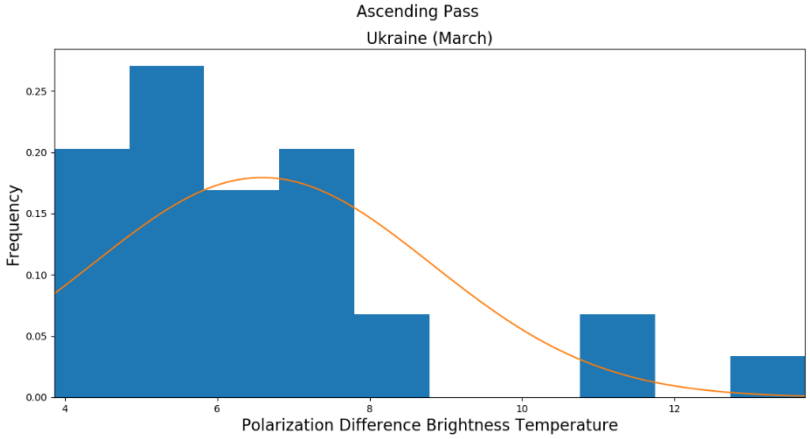

Figure 22. Histograms of the Polarization Difference Brightness Temperature for the ascending pass for days 80-90 for Ukraine

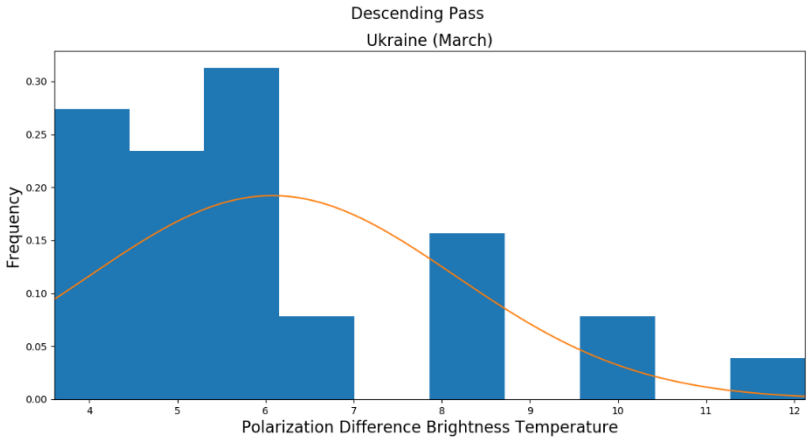

Figure 23. Histograms of the Polarization Difference Brightness Temperature for the descending pass for days 80-90 for Ukraine

In the last case which is the snow event, the PDBT values follow a very different pattern that the previous two cases. It is rather noticeable that some years are standing out than the rest, which might mean that those years the amount of snowfall was either very heavy or very wet. Most of the values are grouped together at the very left side of the plots, indicating very low values of PDBT. However, a few extreme behaviors can be seen from Figure 22 and Figure 23.

For the rest of the cases, see Appendix B1.

3.2.2 Standard deviation and mean plots

For the calculation and creation of the standard deviation and the mean plots the previous created 2D array, with the values of Polarization Difference Brightness Temperature, was used. More specific, the standard deviation and the mean value over the number of years was calculated, resulting in a vector with 36 elements. The values of this array were plotted against time and the time interval was chosen to be 10 days. A graphic representation of the beforementioned is displayed in the following figures.

- *Spain*

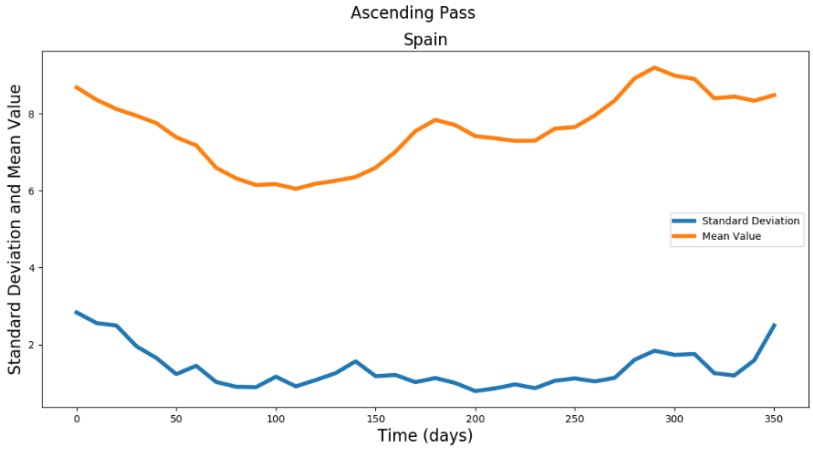

Figure 24. Standard deviation and mean plots for the ascending pass for Spain

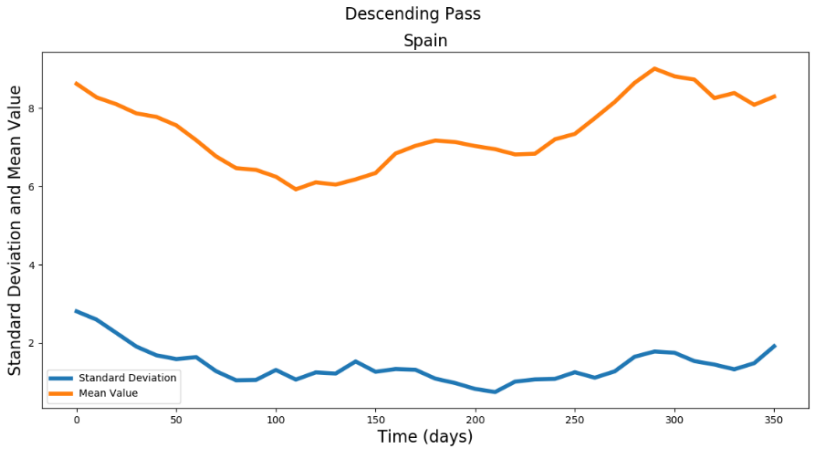

Figure 25.Standard deviation and mean plots for the descending pass for Spain

- *Bosnia and Herzegovina*

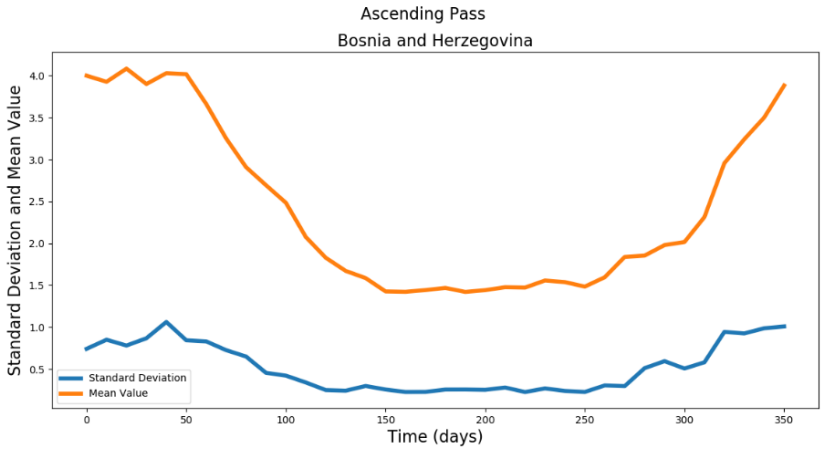

Figure 26. Standard deviation and mean plots for the ascending pass for Bosnia and Herzegovina

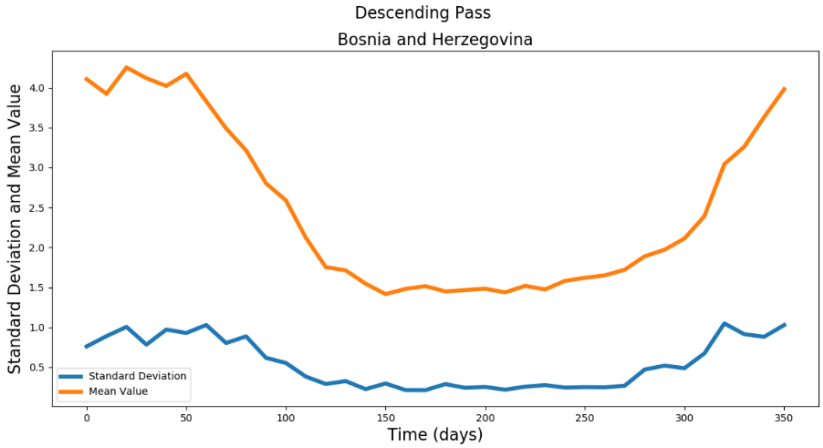

Figure 27. Standard deviation and mean plots for the descending pass for Bosnia and Herzegovina

- *Ukraine*

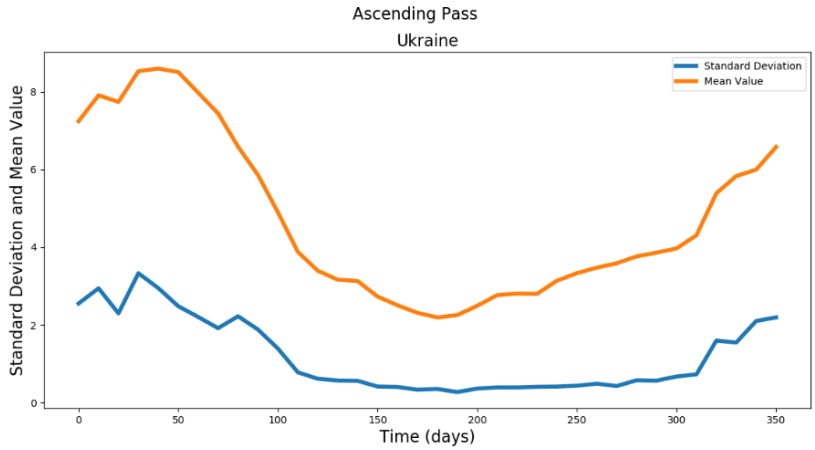

Figure 28. Standard deviation and mean plots for the ascending pass for Ukraine

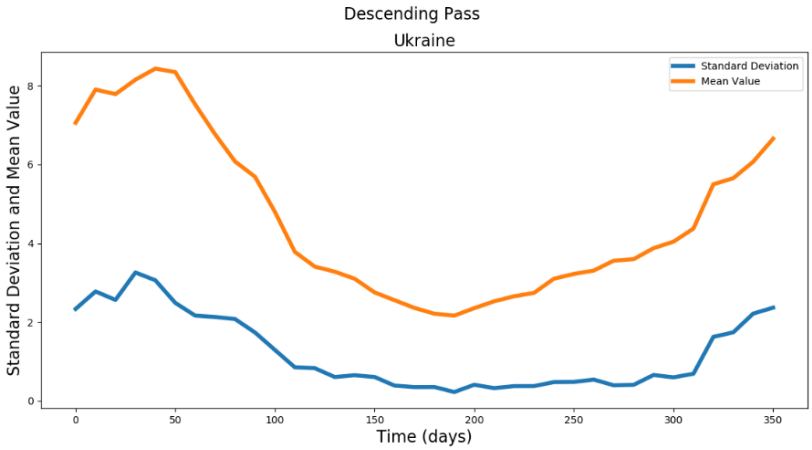

Figure 29. Standard deviation and mean plots for the descending pass for Ukraine

The information that is obtained from the above figures is that there is a difference in the emissivity according to seasonality. It is noticeable that during winter there is more diversity whereas in summer the situation is more uniform. This is quite reasonable since, especially in areas like Bosnia and Herzegovina, during wintertime there might be an alteration of the natural phenomena, meaning that in some periods it might rain, in others it might be relatively dry, whereas in other occasions it might snow as well.

The same pattern follows the area of Ukraine as well, where long-continued rainfall events occur during winter, but also heavy rainfall events occur, especially during January. The snowfall events can also occur in September and May, but they are more frequent during the winter months. During summer the temperatures are becoming higher, they reach up to 40 ^{o}C and these kinds of events are very seldom (Balabukh et al. 2018).

However, in case of Spain the situation is smoother, meaning that there is not such a big difference in the behavior of the data due to seasonality. The reason of this behavior is because of the climate of the specific location. The climate of Spain varies across the country but mainly is characterized as Mediterranean. The climatic changes in these kinds of regions are not so intense, leading to the changes of the emissivity to be less powerful.

The above mentioned could be emphasized with the curve of the mean values of the PDBT. In the winter months it appears to be more rainfall, especially in the areas in the Bosnia and Ukrainian territories, resulting in higher mean values of the PDBT, while during summer months the temperatures are high, meaning that the surface wetness is much lower and the mean values of the PDBT are much lower.

For the rest of the cases, see Appendix B2.

3.3 Spatial Analysis

For the identification of the extreme events a series of procedures had to be followed. All these procedures were achieved in Python environment were first the under-consideration years had to be defined. Also, the region of interest was delineated and more specific the latitude and the longitude limits were set. The latitude and the longitude were set from 35^{o} to 55^{o} and from -10^{o} to 28^{o} respectively. The next step was the creation of functions that return the average values of Brightness Temperature and the average values of Polarization Difference Brightness Temperature for a specific time interval that was chosen.

3.3.1 Brightness Temperature

First the average Brightness Temperature (T_B) values for a time interval of 10 days were calculated, for a specific year. Also, the average T_B values of all the years (31) for the same time interval were calculated and then subtracted from the ones calculated for only a specific year.

$$T_{B_{1year,10days}} - T_{B_{31years,10days}} \quad (5)$$

The next step was to plot these calculated values. On the x-axis is the longitude that these data were selected to be calculated and plotted and on the y-axis is the latitude. These values were calculated and plotted for both polarizations and for both passes as well. In the figures below are presented the values that result from the previous equation for the year of 2014 for the last ten days of May.

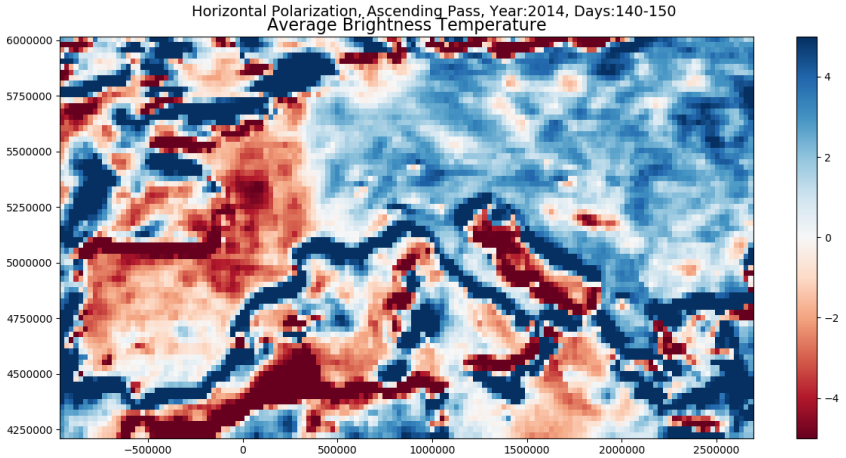

Figure 30. Average T_B for the Horizontal Polarization for the ascending pass for time interval of 10 days

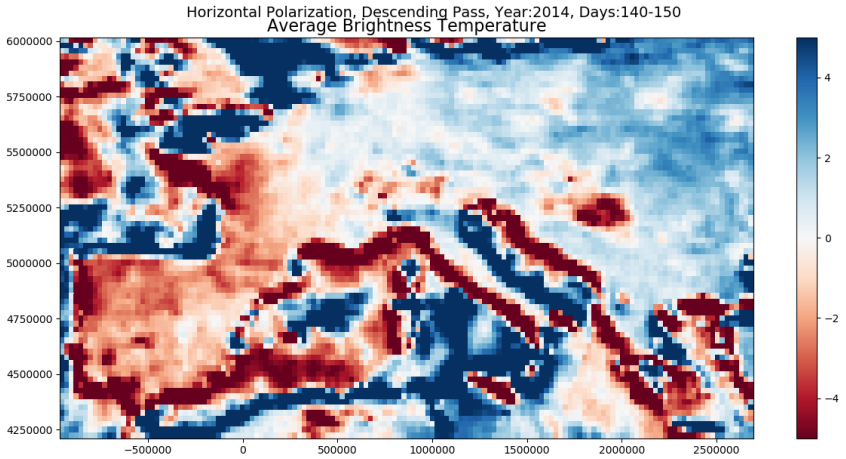

Figure 31. Average T_B for the Horizontal Polarization for the descending pass for time interval of 10 days

For the Horizontal Polarization for both passes it is evident that the T_B values are higher in the North-East and South-East side of Europe, whereas much lower in the South-West. This is a behavior that was not expected, because in South-West the real temperatures in this period are

expected to be higher than the ones North-East because they are closer to the equator. However, this is not the case for the South-East which is also close to the equator.

Another interesting observation is that in both Figure 30 and Figure 31 there are very low values in the middle of the see. The reasoning behind that could be that there might be a storm, causing disturbance in the surface of the sea, making it rough. When the surface is rough, scattering takes place and the emissivity of the horizontal polarization is becoming very high and the polarization differences very low.

Nevertheless, in this specific time interval and year an extreme flooding event occurred in Bosnia and Herzegovina and this is quite evident, especially in Figure 31, because the T_B values are very low.

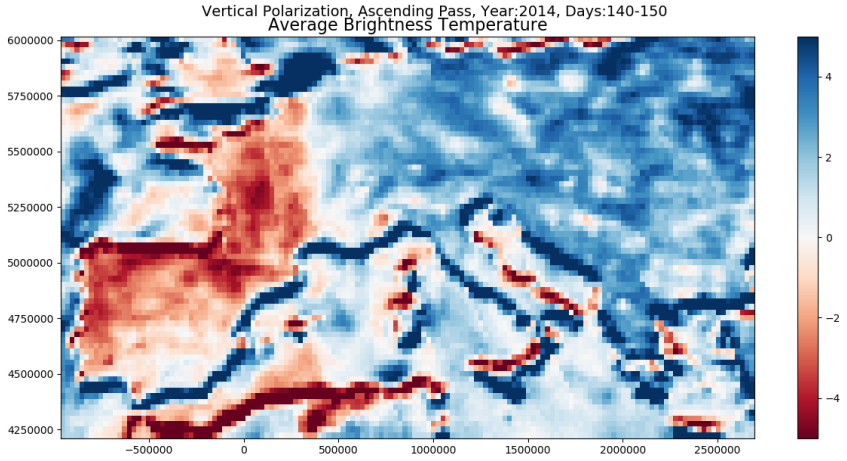

Figure 32. Average T_B for the Vertical Polarization for the ascending pass for a time interval of 10 days

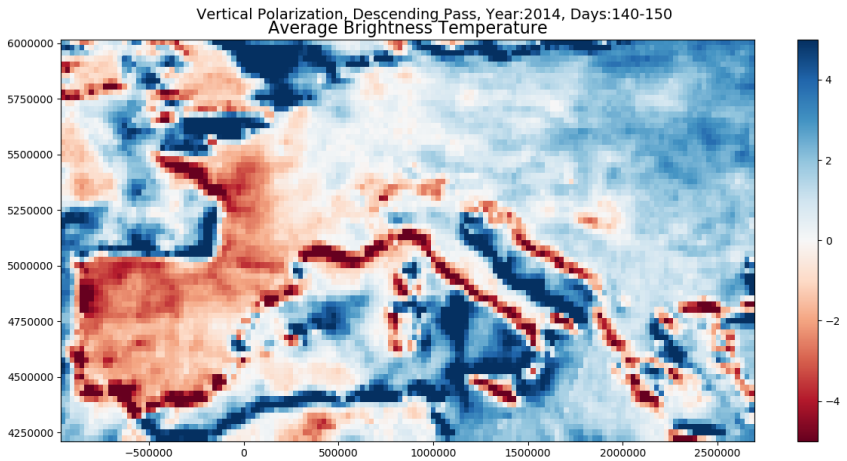

Figure 33. Average T_B for the Vertical Pass for the descending pass for a time interval of 10 days

In the Vertical Polarization the very low values of T_B in the sea are less evident. However, the data behave the same way as the ones in the Horizontal Polarization.

It is very interesting how the values appear in the coastline; they seem very extreme. An initial thought was that maybe the images were not aligned. Though, this was not the case because the

co-registration process was completed. It was not very thorough, but most a good sample of the images were aligned perfectly.

3.3.2 Polarization Difference Brightness Temperature

The same procedure as mentioned before was also followed for the calculation of the average Polarization Difference Brightness Temperature (PDBT) for a specific year and the average PDBT values of all the years (31).

$$PDBT_{1year,10days} - PDBT_{31years,10days} \quad (6)$$

The next step was the graphical representation of these calculated values. On the x-axis and the y-axis are the longitude and the latitude respectively. In the next figures are presented the PDBT values that result from the previous equation for the year of 2014 for the last ten days of May.

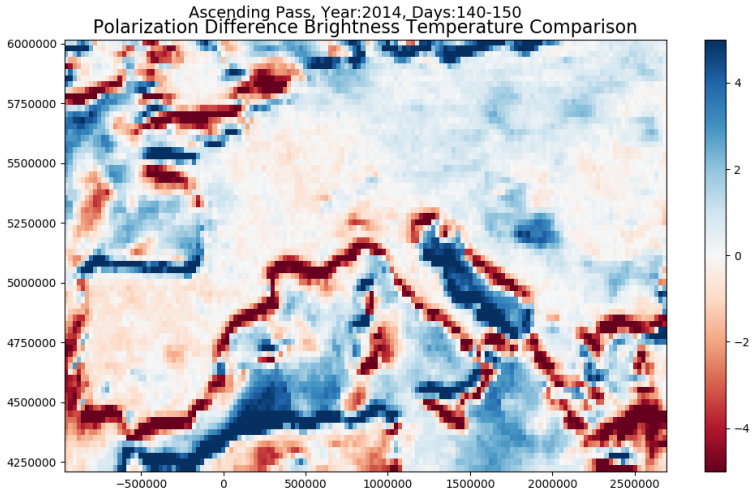

Figure 34. Polarization Difference Brightness Temperature for the ascending pass for a time interval of 10 days

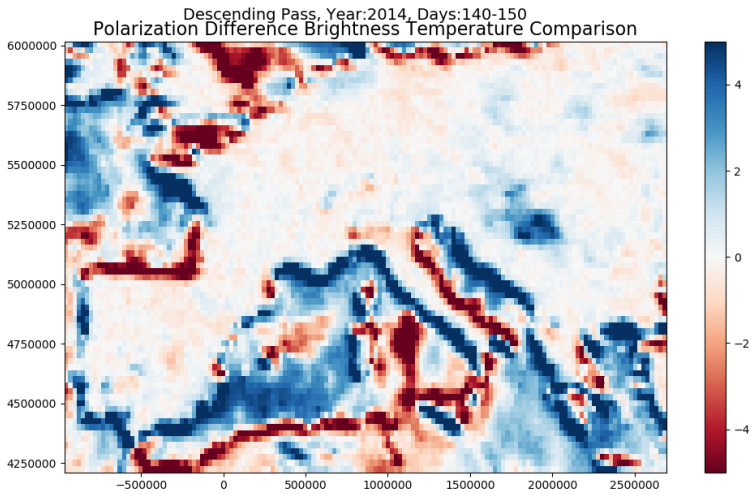

Figure 35. Polarization Difference Brightness Temperature for the descending pass for a time interval of 10 days

As it was described earlier, in Chapter 2 the PDBT is a good indicator of surface wetness. Indeed, this is the case here, that it is being validated that in Bosnia, in 2014 in the last days of May there was a flood. This is being evident by the high values of PDBT.

3.3.3 Normalized Polarization Difference Brightness Temperature

For the last step of this research, which is the identification of the extreme events, the calculation of the Normalized Polarization Difference Brightness Temperature (NPDBT) was achieved. The NPDBT is the same method as the standard score or also known as z-score. The NPDBT indicates how many values appear below or above the mean value. The values that are above the mean have a positive NPDBT, whereas the ones that are below the mean have negative NPDBT value. The NPDBT values extent from -3 standard deviations to 3 standard deviations. The ones that belong to the first category they would fall to the far-left side of the normal distribution, whereas the ones that belong to the second category they would fall to the right side of the normal distribution (Z-Score: Definition, Formula and Calculation - Statistics How To, n.d.).

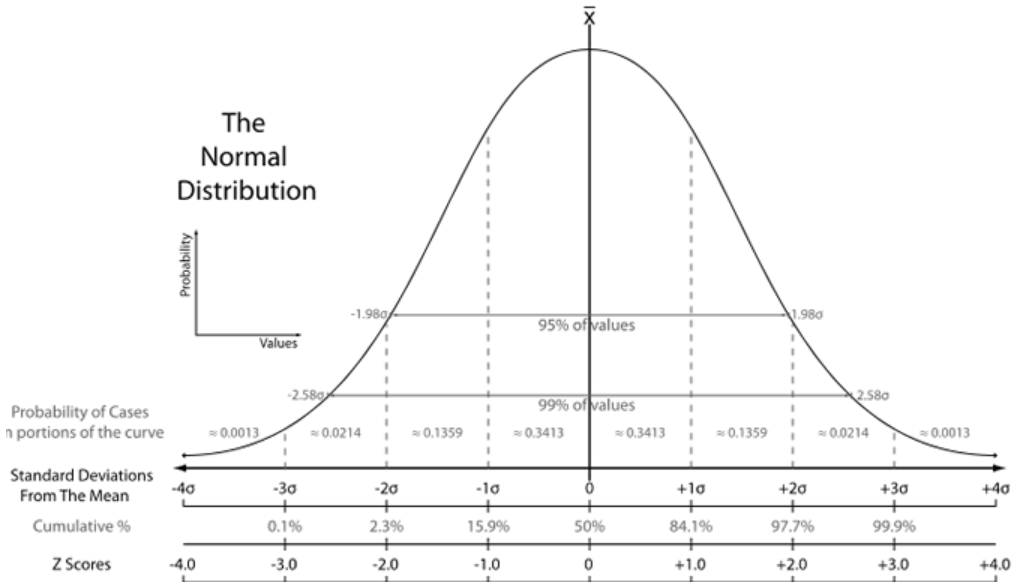

Figure 36. Normal distribution and z-score

The z-score values are calculated by subtracting the mean from an individual value and then dividing this difference with the standard deviation. The exact same procedure is followed for the calculation of the NPDBT values, there the values that were calculated on the previous section are divided by the standard deviation. Below is presented the equation that was used.

$$NPDBT = \frac{PDBT_{1year,10days} - PDBT_{31years,10days}}{\sigma} \quad (7)$$

Where,

$PDBT_{1year,10days}$	is the individual value
$PDBT_{31years,10days}$	is the mean value
σ	is the standard deviation

The values that fall on the far-left side of the normal distribution (-3σ) are assigned with -1 whereas the ones that fall at the far-right side of the normal distribution (3σ) are assigned with the value 1. The rest of the values are assigned with 0. The -1 and 1 values are characterized as the extremes. The negative values indicate that the area is dry, whereas the positive ones that it is wet. In case of snow, there could be two different cases. When the snow is wet, then the values are expected to be 1, because of the wet surface on the top of the snow. On the other hand, when the snow is dry the values are negative. In the next figures there is a representation of some extremes at specific time intervals and specific years. Once again, the year that was chosen to be presented is 2014 and the period is late May. The anomalies were detected only for the ascending pass.

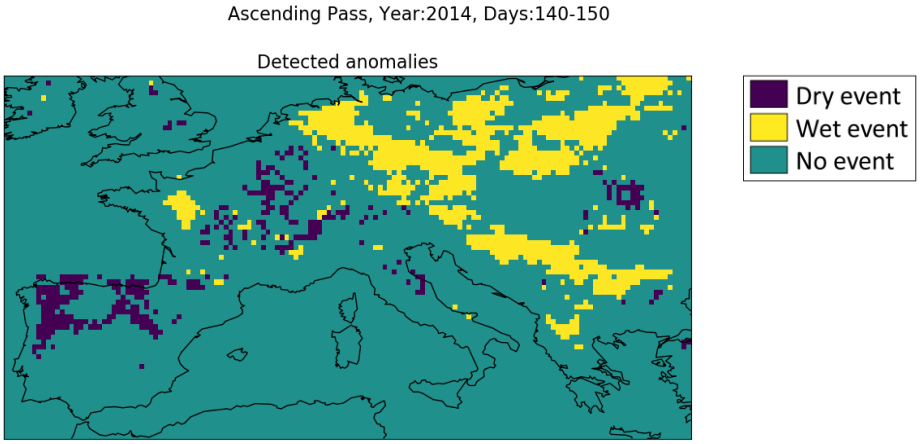

Figure 37. Detected anomalies for 2014 for last days of May

From the above procedure it was expected that not only the anomalies would be detected but also that some outliers would emerge. As outliers they could be characterized the single pixels, especially the dark purples that indicate dry events, just because dry events occupy bigger areas and they are not so local. Also, some of the colored pixels appear to be in the sea, especially North from Spain that either there is a severe event happening between the sea and the coastline (e.g. storm), either they are just outliers.

Chapter 4. Results and discussion

The results of this research will be presented in this chapter in the form of case studies. As it was mentioned earlier in the description of the study area, several different locations were selected to be investigated. The reason of this selection was because these areas suffered from extreme events in the last decade. The results that are presented are focused on the time periods that these extreme events occurred.

In order to investigate the behavior of each pixel, in other words the behavior of each selected area, scatter plots were created. The creation of the scatter plots was achieved by following the steps that are described in the Appendix C.

following, there will be presented some scatter plots. On the x-axis there are the PDBT values ($T_V - T_H$) for each critical period for the investigated area, and on the y-axis, there are the average values of the absolute values of T_B for the specified location ($\frac{T_V+T_H}{2}$) . It should be mentioned that the scatter plots were created for both the ascending and the descending pass as well. The dot that is highlighted with red color in the scatter plots indicate the year that the extreme event occurred. However other years appear as extreme ones and those are being highlighted with green color.

Those scatter plots are expected not only to provide us with information about extreme years but also with information regarding the relationship between the T_B and PDBT. More specific, they would be a good indicator for investigating if those two units are correlated or not. It should be remarked that the detection algorithm is only based on the PDBT values, and hence this 2D analysis would give some useful indication on whether the average temperature should be included in the algorithm as a possible follow-up.

4.1 Spain

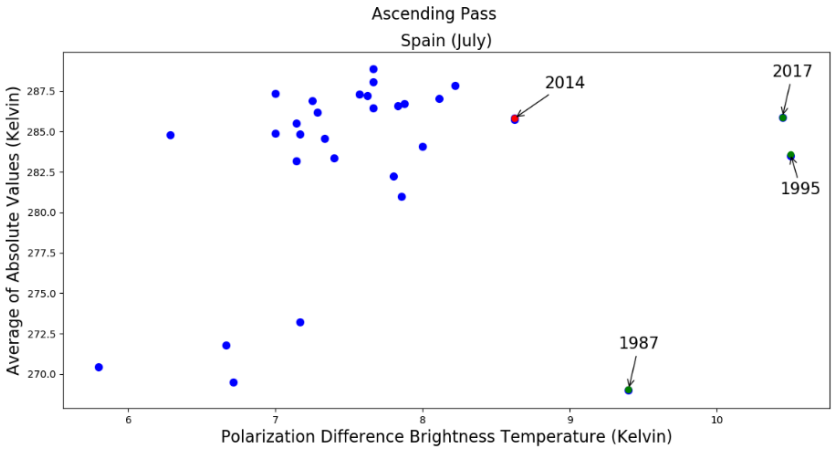

Figure 38. Scatter plots for the ascending pass for the last 10 days of July for Spain

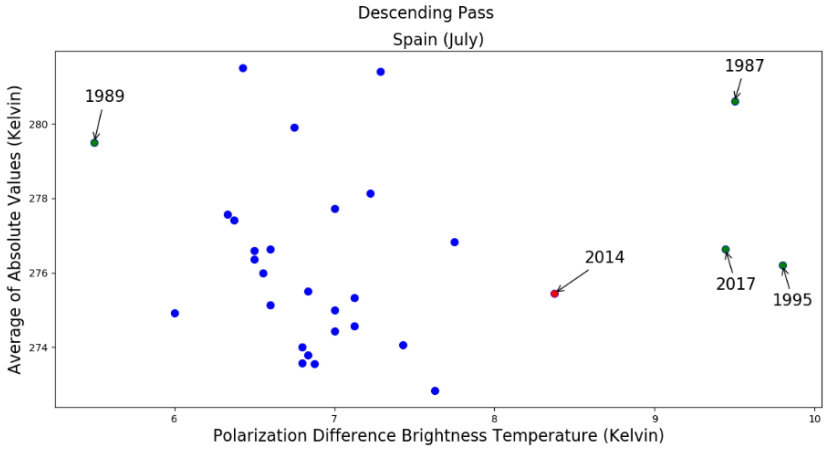

Figure 39. Scatter plots for the descending pass for the last 10 days of July for Spain

According to literature review the July of 2014 was a very dry one for Spain, however 1987, 1989, 1995 and 2017 also stand out from the rest. The year 1987 is not very representative because half of the data are missing for this year. In order to study the algorithm performance, the results for the years 2014 and 2017, i.e. the most recent extreme in both passes, will be presented for a specific time interval.

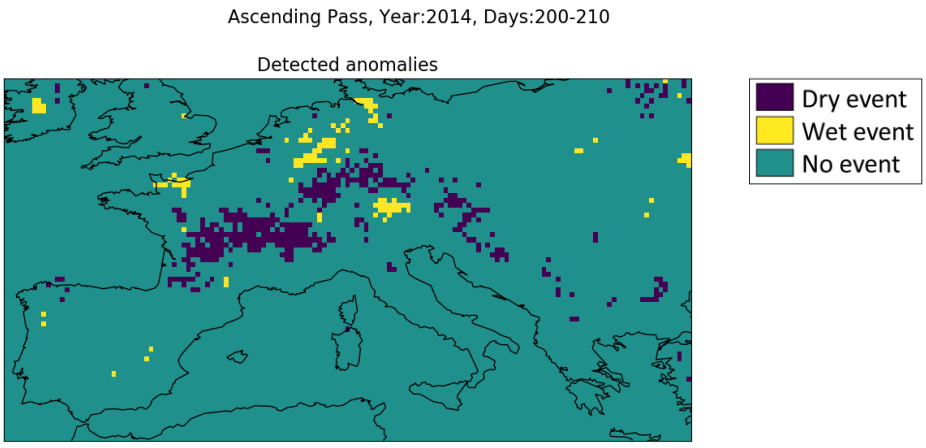

Figure 40. Detected anomalies for 2014 for the last days of July

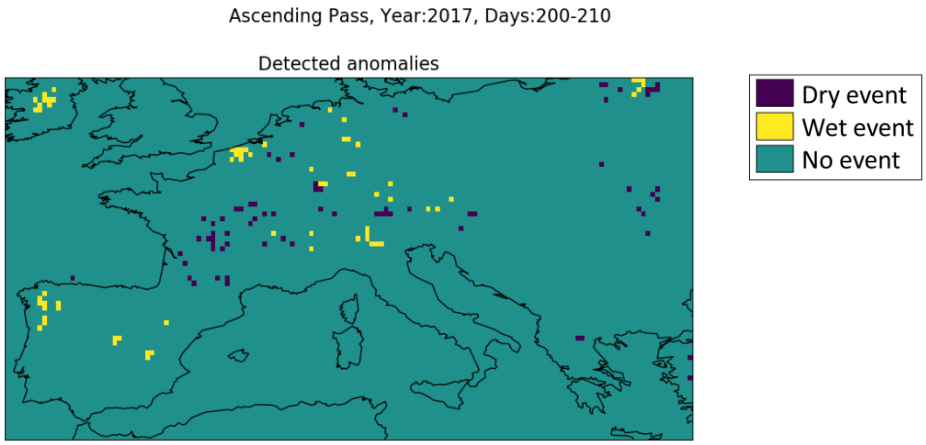

Figure 41. Detected anomalies for 2017 for the last days of July.

From both Figure 40 and Figure 41 it is not evident that Spain suffered form an extreme drought in late July. The explanation behind this is that usually the summers in Spain are very hot and dry, so it would be relatively difficult to detect an even drier event that might not even make a big difference compared to the rest. Also, the detection of the anomalies analysis was based on the assumption that there are no other strong events is the area, which evidently does not apply in this case.

However, further investigation took place and soil moisture data were obtained and plotted for the investigated periods of time.

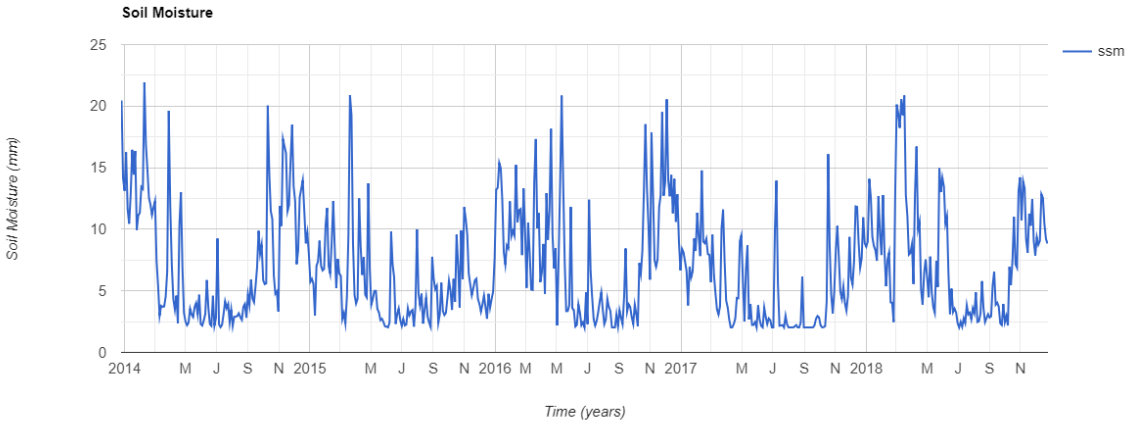

Figure 42. Yearly soil moisture data for Spain

In Figure 42 it is evident that the mean soil moisture values for July of 2014 are slightly lower than the ones for 2017. There is relatively a difference of 0.5-1 mm. So, both years appear to be dry, and this statement could be furthered enhanced, because right after and before July the soil moisture levels are very low for both years.

The next step is the creation of rainfall plots. The rainfall data are obtained hourly and only the critical period for both years will be presented. The rainfall that the area received in one hydrological cycle, which starts on the 1st of October of 2016 and ends on the 30th of September of 2017, was significantly decreased compared to the previous hydrological years, indicating that 2017 had a very dry July in general (Sevillano, 2017).

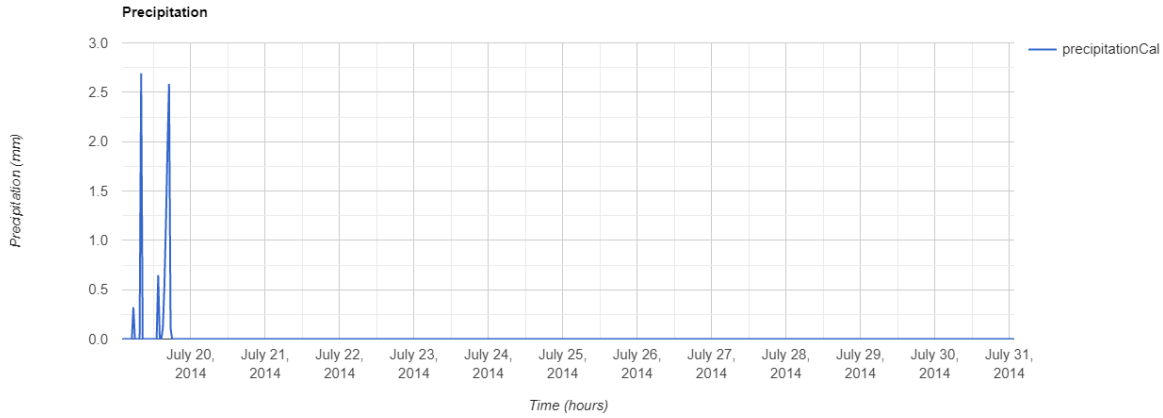

Figure 43.Hourly precipitation data for Spain for July 2014

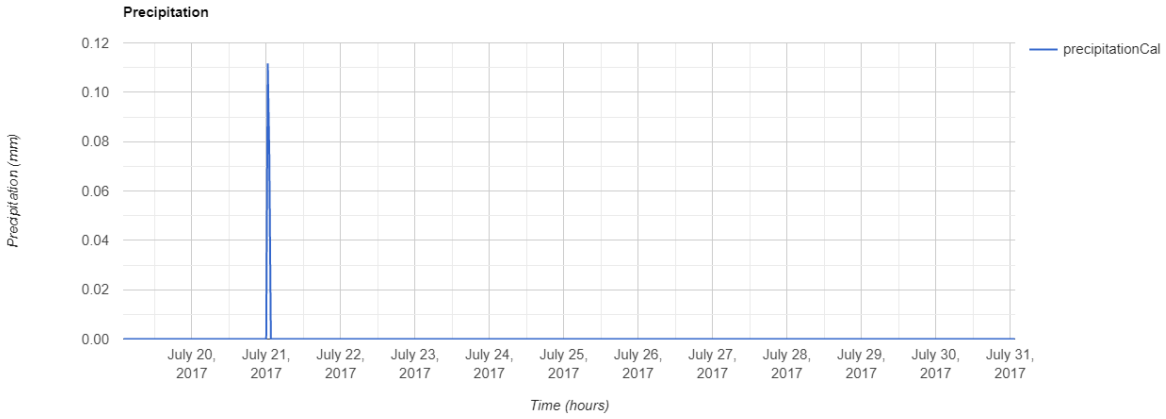

Figure 44. Hourly precipitation data for Spain for July 2017

According to the precipitation events that are presented in Figure 43 and Figure 44, it is noticeable that even in late July, for both years there was a lack of a precipitation event. Prior to that there were just a few rainfall events in 2014 and only one in 2017. Nevertheless, those events were not enough to saturate the soil, especially with the high temperatures that prevail the area. This amount of water that was precipitated can easily be evaporated because of the high temperatures, not making a big difference in the dryness of the area. In 2014 the duration of the precipitation event was not enough, whereas in 2017 neither the duration nor the intensity was enough.

4.2 South France

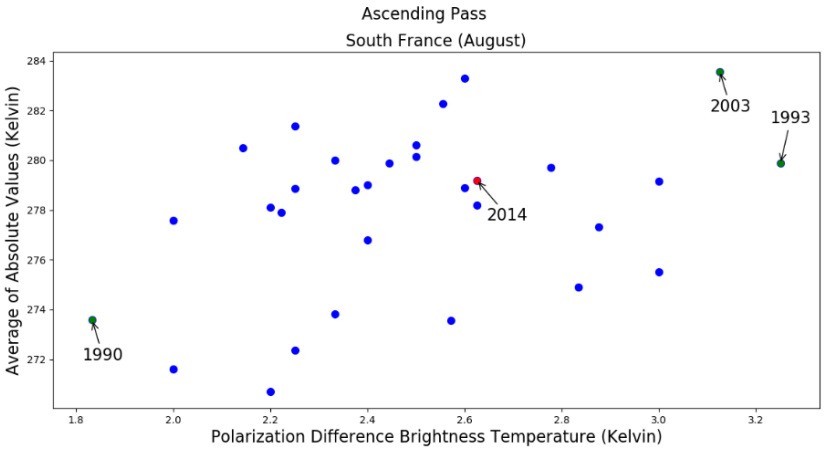

Figure 45. Scatter plots for the ascending pass for the first 10 days for South France

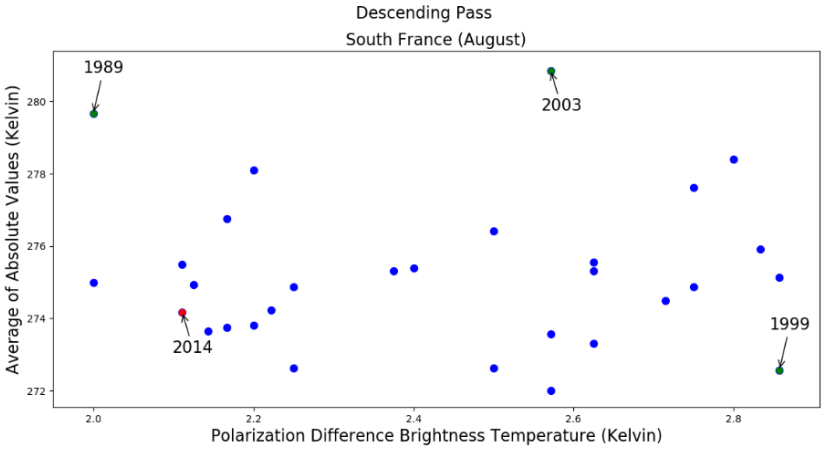

Figure 46. Scatter plots for the descending pass for the first 10 days for South France

The summer of 2014 and especially early August was very hot for Europe and especially for South France that suffered from a drought event. Still, this is not obvious from Figure 45 and Figure 46 since this year does not appear to stand out from the rest. Also, since it is characterized as a dry year it would be expected to be located on the left top corner in both scatter plots. However, the year that appears as extreme in both scatter plots is 2003, so 2014 and 2003 will be investigated for the detection of anomalies.

It is obvious from Figure 47 that close to the borders of France with Spain there is an indication of a dry event. However, it would be expected that the area that suffered a drought would be larger, since drought is not such a local event as a flood. The reason that the dry event is not so obvious, is because in general in August of 2003 there was a great heatwave, making the detection of anomalies very difficult since it was general phenomenon the biggest part of North-East Europe suffered from.

It is quite noticeable that some random pixels that indicate a dry event appear in areas that there is no detection of anomalies in the neighboring locations and this is an indicator that these pixels are just outliers. However, extreme dryness could be identified in central Europe.

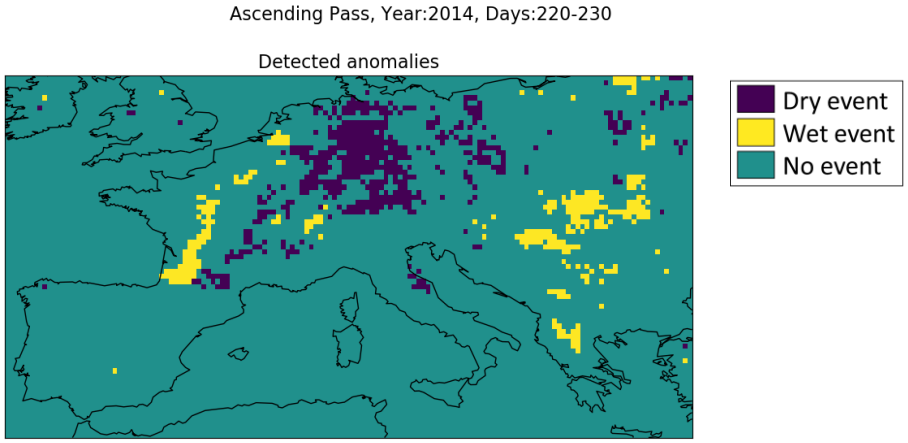

Figure 47. Detected anomalies for 2014 for the first days of August.

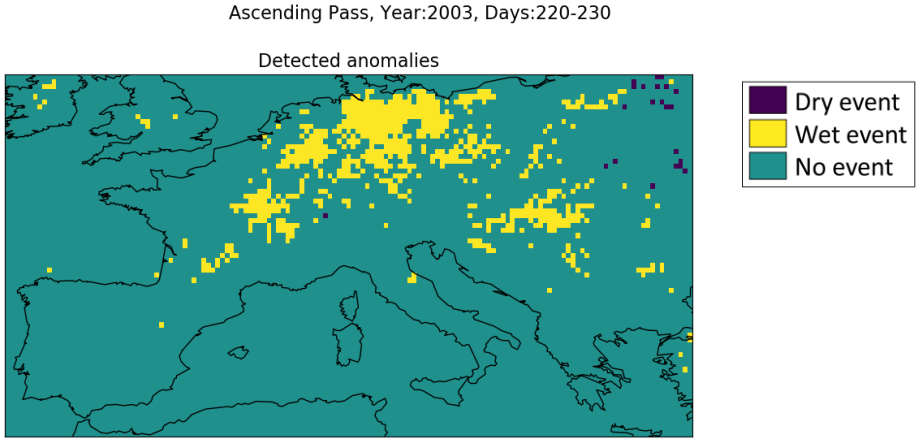

Figure 48. Detected anomalies for 2003 for the first days of August

The year 2003 that appeared to be an extreme one for South France, does not indicate extreme dryness but it does indicate extreme wetness in the area of interest, which agrees with the rest of Europe which appears to be extremely wet for this period. Even though this was not the expected behavior, however it justifies the scatter plots because 2003 was identified as an extreme year, meaning that it was not just an outlier.

Nonetheless, this was not the expected behavior and for this reason the soil moisture will be examined to provide us with an insight in the top layer water content of the area.

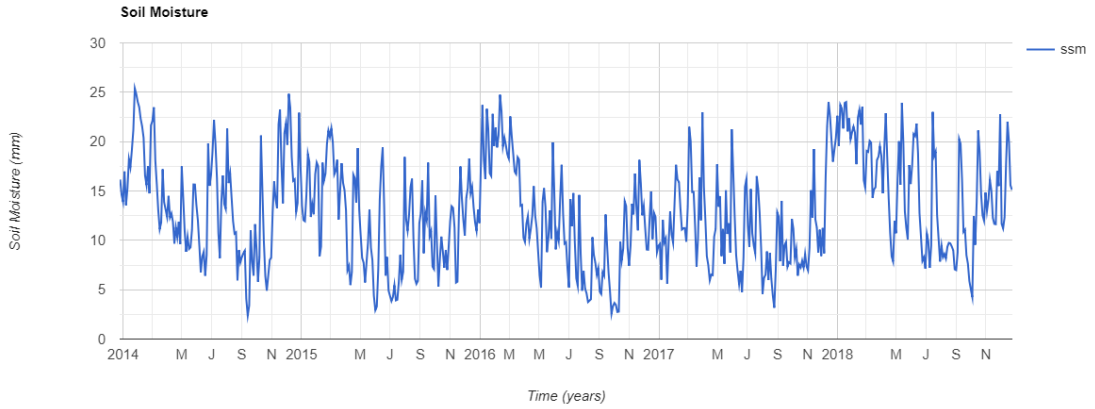

Figure 49. Yearly soil moisture data for South France

A comparison between 2014 and the rest of the years until 2017 will be made according to the obtained data. A specific date was chosen for all those years and this date is at the beginning of August and more specific the 5th of August. On this specific data usually the temperatures are very high, and the soil moisture is expected to be low. For 2014 the value of soil moisture is 15.8 mm which is the highest one than the rest. More specific, for 2015 the value is 10.975 mm, for 2016 is 4.637 mm and for 2017 is 6.497 mm. From external expert knowledge, it would be expected that the 2014 soil moisture values would be the lower ones, but the differences are not so big. Once again, it is very difficult to identify a dry event especially when this area suffers very dry summers.

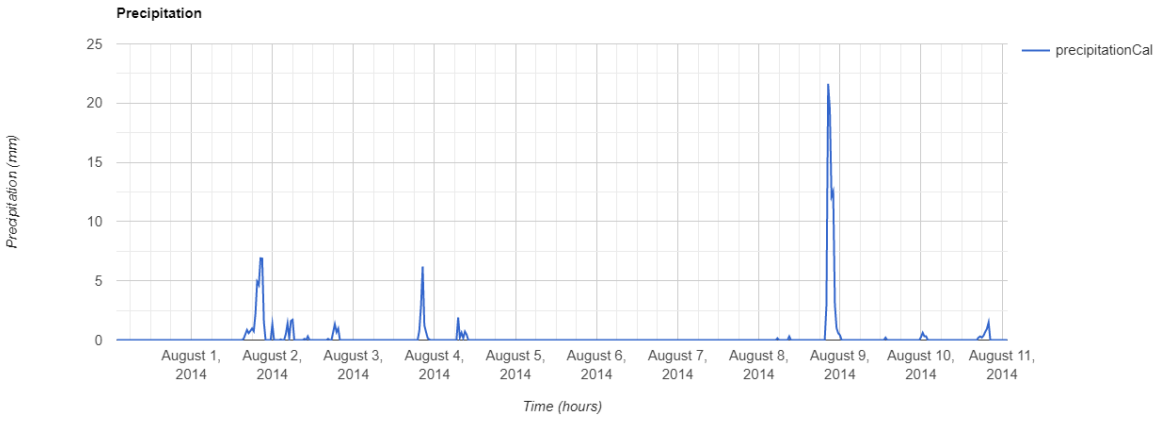

Figure 50. Hourly precipitation data for South France for August 2014

In Figure 50 it is evident that there are some precipitation events that can also be clearly seen in the detection of the anomalies in Figure 47.

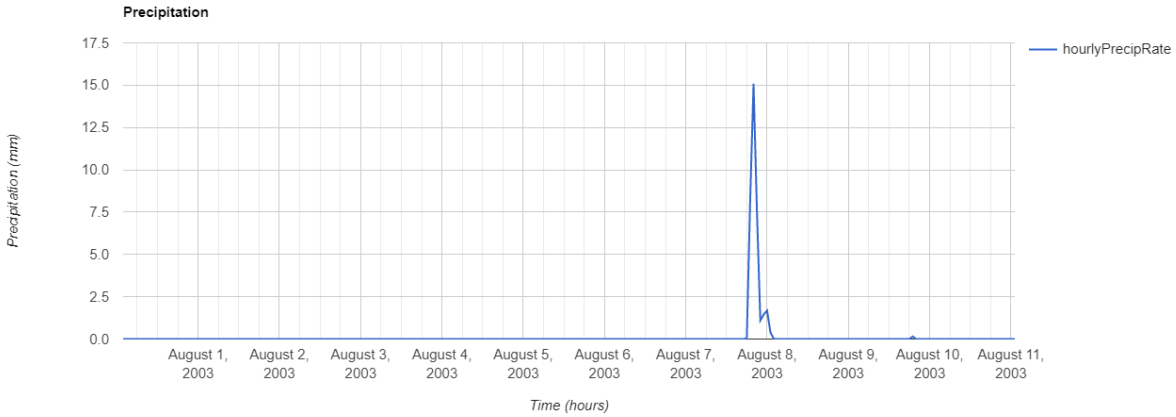

Figure 51. Hourly precipitation data for South France for August 2003

From Figure 51 it is obvious why 2003 appeared as a wet year and not a dry one as it was expected. The reason is because during the whole month of August there was no precipitation at all, and suddenly there is a precipitation event occurring on the 8th of August. This means that the value of the temperature for this day will be highly affected and more specific lowered, affecting significantly the average of the temperatures that was calculated for the time interval of ten days, because the rest of the values were relatively small. This peak is enough to give mixed signs.

4.3 Bosnia and Herzegovina

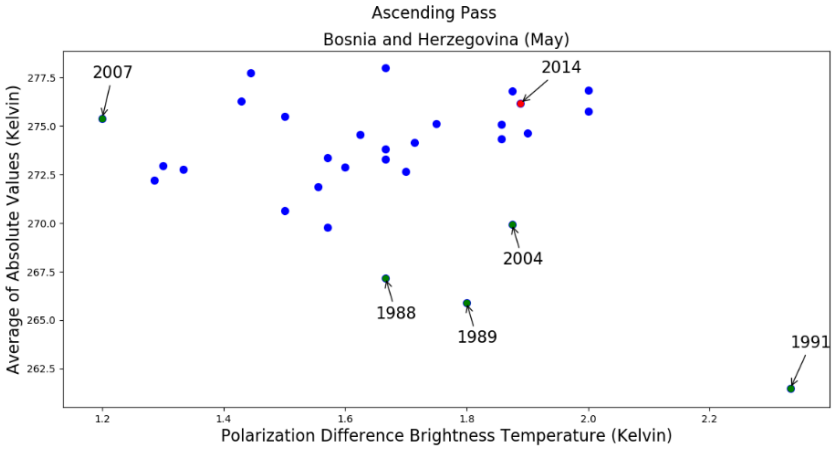

Figure 52. Scatter plots for the ascending pass for the last 10 days for Bosnia and Herzegovina

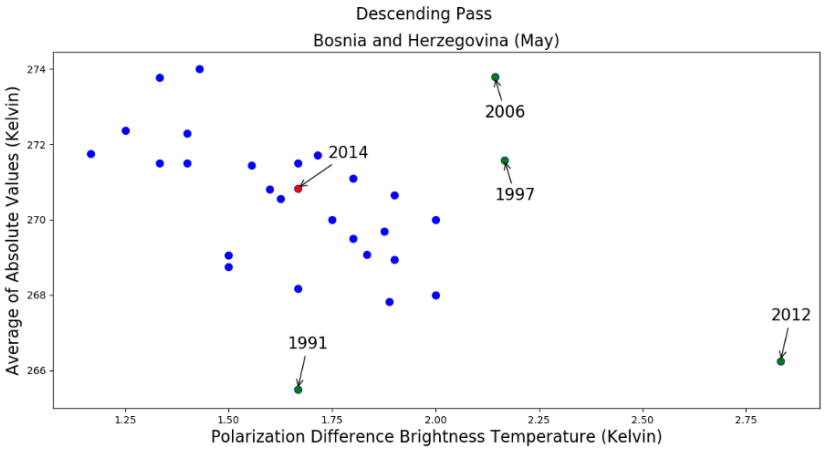

Figure 53. Scatter plots for the descending pass for the last 10 days for Bosnia and Herzegovina

For Bosnia and Herzegovina, a big variety of years appear as extremes for the ascending and the descending pass, besides 2014 that the flood occurred. The one that appears in both cases is 1991.

It is apparent in Figure 54 that indeed Bosnia and Herzegovina suffered an extreme flood in mid-May of 2014. And it is also obvious that most of North-East Europe suffered extreme wetness which could be related to flood events.

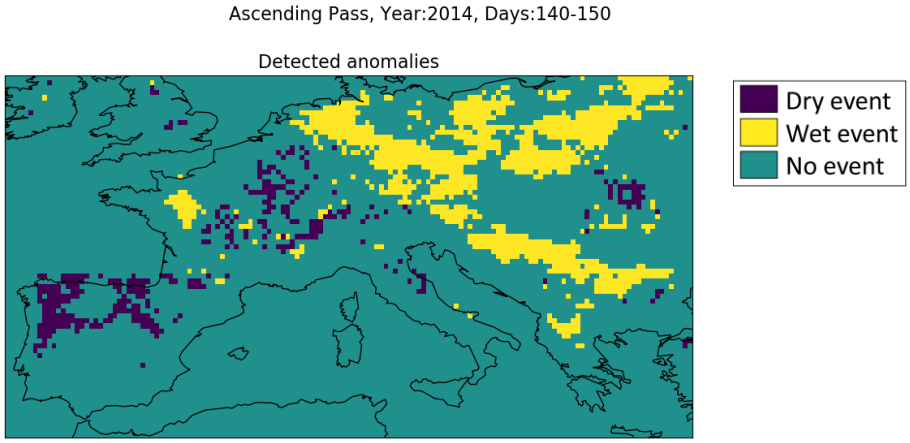

Figure 54. Detected anomalies for 2014 for the last days of May

Also, 1991 appeared to be an extreme year for Bosnia and Herzegovina, which is being justified by Figure 55. In both cases the wet extremes are more obvious in the North-East side of Europe, whereas the drier ones appear in the North-West and South-West Europe.

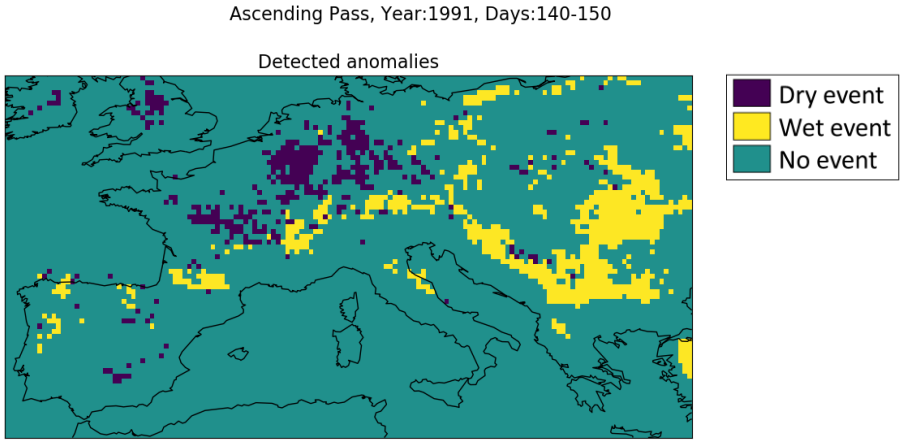

Figure 55. Detected anomalies for 1991 for the last days of May

Unfortunately, there are no available data either for soil moisture or for precipitation for the year of 1991. However, time series of soil moisture for 2014-2017 could be obtained.

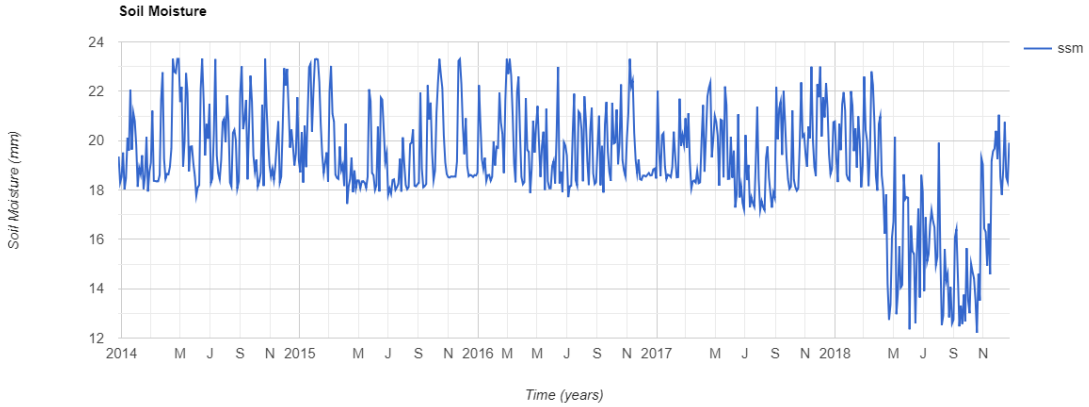

Figure 56. Yearly soil moisture data for Bosnia and Herzegovina

Undeniably, the May of 2014 appeared to have very high values of soil moisture and much higher than the ones in 2015. The rest of the years appear to have slightly lower values of soil moisture. Form Figure 56 it is not so evident that there was a flooding event in the investigated area and that is why the precipitation plots will be further examined.

Figure 57 indicates the precipitation in the area for the month of May. It is obvious that there were some rainfall events that could easily saturate the soil, leading to a flood event. The reason is not the intensity but their frequency which is relatively high for this time interval.

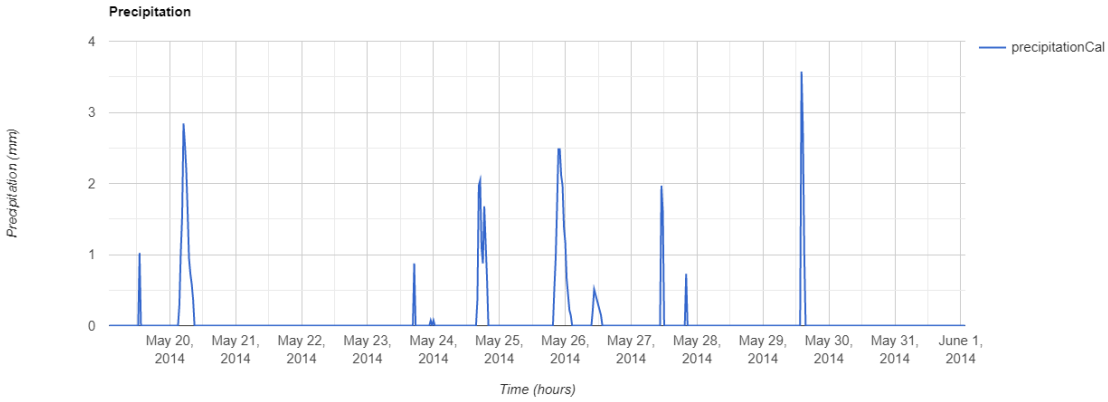

Figure 57. Hourly precipitation data for Bosnia and Herzegovina for May 2014

4.4 Czech Republic

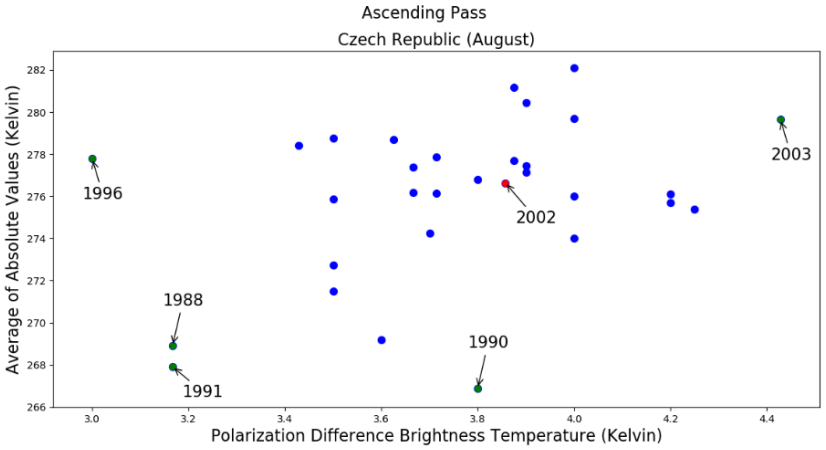

Figure 58. Scatter plots for the ascending pass for the first 10 days for Czech Republic

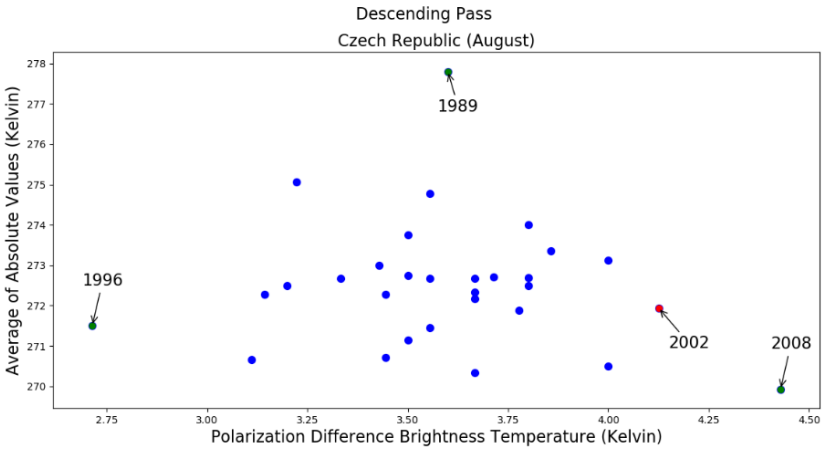

Figure 59. Scatter plots for the descending pass for the first 10 days for Czech Republic

On August of 2002 the city of Prague suffered a big flood. This is not so obvious from the created scatter plot for the ascending pass, whereas in the one for the descending pass is more evident. However, the year that stands out in both cases is 1996. In this year there was not mentioned any extreme climatic condition, but still it will be investigated.

Figure 60 justifies the extreme wetness which is the result of a flooding event. The yellow pixels

indicate high surface wetness. Also, for the same period there is a pattern in the surrounding area, which means that the event was not so local, and it was the result of heavy rainfall.

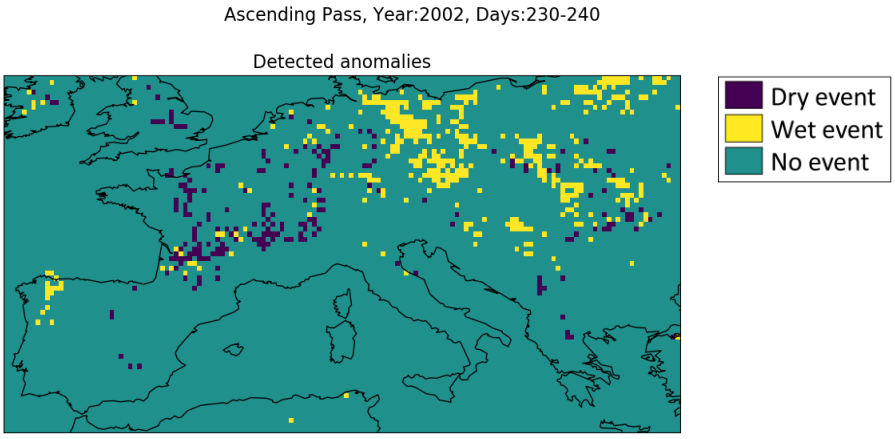

Figure 60. Detected anomalies for 2002 for the last days of August

Even though 1996 appeared to be an extreme year for the under-consideration area, the following figure does not indicate that. In Czech Republic and more specific in the city of Prague, there are some pixels that indicate high surface wetness but are less evident than the ones in Figure 60. The year of 1996 might appear as an extreme one because the behavior of the surrounding area is mixed and two extreme conditions appear to happen at the same time in a very close distance. However, these extremes is possible that could get affected by the morphology of the area as well. If the area is mountainous and there is dry snow on top of it, then very low values are expected as shown in Figure 61.

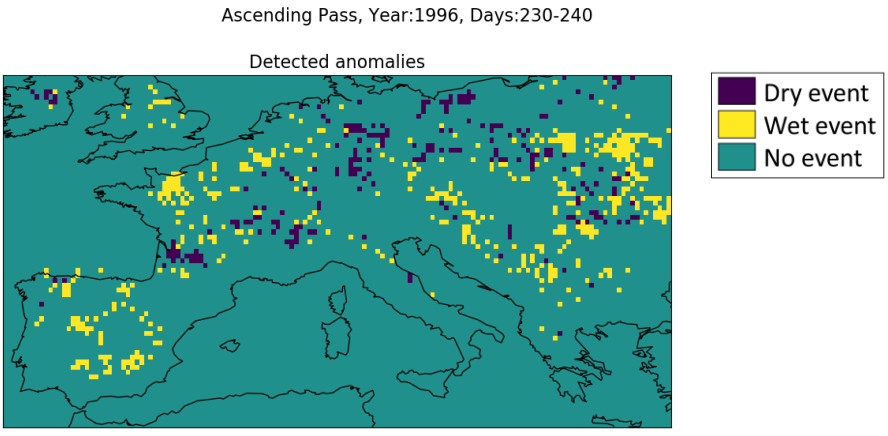

Figure 61. Detected anomalies for 1996 for the last days of August

Neither for year 2002 nor 1996, soil moisture time series were available. However, precipitation hourly data were available for 2002, which will give us an insight of the amount of precipitation that the area received over time.

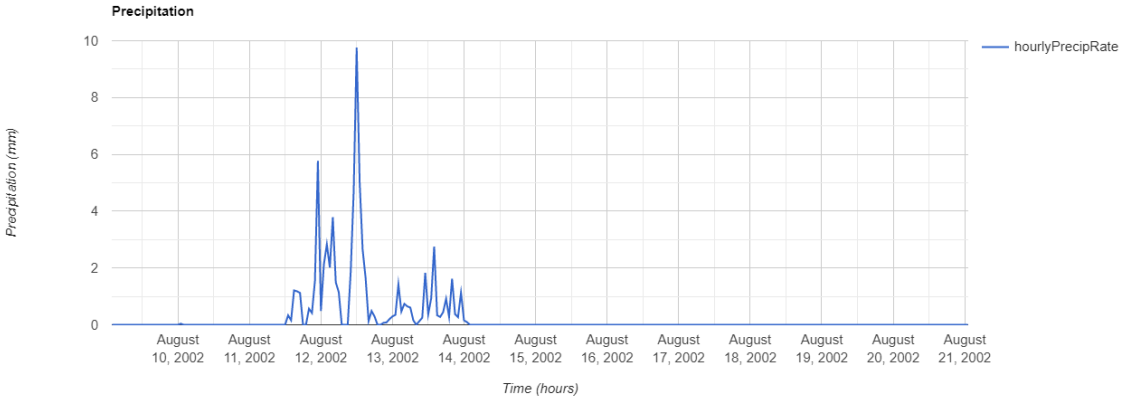

Figure 62. Hourly precipitation data for Czech Republic for August 2002

In Figure 62 it is obvious that late at night of 12/08/2012 there was almost 10mm of rainfall. Prior and later to that event there was also a significant amount of precipitation occurring in the area. The duration might not be considered as long, however the intensity was high. These series of events could justify the fact that indeed there was a flood in the area.

4.5 Poland

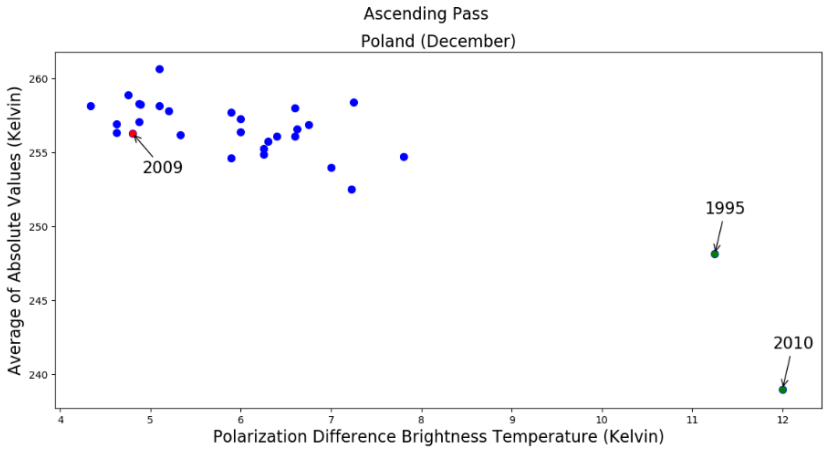

Figure 63. Scatter plots for the ascending pass for the first 10 days for Poland

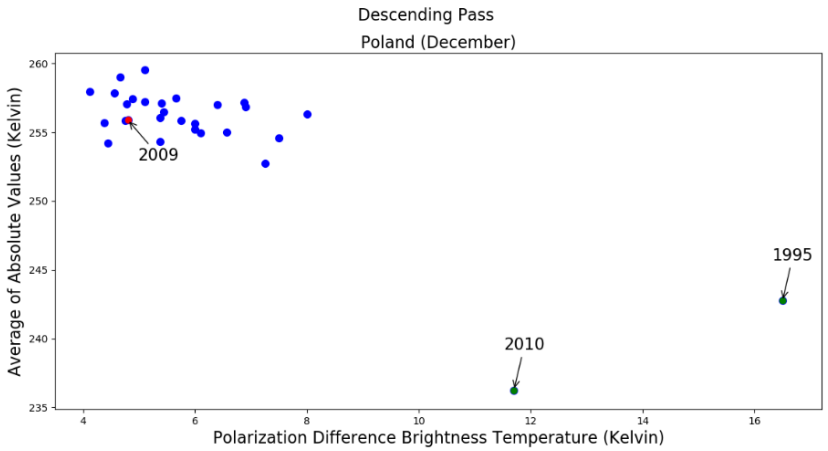

Figure 64. Scatter plots for the descending pass for the first 10 days for Poland

Poland suffered from heavy snowfall in December of 2009 with 62 casualties. However, this is not obvious from Figure 63 and Figure 64, since it is not prominent in either of the scatter plots.

The ones that do stick out in both cases are 1995 and 2010. Year 1995 appeared to have a warm winter that was even considered as irregular (Kejna et al. 2009). However this statement does not agree with the results of the scatter plots, because if this was the case then 1995 should be placed in the top-left corner of the plots. However, this does not mean that the scatter plots are mistaken, because indeed they detected 1995 as an extreme one. The year of 2010 appears to be a very interesting case, because it has relatively high PDBT values and very low average T_B. For this reason, anomalies will be detected for the year of 2009 and 2010, because it will be very interesting to see the changes in two subsequent years.

Figure 65 does not indicate any extreme event in the investigated area and in general in Poland. This result was very interesting because there is also not an evident pattern in the neighboring countries. The reasoning behind that might be that the temperatures in the rest of the years were not so different than the ones in 2009, so the event did not become evident. In general Poland is a country that suffers extremely cold winters with heavy snowfall events. Also the initial assumption was that there are no strong events in the area, which does not apply in this situation.

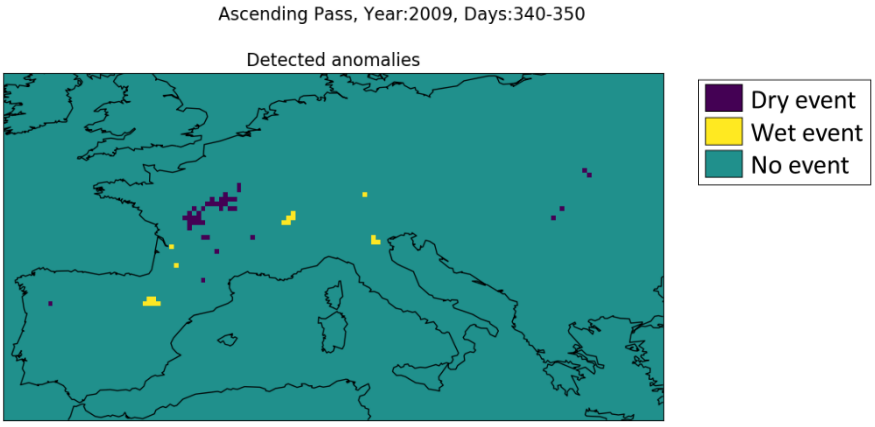

Figure 65. Detected anomalies for 2009 for the first days of December

On the other hand, in 2010 there is an indication of high wetness in the investigated location. Once again, this would be an indication that there is wet snow, behaving in the same way as surface water, rather than dry snow, which behaves as dry soil (low NPDBT values).

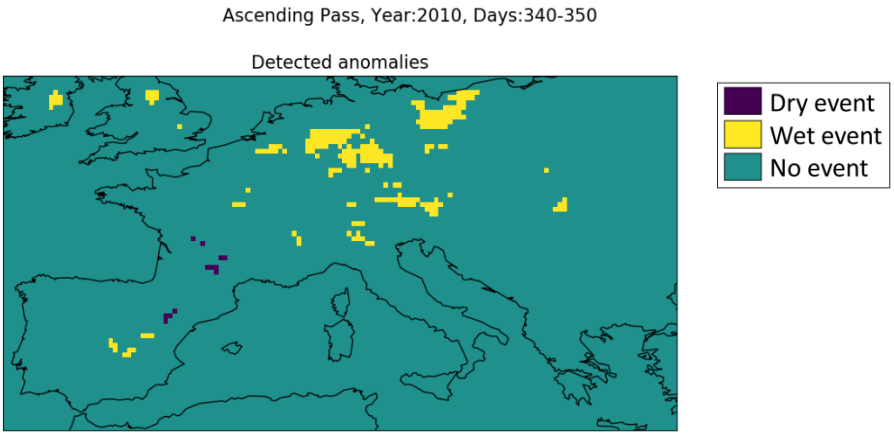

Figure 66. Detected anomalies for 2010 for the first days of December

A better insight in the assessment of those events would be the precipitation data of the period and the area that the anomalies were or not detected.

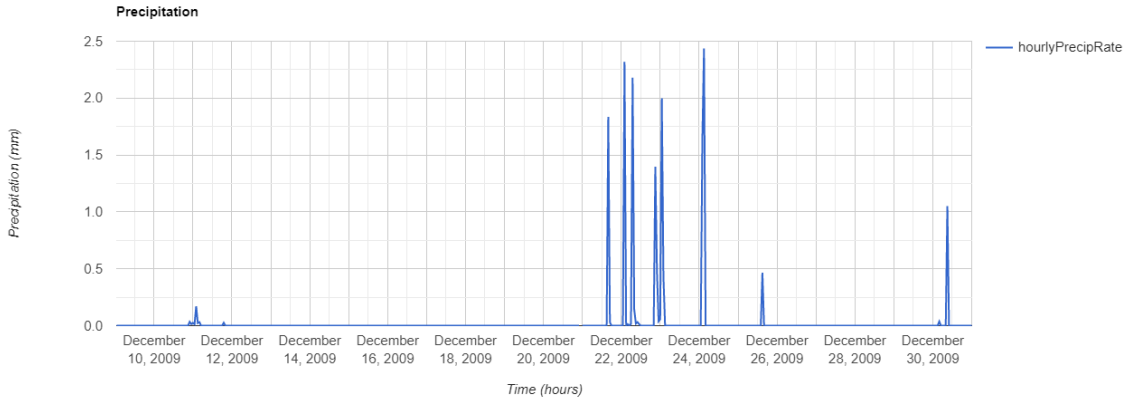

Figure 67. Hourly precipitation data for Poland for December 2009

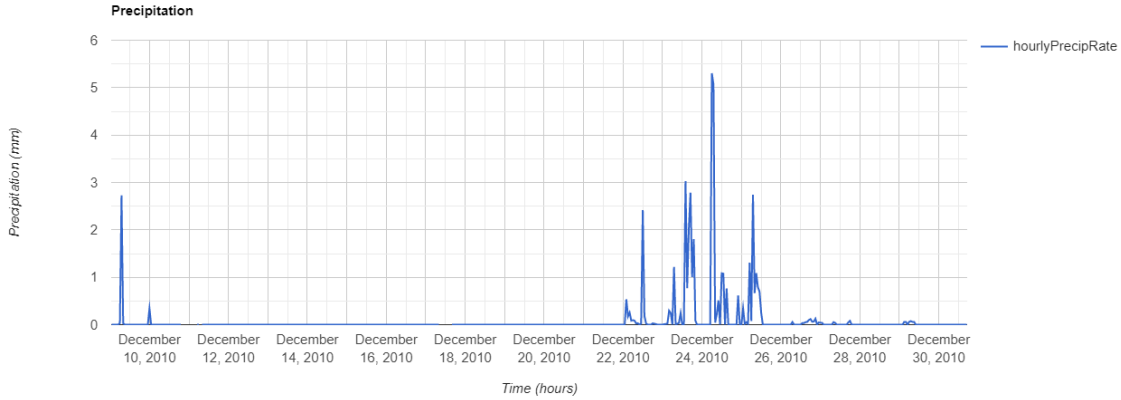

Figure 68. Hourly precipitation data for Poland for December 2010

As it is seen, for the same days of December, in 2009 the precipitation (snowfall) values are much lower than the ones in 2010. More specific, in 2009 the maximum precipitation rate is almost 2.5mm/hour, whereas in 2010 is nearly 5.5mm/hour. This is a big difference, indicating that 2010 correctly demonstrated high values of NPDBT, meaning that the surface wetness, in this case heavy snowfall, was high.

4.6 Ukraine

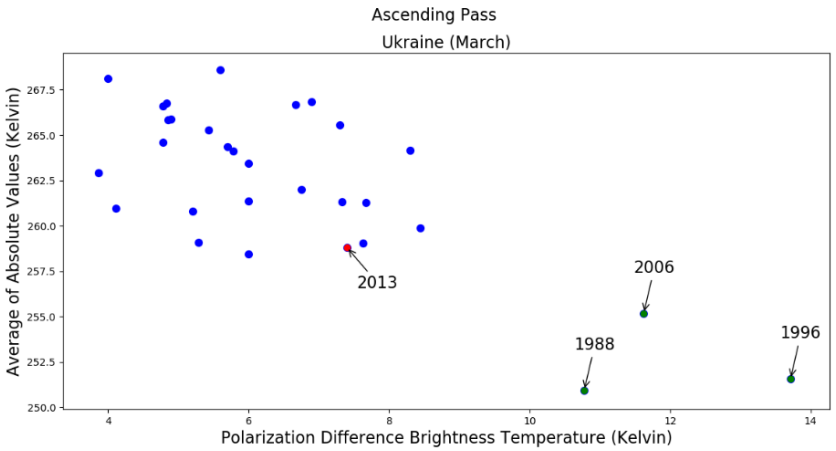

Figure 69. Scatter plots for the ascending pass for Ukraine

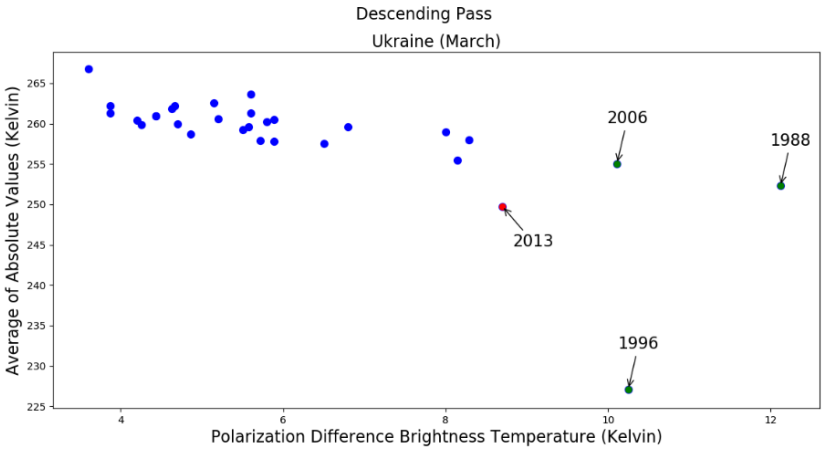

Figure 70. Scatter plots for the descending pass for Ukraine

For the case of Ukraine, the critical period was in March of 2013 and it appears to stand out in the descending pass, but not in the ascending one. However, for both passes the years 1988, 1996 and 2006 appear to have an extreme behavior comparing to the rest. Between the years of 1971 and 1990 the repetition and the intensity of the snowfall events in Ukraine and especially in the West part where Lviv is, were extremely high. The amount of snowfall events that occurred in 1996, 1988 and 2006 are not that many, but the maximum precipitation (snowfall) that occurred was considerable high (Balabukh et al. 2018). Therefore those years behave differently than the rest.

The year of 2013 and 2006 will be investigated for the detection of anomalies, because they are the most recent ones and soil moisture and precipitation data are available for them.

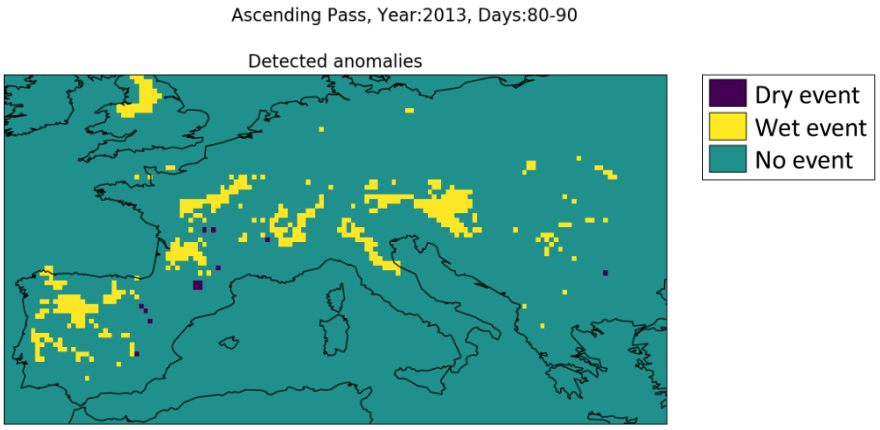

Figure 71. Detected anomalies for 2013 for the last days of March

In 2013, in the examined area there is not a clear indication of high surface wetness due to heavy snowfall. However, there is a trend indicating high surface wetness in other areas of Europe for this period. In the rest of the Europe it might not be snow in all the cases, but it was high surface wetness, which could be related to heavy rainfall events that might lead to the saturation of the soil and finally in a flooding event. Once again, due to the geographical position of Ukraine, the heavy snowfall events and the low temperatures are very common, so the investigated event does not stand out as an extreme. It is noticeable that there are some random pixels that indicate a dry event. These are probably outliers because they do not follow a pattern.

Going further back in time and more specific in 2006 that the detected anomalies are depicted in Fig.71, once again patterns of high surface wetness are obvious and more consistent. This is a validation of the scatter plots that the year of 2006 stood out as an extreme one.

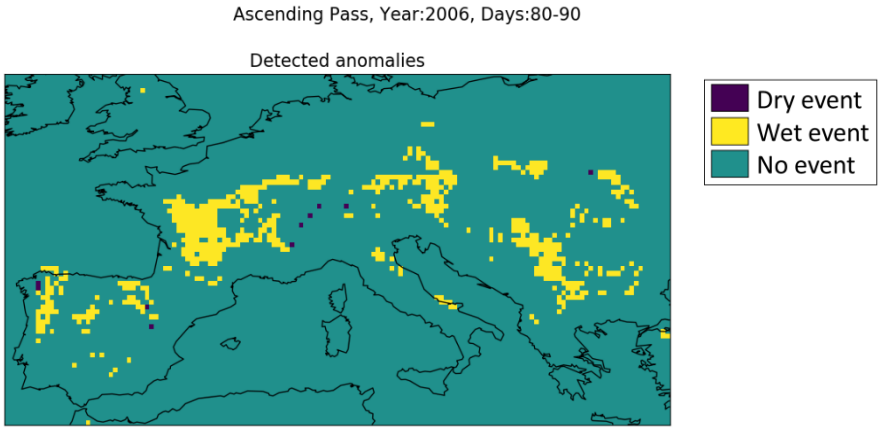

Figure 72. Detected anomalies for 2006 for the last days of March

The soil moisture data in Figure 73showed that in March of 2013 the value is 23.479mm which is bigger than the ones for 2014, 2015 and 2016 respectively. Although, it is quite interesting that it is lower than the soil moisture value for 2017 which was 23.971mm. Nevertheless, this is a negligible difference.

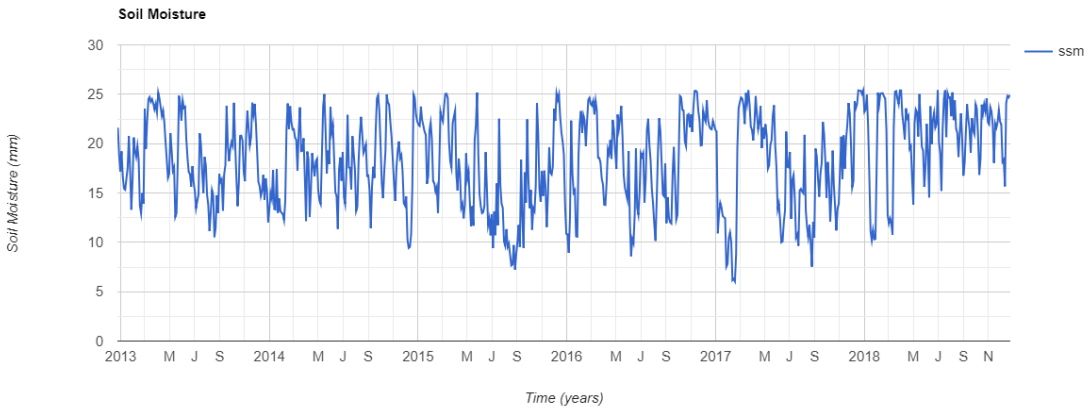

Figure 73. Yearly soil moisture data for Poland

Yet, the precipitation data appear to be more useful for wet-snow events. In Figure 74 the precipitation data for 10 days of March of 2013 are presented and they indicate that at the day of the event there was no precipitation. Once again, this might be happening because the areas were analyzed in a pixel size and the time interval that was used was 10 days. Besides that, it is noticeable that before the date of the extreme event, there is a continuous rate of precipitation events and one of them almost reaches 7mm. Also, the precipitation continuous for three more days. This amount of precipitation (snow) was enough in order to cause an extreme event.

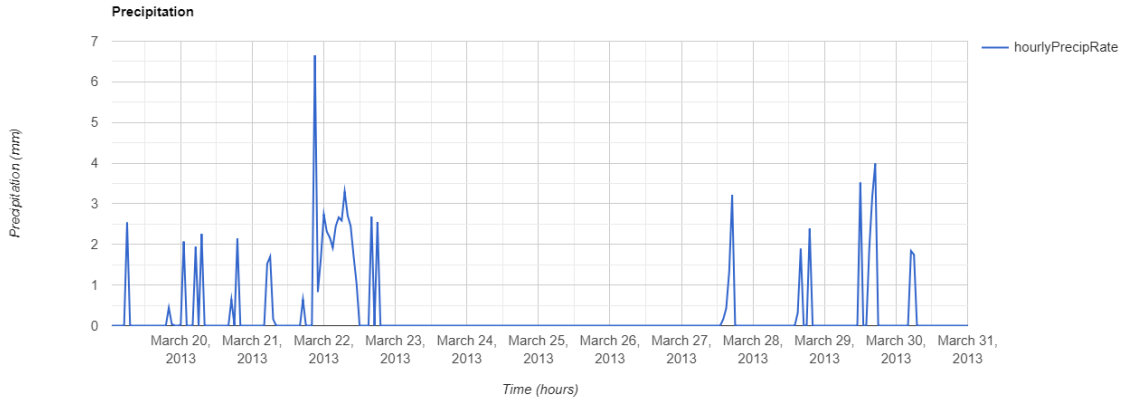

Figure 74. Hourly precipitation data for Poland

Going seven years back in 2006, for the same time interval, there are less precipitation events occurring, but their intensity is higher than the smaller ones that occurred in 2013. So, this is a good reason why 2006 stood out as an extreme year, because the precipitation events (snowfall events) that occurred could not be neglected.

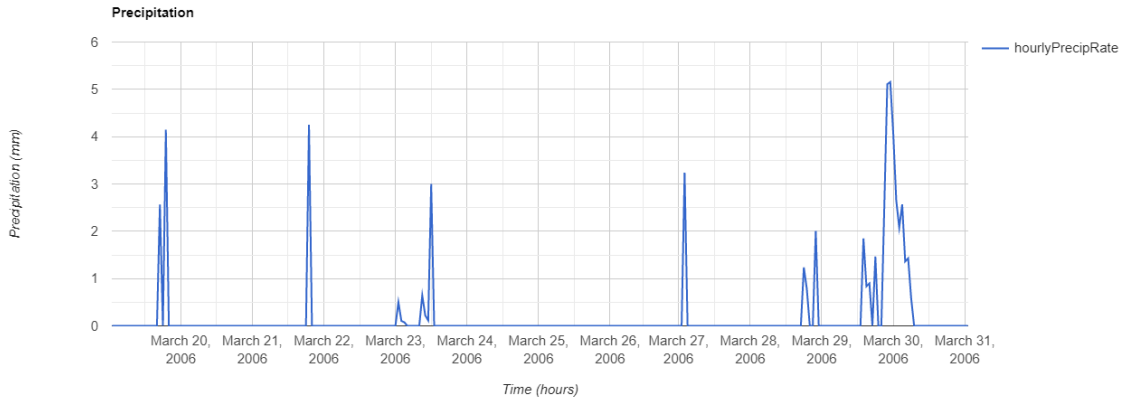

Figure 75. Hourly precipitation data for Ukraine for March 2006

Chapter 5. Conclusions and Recommendations

A detailed study was performed for the identification of extreme events in the area of Europe with the selection of the 37GHz channel of SSM/I. The first part of this study focused on the creation of T_B and PDBT time series to get an indication of the behavior of the data. The high values of PDBT show high surface wetness. The reason behind that statement is because the surface emissivity decreases while the polarization difference increases with surface wetness. The next step was the statistical analysis to provide us with information about any outliers and actual extreme behaviors. Lastly, the creation of the scatter plots delivered other years as well to stand out as extremes. Those years that stood out were used for the detection of the anomaly's procedure.

The results show that the methodology that was followed does not work the same for all the cases. More specific, it performed better in the wet and snow events than the dry ones. The reasoning behind that is that in general in summer months and especially in areas that belong in the Mediterranean region, the temperatures (real and T_B) are very high and the climate is already dry, so the identification of drought events is very difficult.

However, this does not seem to be the case for the identification of wet events. As wet events are characterized the flooding events that are usually more spontaneous and do not need a lot of time to evolve as for example a drought event. From the results of this research it is concluded that the anomaly detection technique provides the suspected behavior.

For the identification of snow events the research showed mixed results. In the detection of anomalies for snow coverage, in one the cases there was no indication of an extreme event, however in another one it was more evident. If the snow is dry, meaning that it is frost, then the scattering effect takes place and the emissivity is not so high. On the other hand, if the snow is fresh and wet then the polarization difference is expected to be much higher. However, this does not mean that in both cases there was no snowfall. It means that in the first case the temperatures were so low that turned snow into frost, whereas in the second one they were close to zero or even higher, keeping the snow wet.

The soil moisture and precipitation data were used as a form of validation. Soil moisture appears to be more helpful in the cases of the drought events, whereas for the cases of flooding and snow events the precipitation data appear to be more suitable for investigation. Soil moisture is the amount of water that is contained in the very first centimeters of soil. This is usually related to the water that evaporates from the soil surface and transpires from vegetation when the temperatures are very high. So, it is more useful for a drought event to see how much water is contained in the first layers of soil. The less the contained amount of water, the drier the area.

On the other hand, for wet and snow events the precipitation was much more helpful. Precipitation is defined as any kind of water in the form of liquid or solid that falls to the ground surface. This might be rain, snow, hail and sleet. The precipitation is measured in mm. It is more useful to get information about how much water was received than how much water is

available to be evaporated. Even if on the expected days the amount of precipitation was not very high, that does not mean that the flooding event could not occur at that day. When multiple events occur prior to the extreme one, then the aquifer becomes saturated and cannot absorb and store any more water which leads to flooding.

In case of snow events the heavy snowfall is also related to accumulated events, since the time interval that was used for the detection of the anomalies was 10 days. When the events are frequent over the investigated period that means that more snow is being accumulated to the studied area. Also, the high intensity of the snow events could cause a heavy snowfall event. So in case of the snowfall events both intensity and frequency are very important parameters.

From this study is concluded that the T_B values are more unpredictable than the PDBT values, and the user cannot be sure if they expect high or low values of T_B according to the occurring event. Therefore further investigation and modelling is needed to exploit T_B.

One of the limitations of this research is that the resolution of the data is too big for the identification of extreme events. If the spatial resolution was lower, then the data would be more detailed. In bigger resolutions they appear to work better for ocean climate measurements and for soil moisture retrievals. For the soil moisture retrievals in situ measurements would be very helpful as well, in order to make comparisons and for validation reasons.

Another limitation was the scale of the study area. It would be easier if the scale of the investigated areas would be smaller. For example, if only one country or better a fraction of it would be studied, then obtaining other kind of information such as vegetation type and cover and surface roughness would be extremely helpful for a more detailed analysis. For example for the vegetation type and coverage NDVI maps could be used. In general the land surface conditions should be taken into consideration because each surface has different characteristics and emissivity properties. For instance, a smoother surface has higher emissivity than a rougher one. Also the landscape and the different topography of each area should be taken into consideration. If the study area was smaller, maybe in situ measurements of actual temperatures and rainfall could be provided form stations and help in the validation of the data and the detection of the anomalies.

Also if the scale was smaller, it would be much easier to estimate the atmosphere emittance and the attenuation from vegetation, with the use of a radiative transfer model, because those two appear to be very important parameters that really affect the quality of the obtained data.

One recommendation would be to pre-process the SSM/I data before using them. The pre-processing, also called filtering could help remove the contribution from clouds, atmosphere, rain and observation gaps which could be called noise. By filtering the data the noise is being eliminated and the surface emissivity is more accurate. Otherwise the obtained signal might contain fluctuations of the atmospheric conditions.

This research was based on a big assumption. This assumption was that the area was fully vegetated and that is why in the calculation of the PDBT was done with Eq.3. Even though the selection of each area was done very carefully, away from nonrural areas, that does not mean that there is zero chance that urbanized parts might also be included or more simply that the area is partially vegetated. In that case the fractional area of vegetation, the difference of vertical and horizontally polarized emissivity, the surface temperature and the transmission function of the vegetation canopy are needed to be concluded in the calculation of the PDBT.

Another assumption that was made in this analysis for the detection of the anomalies, was that in the surface there were no strong events. This is not always the case and it might be a reason that in some of the investigated areas the results did not agree with what it was expected. The analysis was comparative, since there was just a comparison of an extreme year with the rest, assuming that no other significant events took place.

This research could be a useful tool for future research, used as a base and including new parameters and indicators that could either help detect anomalies with better precision or predict them for the near future.

Appendix A. Time series

A.1. Brightness Temperature time series

The T_B time series for the rest of the case studies will be presented in the figures below.

- *Dry event*

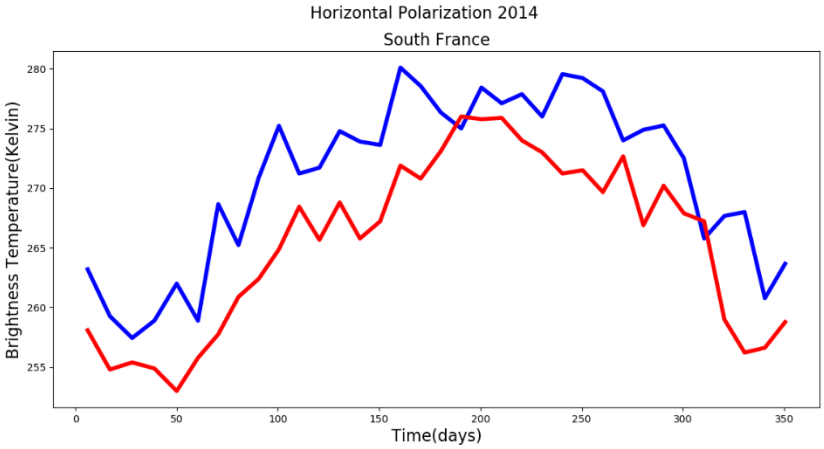

Figure 76. Brightness Temperature time series for the Horizontal Polarization for South France, event occurring in days 200-210

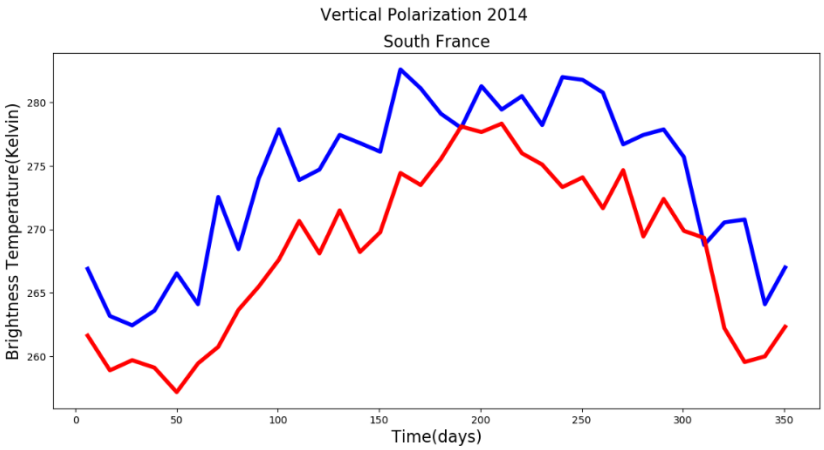

Figure 77. Brightness Temperature time series for the Vertical Polarization for South France, event occurring in days 200-210

- *Wet event*

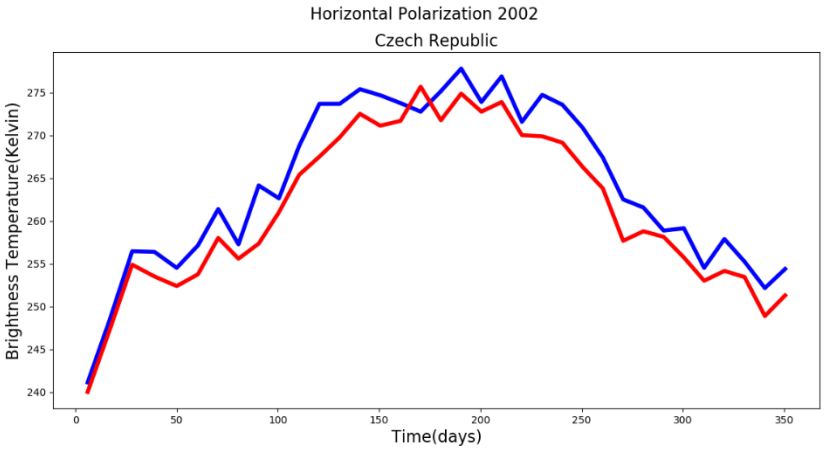

Figure 78. Brightness Temperature time series for the Horizontal Polarization for Czech Republic, event occurring in days 220-230

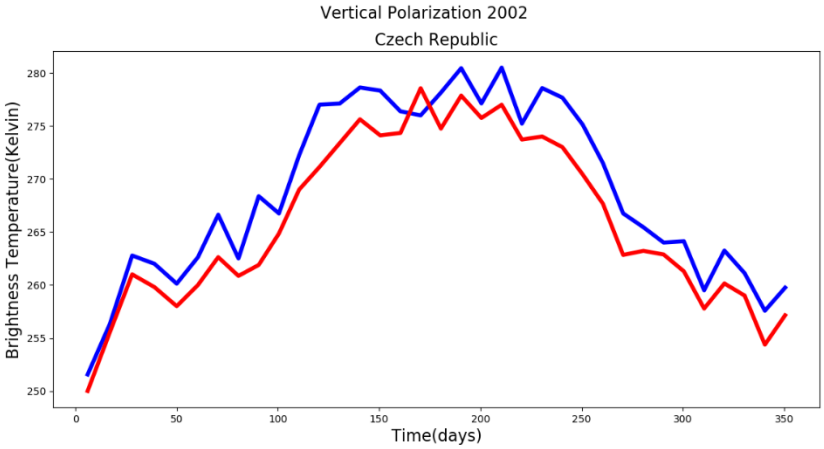

Figure 79. Brightness Temperature time series for the Vertical Polarization for Czech Republic, event occurring in days 220-230

- *Snow event*

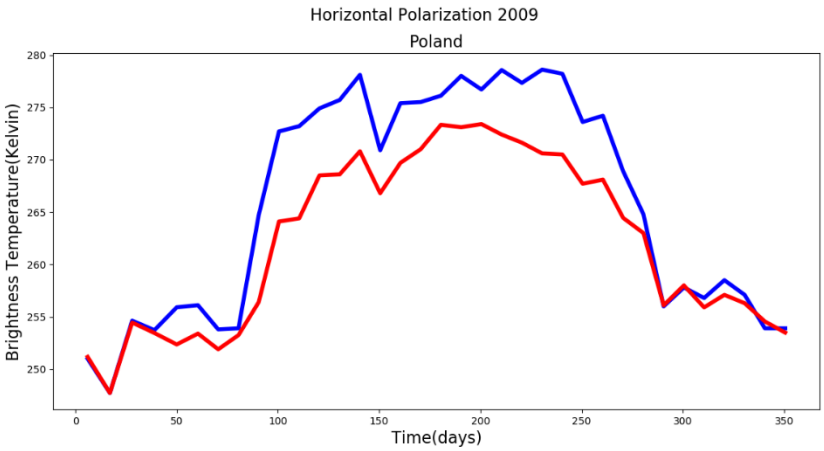

Figure 80. Brightness Temperature time series for the Horizontal Polarization for Poland, event is occurring in days 340-350

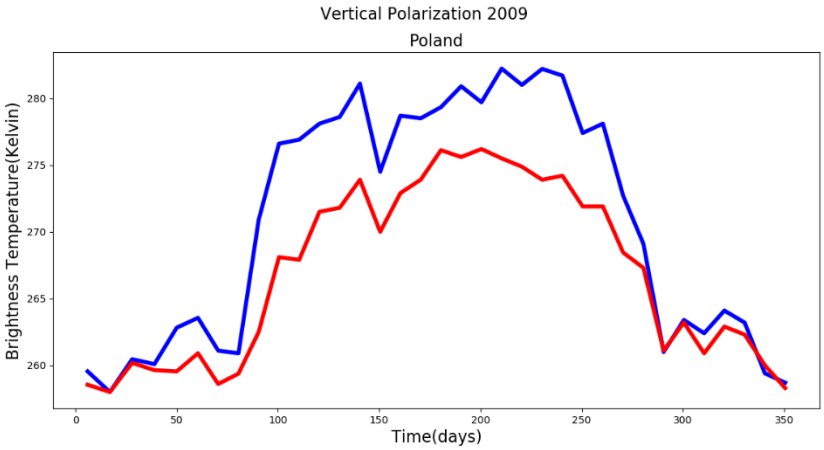

Figure 81. Brightness Temperature time series for the Vertical Polarization for Poland, event occurring in days 340-350

A.2. Polarization Difference Brightness Temperature time series

The PDBT time series for the rest of the case studies will be presented in the figures below.

- *Dry event*

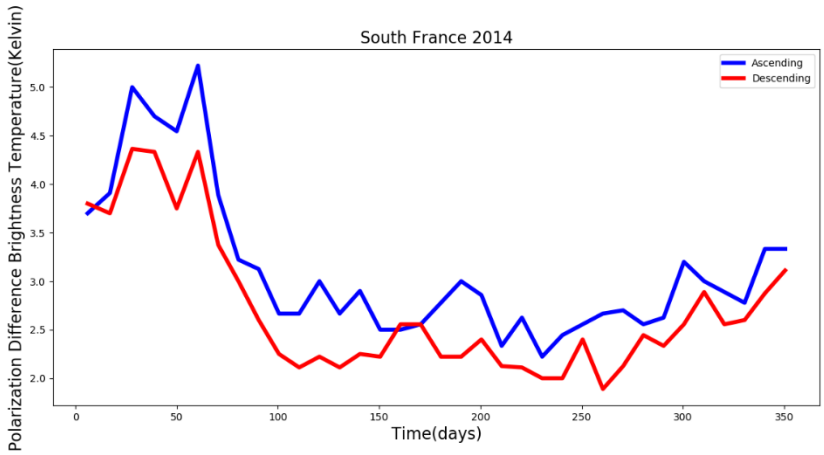

Figure 82. Polarization Difference Brightness Temperature time series for South France, event occurring in days 200-210

- *Wet event*

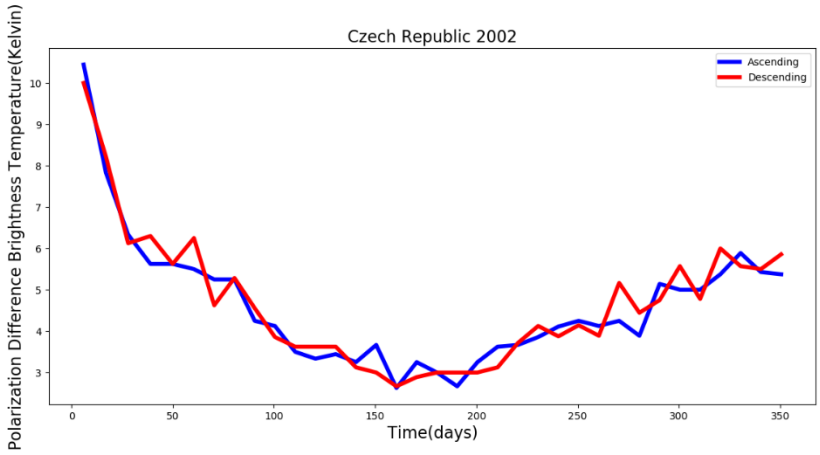

Figure 83.Polarization Difference Brightness Temperature time series for Czech Republic, event occurring in days 220-230

- *Snow event*

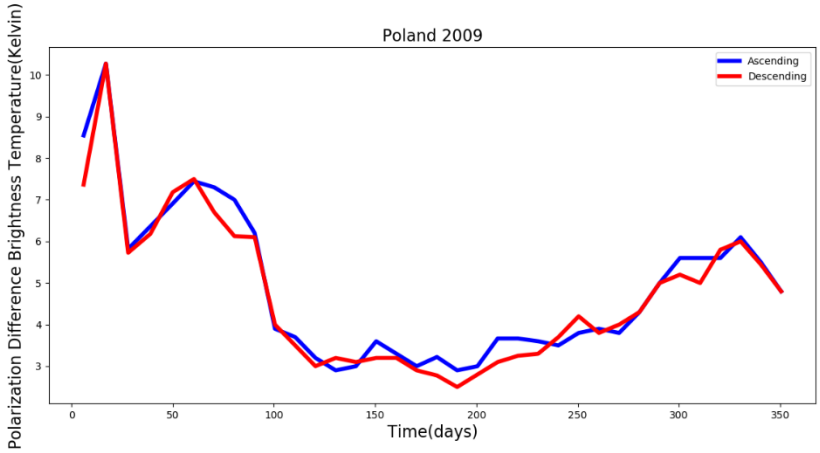

Figure 84. Polarization Difference Brightness Temperature time series for Poland, event occurring in days 340-350

A.3. Microwave Polarization Difference Index time series

The MPDI time series for the rest of the case studies will be presented in the figures below.

- *Dry event*

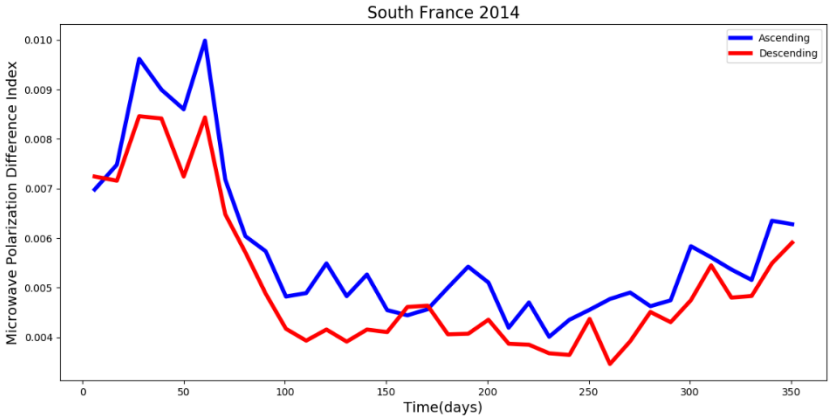

Figure 85. Microwave Polarization Difference Index time series for South France, event occurring in days 200-210

- *Wet event*

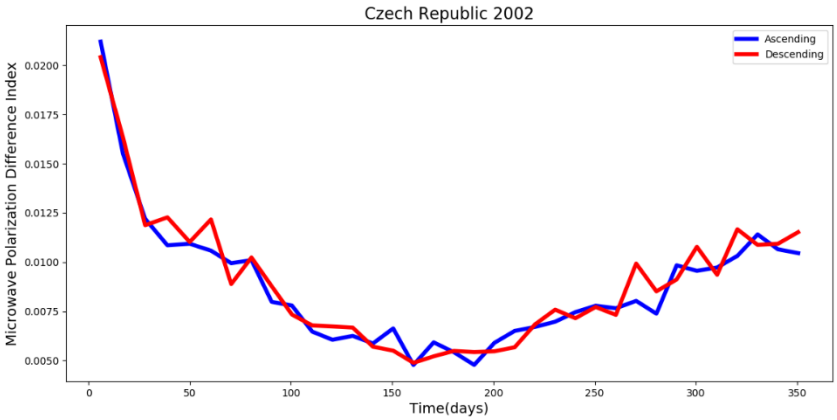

Figure 86. Microwave Polarization Difference Index time series for Czech Republic, event occurring in days 220-230

- *Snow event*

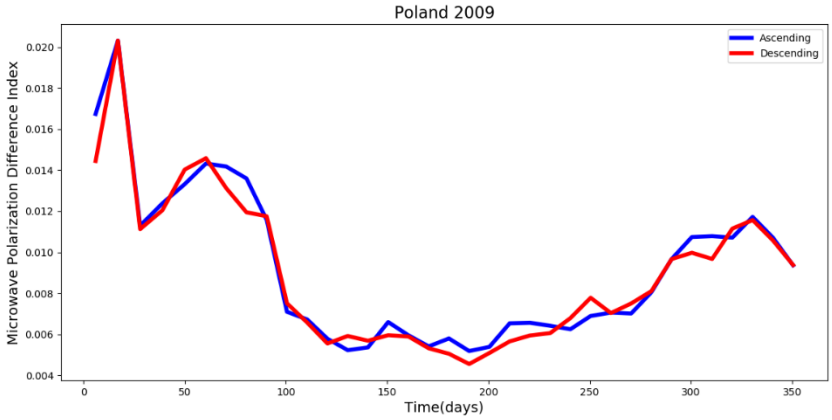

Figure 87. Microwave Polarization Difference Index time series for Poland, event occurring in days 340-350

Appendix B. Polarization Difference Brightness Temperature statistics

B.1. Histogram plots

The histograms for the rest of the case studies will be presented in the figures below.

- *Dry event*

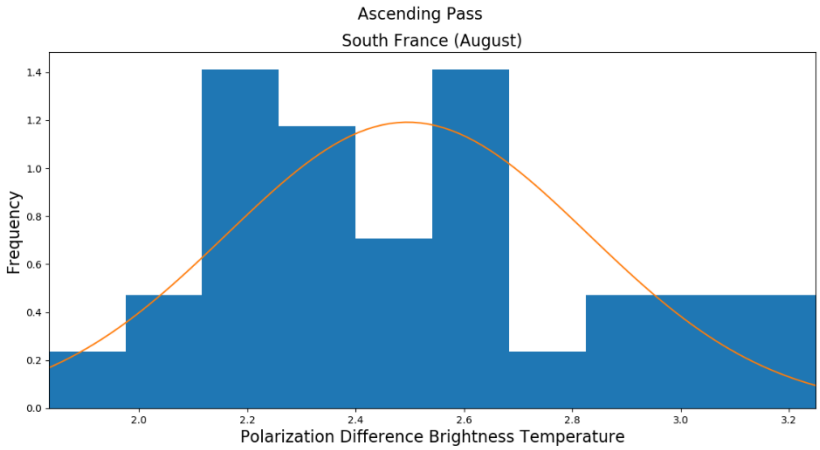

Figure 88. Histogram of the Polarization Difference Brightness Temperature for the ascending pass for days 200-210 for South France

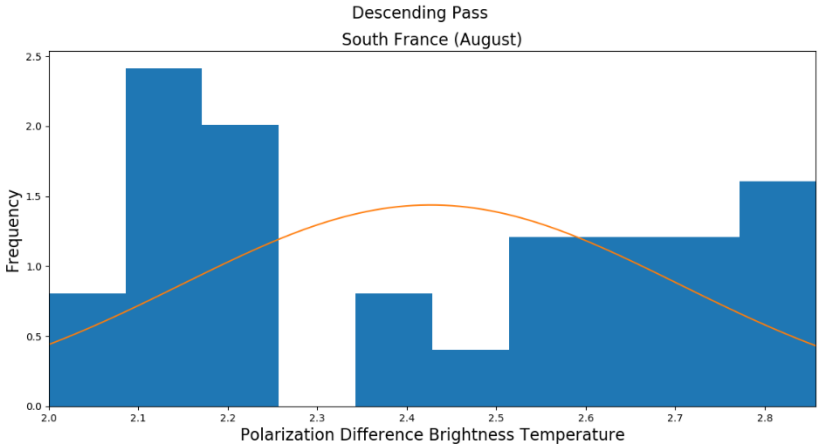

Figure 89. Histogram of the Polarization Difference Brightness Temperature for the descending pass days 200-210 for South France

- *Wet event*

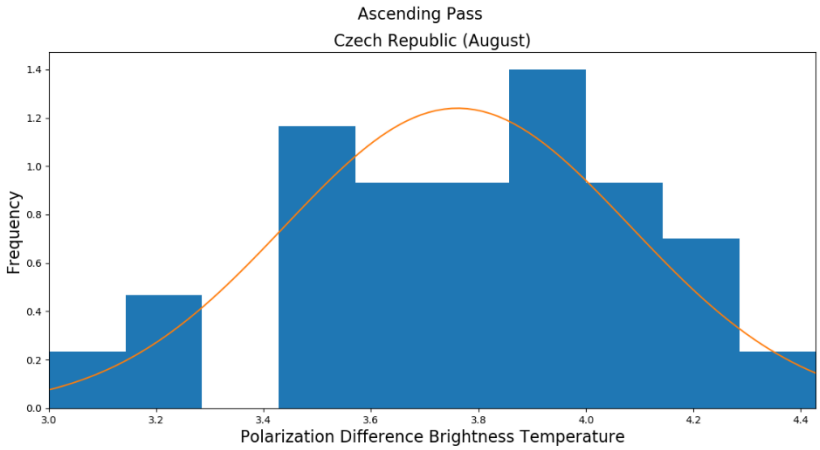

Figure 90. Histogram of the Polarization Difference Brightness Temperature for the ascending pass for days 220-230 for Czech Republic

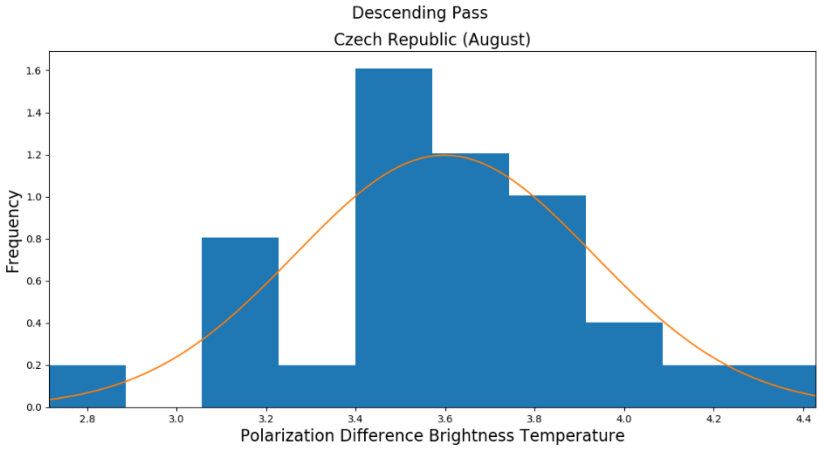

Figure 91. Histogram of the Polarization Difference Brightness Temperature for the descending pass for days 220-230 for Czech Republic

- *Snow event*

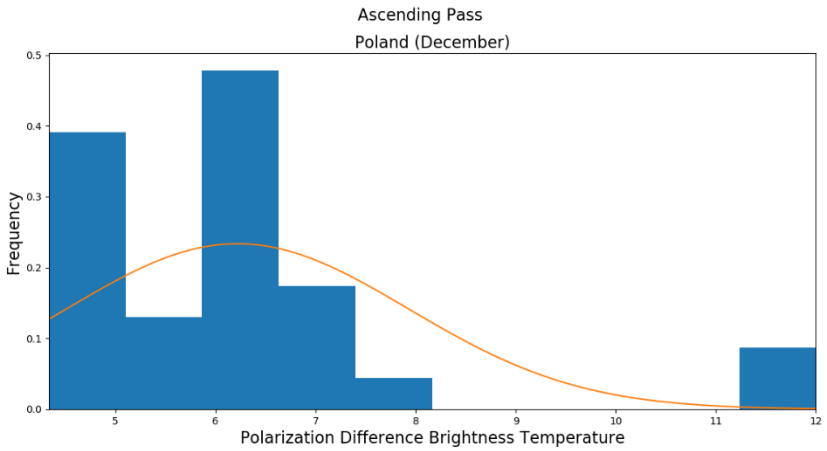

Figure 92. Histogram of the Polarization Difference Brightness Temperature for the ascending pass for days 340-350 for Poland

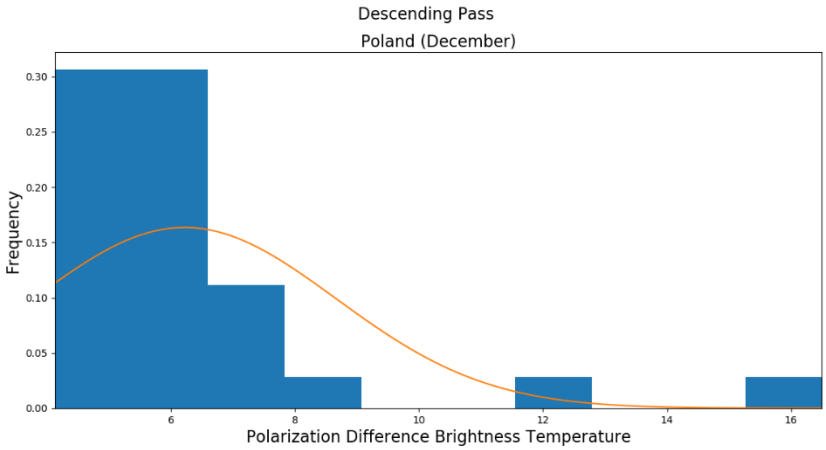

Figure 93. Histogram of the Polarization Difference Brightness Temperature for the descending pass for days 340-350 for Poland

B.2. Standard deviation and mean plots

The standard deviation and the mean plots for the rest of the case studies will be presented in the figures below.

- *South France*

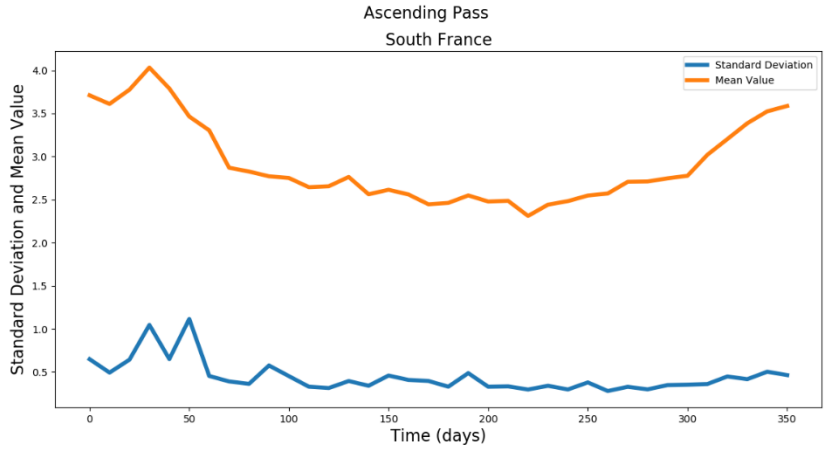

Figure 94. Standard deviation and mean plots for the ascending pass for South France

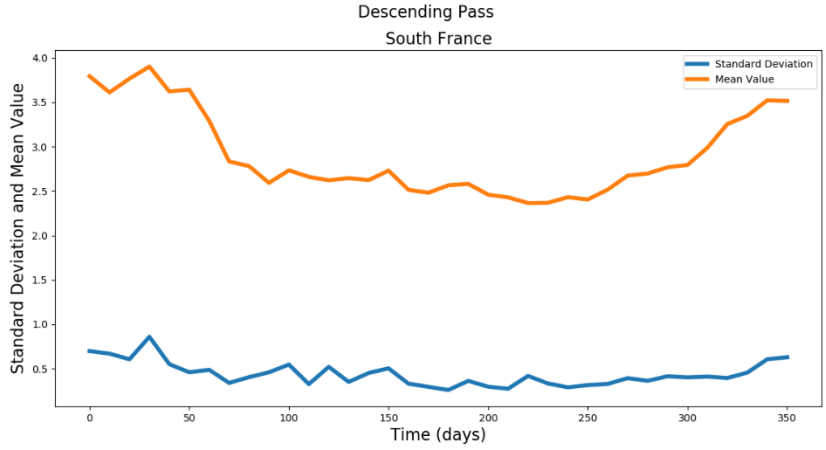

Figure 95. Standard deviation and mean plots for the descending pass for South France

- *Czech Republic*

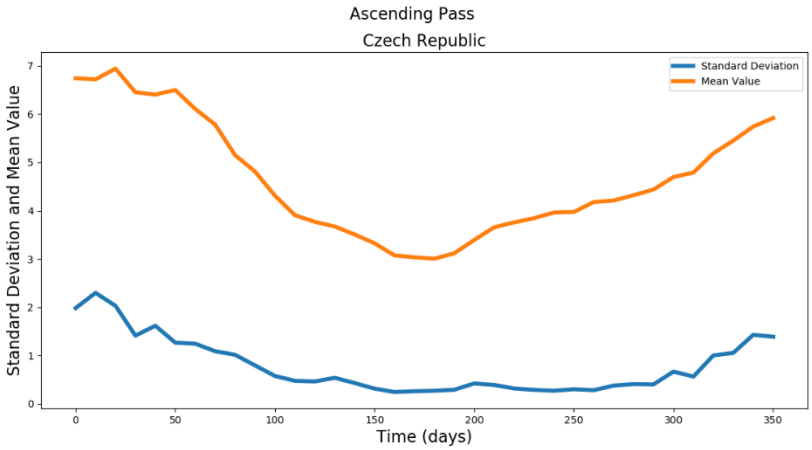

Figure 96. Standard deviation and mean plots for the ascending pass for Czech Republic

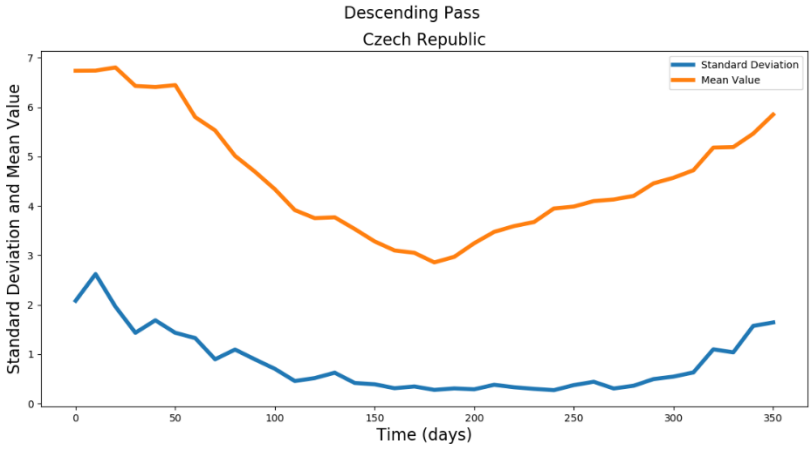

Figure 97. Standard deviation and mean plots for the descending pass for Czech Republic

- *Poland*

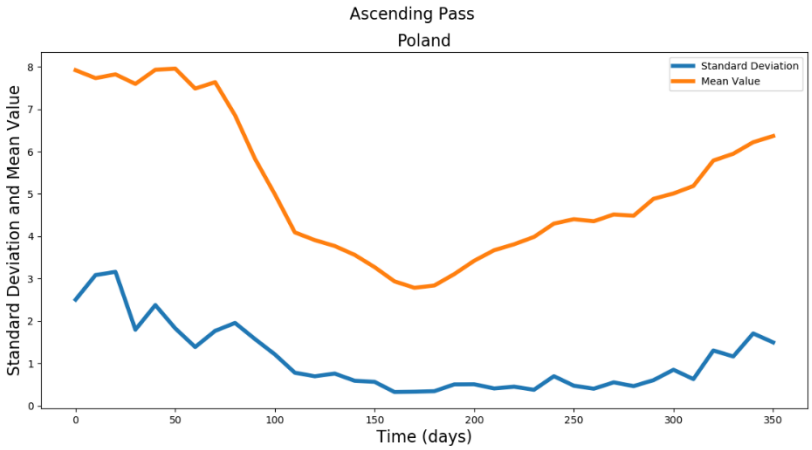

Figure 98. Standard deviation and mean plots for the ascending pass for Poland

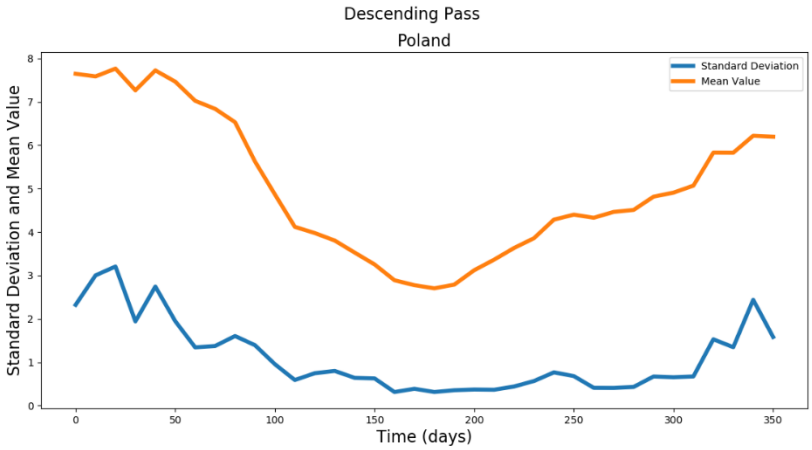

Figure 99. Standard deviation and mean plots for the descending pass for Poland

Appendix C. Methodology of creation of scatter plots

In this section the description of the methodology that was followed for the creation of the scatter plots will be presented.

As described in part 3.1 the data were binned in groups of 10 days according to a fixed DoY index, generating hence 36 groups for every year, leading to the creation of a 3D array. Then, the mean value of the previous created array was found, according to the number of days, resulting in a 2D array with shape (36,31). Following, the PDBT was once again calculated for each selected area, but it was calculated for a specified time interval of ten days that it was the critical one that an extreme had occurred in the area, resulting in the creation of a 2D array with shape (31L,). The same was also completed for the calculation of the average of the absolute values.

Bibliography

Armstrong Richard, Knowles Kenneth, Brodzik Mary, & Hardman Molly. (1994). *DMSP SSM/I-SSMIS Pathfinder Daily EASE-Grid Brightness Temperatures, Version 2 | National Snow and Ice Data Center*. Retrieved from https://nsidc.org/data/NSIDC-0032/versions/2

Differences Between Optical & Radar Satellite Data | Pixalytics Ltd. (n.d.). Retrieved from https://www.pixalytics.com/optical-vs-radar/

Electromagnetic Radiation | Natural Resources Canada. (n.d.). Retrieved from https://www.nrcan.gc.ca/node/14621

Entekhabi, D., Njoku, E., O'Neill, P., Kellogg, K., Crow, W., Edelstein, W., . . . Van Zyl, J. (2010, 5). The Soil Moisture Active Passive (SMAP) Mission. *Proceedings of the IEEE, 98*(5), 704-716.

Europe – FloodList. (n.d.). Retrieved from http://floodlist.com/europe

Greicius, T. (2014). Smap - Launch.

Horizontal polarization vs Vertical polarization- Difference between Horizontal polarization and Vertical polarization. (n.d.). Retrieved from http://www.rfwireless-world.com/Terminology/Horizontal-polarization-vs-Vertical-polarization.html

Importing Passive Microwave EASE-Grid Data into a GIS | National Snow and Ice Data Center. (n.d.). Retrieved from http://nsidc.org/data/ease/gis.html#import-original-ease

Microwave remote sensing | Natural Resources Canada. (n.d.). Retrieved from https://www.nrcan.gc.ca/node/9371

Passive vs. Active Sensing | Natural Resources Canada. (n.d.). Retrieved from http://www.nrcan.gc.ca/node/14639

Precipitation -The Water Cycle. USGS Water Science School. (n.d.). Retrieved from https://water.usgs.gov/edu/watercycleprecipitation.html

Principles of Remote Sensing - Centre for Remote Imaging, Sensing and Processing, CRISP. (n.d.). Retrieved from https://crisp.nus.edu.sg/~research/tutorial/optical.htm

Remote Sensing - Overview, Types and Applications. (n.d.).

Remote Sensing Systems. (n.d.). Retrieved from http://www.remss.com/missions/ssmi/

Satellite Characteristics: Orbits and Swaths | Natural Resources Canada. (n.d.). Retrieved from http://www.nrcan.gc.ca/node/9283

Sevillano, E. (2017). *Environment in Spain: After a long, dry summer, Spain's drought intensifies | In English | EL PAÍS*. Retrieved from https://elpais.com/elpais/2017/09/04/inenglish/1504524138_478794.html

Shaik, A. (n.d.). *LIDAR (Light Detection And Ranging) | Physics and Radio-Electronics*. Retrieved from https://www.physics-and-radio-electronics.com/blog/lidar-light-detection-ranging/

SMOS operations / Operations / Our Activities / ESA. (n.d.). Retrieved from https://www.esa.int/Our_Activities/Operations/SMOS_operations

Snow and Climate | National Snow and Ice Data Center. (n.d.). Retrieved from https://nsidc.org/cryosphere/snow/climate.html

Spatial coverage. (n.d.). Retrieved from https://documentation.ands.org.au/display/DOC/Spatial+coverage

Spatial Resolution | fis.uni-bonn.de. (n.d.). Retrieved from http://www.fis.uni-bonn.de/en/recherchetools/infobox/professionals/resolution/spatial-resolution

SSM/I | PO.DAAC. (n.d.). Retrieved from https://podaac.jpl.nasa.gov/SSMI

Standard Score - Definition of the Standard Score (Z-Score). (n.d.). Retrieved from https://statistics.laerd.com/statistical-guides/standard-score-2.php

Thermal Imaging | Natural Resources Canada. (n.d.). Retrieved from https://www.nrcan.gc.ca/node/9319

Types of Disasters and Their Consequences. (n.d.). Retrieved from https://www.medscape.com/viewarticle/513258_3

What is remote sensing and what is it used for? (n.d.). Retrieved from https://www.usgs.gov/faqs/what-remote-sensing-and-what-it-used?qt-news_science_products=7#qt-news_science_products

Z-Score: Definition, Formula and Calculation - Statistics How To. (n.d.). Retrieved from https://www.statisticshowto.datasciencecentral.com/probability-and-statistics/z-score/

Aonashi, Kazumasa et al. 2009. "GSMaP Passive Microwave Precipitation Retrieval Algorithm : Algorithm Description and Validation." *Journal of the Meteorological Society of Japan* 87A(June 2008): 119–36.

Baghdadi, Nicolas., and Mehrez. Zribi. 2016. *Land Surface Remote Sensing in Continental Hydrology*. Elsevier. https://books.google.nl/books?id=2Ha0CwAAQBAJ&pg=PA68&lpg=PA68&dq=frequencies+that+SMOS+operates&source=bl&ots=m6jSyDdJrf&sig=ACfU3U3IX5Kff4lmHakoKGkTqsM5GVAGmQ&hl=el&sa=X&ved=2ahUKEwjwqvTZvK_hAhWHL1AKHXxBDjcQ6AEwBXoECAcQAQ#v=onepage&q=frequencies that SMOS operates&f=false (April 1, 2019).

Bakker, Wim et al. 2004. *Principles of Remote Sensing*. eds. Norman Kerle, Lucas Janssen, and Gerrit Huurneman. Enschede: The International Institute for Geo-Information Science and Earth Observation (ITC).

Balabukh, Vira et al. 2018. "Extreme Weather Events in Ukraine: Occurrence and Changes." In *Extreme Weather*, ed. Philip John Sallis.

Bolten, J. D., and W. T. Crow. 2012. “Improved Prediction of Quasi-Global Vegetation Conditions Using Remotely-Sensed Surface Soil Moisture.” *Geophysical Research Letters* 39(19): 1–5.

Bolten, John D et al. 2010. “Evaluating the Utility of Remotely Sensed Soil Moisture Retrievals for Operational Agricultural Drought Monitoring and Grant NNS06AA051 Entitled "Integrating NASA’s Global Soil Moisture Remote Sensing and Modeling Data into the USDA’s Global Crop Pro.” *Ieee Journal of Selected Topics in Applied Earth Observations and Remote Sensing* 3(1): 57. http://ieeexplore.ieee.org.

Brown, Molly E. et al. 2013. “NASA’s Soil Moisture Active Passive (SMAP) Mission and Opportunities for Applications Users.” *Bulletin of the American Meteorological Society* 94(8): 1125–28. http://journals.ametsoc.org/doi/abs/10.1175/BAMS-D-11-00049.1 (April 1, 2019).

Csornai, G. 2006. “Flood and Drought Monitoring by Remote Sensing.”

Europe, Central-northern. 2018. “EDO Analytical Report EDO Analytical Report.” (July): 1–13.

Ferraro, Ralph R, Fuzhong Weng, Norman C Grody, and Alan Basist. 1996. “An Eight-Year (1987 – 1994) Time Series of Rainfall , Clouds , Water Vapor , Snow Cover , and Sea Ice Derived from SSM / I Measurements.” (January): 891–905.

Fily, M, A Royer, and K Goı. 2003. “A Simple Retrieval Method for Land Surface Temperature and Fraction of Water Surface Determination from Satellite Microwave Brightness Temperatures in Sub-Arctic Areas.” *Elsevier* 85: 328–38.

Fournier, S. et al. 2016. “SMAP Observes Flooding from Land to Sea: The Texas Event of 2015.” *Geophysical Research Letters* 43(19): 10,338-10,346. http://doi.wiley.com/10.1002/2016GL070821 (April 1, 2019).

Grody, Norman C. 1991. “Classification of Snow Cover and Precipitation Using the Special Sensor Microwave Imager.” *JOURNAL OF GEOPHYSICAL RESEARCH*, 96: 7423–35.

“Horizontal Polarization vs Vertical Polarization- Difference between Horizontal Polarization and Vertical Polarization.” http://www.rfwireless-world.com/Terminology/Horizontal-polarization-vs-Vertical-polarization.html (August 2, 2018).

“Introducing SMOS / SMOS / Observing the Earth / Our Activities / ESA.” https://www.esa.int/Our_Activities/Observing_the_Earth/SMOS/Introducing_SMOS (April 1, 2019).

Jackson, J. 1997. “Soil Moisture Estimation Using Special Satellite Microwave / Imager Satellite Data over a Grassland Region.” *Water Resources Research* 33(6): 1475–84.

Kaya, Gulsen Taskin. 2014. ITU Insitute of Earthquake Engineering and Disaster Management *Introduction to Optical & Thermal Remote Sensing Remote Sensing Components*. http://bte.bilgem.tubitak.gov.tr/sites/images/g1-6.pdf.

Kejna, Marek et al. 2009. “AIR TEMPERATURE IN POLAND.” *Bulletin of Geography-physical geography series* (December).

Kubota, Takuji et al. 2006. “Global Precipitation Map Using Satelliteborne Microwave Radiometers by the GSMaP Project: Production and Validation.” *International Geoscience and Remote Sensing Symposium (IGARSS)* 45(7): 2584–87.

Kubota, Takuji, and Ken’ichi Okamoto. 2007. “The Global Satellite Mapping of Precipitation

(GSMaP) Project."

Kumar, Nagesh, and Resmidevi Tv. 2013. "Remote Sensing Applications in Water Resources Engineering." *Indian Institute of Science*.

Kundzewicz, Zbigniew W. et al. 2005. "Summer Floods in Central Europe - Climate Change Track?" *Natural Hazards* 36(1–2): 165–89.

Kundzewicz, Zbigniew W et al. 2013. "Large Floods in Europe , 1985 – 2009." *Hydrological Sciences Journal* 6667.

Lakshmi, Venkataraman, Eric Wood, and Bhaskar Choudhury. 1997. "Evaluation of Special Sensor Microwave / Imager Satellite Data for Regional Soil Moisture Estimation over the Red River Basin." *Journal of applied meteorology* 36(Schmugge 1985).

Li, Yang-yang, Kai Zhao, Xing-ming Zheng, and Jian-hua Ren. 2013. "Analysis of Microwave Polarization Difference Index Characteristics about Different Vegetation Types in Northeast of China." *International Conference on Remote Sensing, Environment and Transportation Engineering (RSETE 2013)* (Rsete): 36–38.

Marchi, L, M Borga, E Preciso, and E Gaume. 2010. "Characterisation of Selected Extreme Flash Floods in Europe and Implications for Flood Risk Management." *Journal of Hydrology* 394(1–2): 118–33. http://dx.doi.org/10.1016/j.jhydrol.2010.07.017.

McColl, Kaighin A. et al. 2017. "The Global Distribution and Dynamics of Surface Soil Moisture." *Nature Geoscience* 10(2): 100–104. http://www.nature.com/articles/ngeo2868 (April 1, 2019).

Mladenova, Iliana E. et al. 2017. "Intercomparison of Soil Moisture, Evaporative Stress, and Vegetation Indices for Estimating Corn and Soybean Yields Over the U.S." *IEEE Journal of Selected Topics in Applied Earth Observations and Remote Sensing* 10(4): 1328–43. http://ieeexplore.ieee.org/document/7811273/ (April 4, 2019).

Owe, Manfred, Richard de Jeu, and Thomas Holmes. 2008. "Multisensor Historical Climatology of Satellite-Derived Global Land Surface Moisture." *Journal of Geophysical Research: Earth Surface* 113(1): 1–17.

Paloscia, Simonetta, Giovanni Macelloni, Emanuele Santi, and Toshio Koike. 2001. "A Multifrequency Algorithm for the Retrieval of Soil Moisture on a Large Scale Using Microwave Data from SMMR and SSM / I Satellites." 39(8): 1655–61.

Prigent, Catherine, William B. Rossow, and Elaine Matthews. 1997. "Microwave Land Surface Emissivities Estimated from SSM/I Observations." *Journal of Geophysical Research: Atmospheres* 102(D18): 21867–90. http://doi.wiley.com/10.1029/97JD01360.

"Remote Sensing: Passive Microwave | National Snow and Ice Data Center." https://nsidc.org/cryosphere/seaice/study/passive_remote_sensing.html (March 31, 2019).

"Remote Sensing Systems." http://www.remss.com/missions/ssmi/ (August 2, 2018).

Resources, Natural. 2016. "Fundamentals of Remote Sensing." *Forestry*.

Rybicki, George B, and Alan P Lightman. 1991. *RADIATIVE PROCESSES IN ASTROPHYSICS*. Wiley & Sons.

Shang, Haolu. 2017. 91 TU Delft University "Applications of Passive Microwave Data to Monitor Inundated Areas and Model Stream Flow." Delft University of Technology.

Sippel, Suzanne J., Stephen K. Hamilton, John M. Melack, and Bhaskar J. Choudhury. 1994. "Determination of Inundation Area in the Amazon River Floodplain Using the SMMR 37 GHz Polarization Difference." *Remote Sensing of Environment* 48(1): 70–76.

Spinoni, Jonathan, Gustavo Naumann, Paulo Barbosa, and Jürgen Vogt. 2016. *Meteorological Droughts in Europe Events and Impacts*. European Comission.

Spinoni, Jonathan, Gustavo Naumann, Jürgen V. Vogt, and Paulo Barbosa. 2015. "The Biggest Drought Events in Europe from 1950 to 2012." *Journal of Hydrology: Regional Studies* 3: 509–24.

"Surface Soil Moisture (WMO)." https://ipad.fas.usda.gov/cropexplorer/description.aspx?legendid=207&regionid=useast (April 4, 2019).

Velde, R Van Der et al. 2014. "Long Term Soil Moisture Mapping over the Tibetan Plateau Using Special Sensor Microwave / Imager." : 1323–37.

"What Is RFI (EMI) / EMC? - FuseCo." https://www.fuseco.com.au/rfi-filters/knowledge-centre/articles/what-is-rfi-emi-emc (April 1, 2019).